EMPIRICAL ANALYSIS OF SINGLE-CELL ELECTROPORATION WITH AN ELECTROLYTE-FILLED CAPILLARY

by

Aparna Agarwal

B.S., University of Delhi, 1998

M.S., Indian Institute of Technology, Kanpur, 2001

Submitted to the Graduate Faculty of

Arts and Sciences in partial fulfillment

of the requirements for the degree of

Doctor of Philosophy

University of Pittsburgh

2009

UNIVERSITY OF PITTSBURGH

FACULTY OF ARTS AND SCIENCES

This dissertation was presented

by

Aparna Agarwal

It was defended on

March 26th, 2009

and approved by

Stephen G. Weber, Professor, Department of Chemistry

Adrian Michael, Associate Professor, Department of Chemistry

Shigeru Amemiya, Associate Professor, Department of Chemistry

c, Professor, Department of Pharmaceutical Sciences

Dissertation Advisor: Stephen G. Weber, Professor, Department of Chemistry

EMPIRICAL ANALYSIS OF SINGLE-CELL ELECTROPORATION WITH AN ELECTROLYTE-FILLED CAPILLARY

Aparna Agarwal, PhD

University of Pittsburgh, 2009

Electroporation is a technique that uses electric fields to create transient nanopores in a cell's membrane thereby increasing its permeability. This technique has been most frequently used to transport molecules, chiefly DNA, across cell membranes for a wide range of applications such as gene therapy, molecular biology, and clinical chemotherapy. There are two types of electroporation, bulk and single-cell electroporation. In single-cell electroporation, a localized electric field is applied to a single cell to achieve selective permeabilization of the targeted cell without affecting its neighbors. However, there are no experimental reports on the quantitative treatment of single-cell electroporation. We have developed a quantitative approach to control and maximize cell permeabilization and viability in single-cell electroporation. Single-cell electroporation experiments have been performed using small-sized electrolyte-filled capillaries. A549 cells are exposed to the thiol-reactive dye Thioglo-1 leading to green fluorescence from intracellular thiol adducts. The fluorescent cells are exposed to brief (50-500 ms) electric field pulses (500 V across a 15 cm capillary) at varying cell-capillary tip distances (2-10 μm). Loss of fluorescence from diffusion of Thioglo-1 conjugates out of the cell is measured as a function of time. Results revealed that longer pulses and a shorter cell-capillary tip distance led to a greater decrease in the cell's fluorescence and are more deadly. A large variability in single-cell electroporation within a set of experimental conditions has been observed. In order to understand the variability in single-cell electroporation, logistic regression has been performed to determine the probabilities of cell survival and electroporation dependence on experimental conditions and

cell parameters. The results revealed that the cells are more readily permeabilized and are more likely to survive if they are large and hemispherical as opposed to small and ellipsoidal with a high aspect ratio. Further, a quantitative approach has been developed to determine the experimental and cell parameters that influence the outcome of a single-cell electroporation experiment. The regression analysis results revealed that the outcome of electroporation can be related to the cell-capillary tip distance and cell size. The relationship obtained has been used to control the magnitude of molecular flux from single cells, and decrease the variability in the outcome of electroporation of A549, and two more cell lines DU 145, and PC-3 cells. It has also been found that there is a significant relationship between cell survivability and the molecular efflux from single fluorescent cells. Results revealed that cell survivability could be retained across the three cell lines A549, DU 145 and PC-3 by controlling the magnitude of molecular efflux to 55 % or less.

TABLE OF CONTENTS

LIST OF TABLES

LIST OF FIGURES

ACKNOWLEDGEMENTS

"You can understand perfectly, if you give your mind to it."- Lord Kelvin

First and foremost, I would like to thank my research advisor, Prof. Stephen G. Weber. It was a great pleasure to have a chance to work with him and to learn from him. With his vast knowledge of science, he has always provided me with proper guidance and encouraging advice and for that I am eternally grateful. Thank you for your continuous support.

I would like to thank current and former Weber group members for their fruitful discussions and kind support. They have been good friends in many ways. We are more of a family rather than a research group. I would also like to thank my dear friends whom I met along this journey.

I thank all the administrative and technical staff at the Department of Chemistry. They have been a great support.

I am eternally indebted to my parents for their continued love and support. Lastly, I would like to thank my husband, Amit, for always being there for me.

1.0 INTRODUCTION

1.1 ELECTROPORATION

The ability to introduce macromolecules into cells, including DNA, RNA, protein, and other bioactive compounds has facilitated a broad range of biological studies, from biochemistry and biophysics to molecular and cell biology. It has been known since the 1970s that the cell membrane can be transiently permeabilized by exposing the cell to a high intensity electric field pulse.[1-3] Neumann et al. first showed the successful transfer of DNA into mouse L cells by applying electric field pulses of 8 kV/cm with a 5 μs pulse duration.[4] The term electroporation was then introduced by Neumann and is now generally accepted to refer to the phenomenon of formation of pores at high electric field strengths.

1.1.1 Electroporation Overview

The intact cell membrane acts as a barrier to the free diffusion of molecules and ions between the cytoplasm and the external medium. When a cell is exposed to an electric field, a transmembrane voltage is induced on the membrane. If this voltage exceeds a certain value, which has been experimentally determined to be about 250 mV for most cell types,[5] it leads to a significant increase of the conductivity and the permeability of the membrane. Formation of a state of increased permeability of the membrane caused by an exposure to the electric field is

called electroporation (also electropermeabilization). As a result of the increased permeability of the membrane, charged, polar molecules such as DNA, dyes, drugs or proteins can be transported across the membrane.[4, 6] With appropriate duration and amplitude of the electric field, the membrane returns into its normal state after the end of the exposure to the electric field (reversible electroporation). However, if the exposure is too long or the amplitude of the electric field is too high, the membrane does not revert to its normal state after the end of the exposure, leading to cell death (irreversible electroporation).[7] Electroporation is now being used in many fields such as cell biology and biotechnology for gene transfer[4, 8-11] and in medical application for gene therapy,[12-14] cancer chemotherapy,[15, 16] and transdermal drug delivery.[17-19]

There are two types of electroporation, namely bulk electroporation and single-cell electroporation. Traditionally, electroporation has been performed in batch or bulk mode on cells in suspension. In bulk electroporation, a batch of cells in suspension is exposed to a uniform electric field of a few kilovolts per centimeter resulting in the permeabilization of many cells at the same time.[4, 5, 14, 18, 20-22] This gives a distribution of outcomes among the cells in the suspension. Single-cell electroporation has shown promise, especially in applications to natural adherent cells, but is not well studied as bulk electroporation. In single-cell electroporation, a localized field is applied to a single adherent cell or a cell in suspension flowing through a microfabricated device, while the neighboring cells are exposed to very low or no field. Data collected from single cells generates unique information about cell-to-cell variations and avoids information loss due to averaging across the population of cells.[23-25] In the next few sections (1.2 - 1.5) an overview of bulk electroporation in literature is presented. Section 1.6 gives an overview of various techniques that have been used in single cell electroporation.

1.2 TRANSMEMBRANE POTENTIAL

The primary event that leads to the pore formation by electroporation is the induction of a large transmembrane potential by the applied electric field. The potential difference $\Delta\psi_m$ across a cell membrane consists of two major contributions, natural $\Delta\psi_0$ and induced $\Delta\psi_E$ membrane potential differences. $\Delta\psi_0$ is the intrinsic membrane potential difference which is typically about -40 to -60 mV.

The electrically induced potential difference $\Delta\psi_E$ is the difference between the potential inside the cell ψ_{in} and the potential outside the cell ψ_{out}. The $\Delta\psi_E$ induced at a point on the membrane of a single cell placed in a homogeneous field (Figure 1.1) is given by:

$$\Delta\psi_E(t) = \psi_{in} - \psi_{out} = -f(d_c/2)E\cos\varphi(1-\exp(-t/\tau)) \qquad (1.1)$$

where $\Delta\psi_E$ is the induced transmembrane voltage, *f* is a function that describes geometrical and electrical properties, d_c is the diameter of a cell, *E* is the external electric field, and φ is the polar angle measured from the center of the cell with respect to the direction of the field, and τ is the charging time of the pulsed cell membrane.

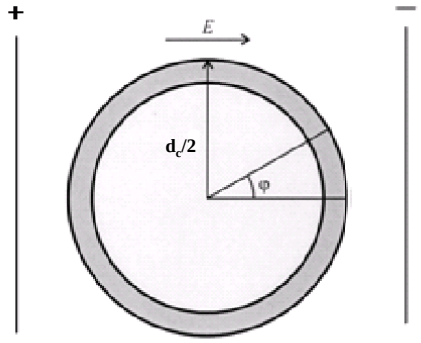

Figure 1.1. Induction of transmembrane on a spherical cell placed in a homogeneous electric field. Adapted from reference. [26]

In most cases, the exponential term can be neglected because the duration of the applied electrical pulse is much larger than the membrane charging time (< 1 μs). By further assuming the cell is spherical with a shape factor of 1.5 and that the cell membrane is pure dielectric, the transmembrane potential can be deduced as following:

$$\Delta\psi_E = -1.5(d_c / 2)E\cos\varphi \qquad (1.2)$$

As the induced potential difference $\Delta\psi_E$ is dependent on an angular parameter φ (Eq. 1.1 and 1.2), the field effect is position dependent on the cell surface. Therefore, the anode facing side of the cell is hyperpolarized while the cathode facing side is depolarized. The spatial distribution of the transmembrane potential induced in nonexcitable cells by external electric field was first imaged by Gross et al. by using potential-sensitive fluorescent dye.[27]

1.3 THEORETICAL MODELS FOR ELECTROPORATION

Despite the common use of electroporation in biotechnology and medicine, the molecular mechanisms of electroporation and electrodelivery of macromolecules is not very well understood. Nevertheless, the theory of formation of aqueous pores in the cell membrane is widely considered as the most convincing theoretical explanation of electroporation.[6] According to this theory a sufficiently long and strong exposure to an electric field leads to the formation of hydrophilic pores, in which the lipids adjacent to the aqueous inside of the pore are reoriented in a manner that their hydrophilic heads are facing the pore, while their hydrophobic tails are hidden inside the membrane. The hydrophilic state of the pores can only be reached through a transition from an initial hydrophobic state in which the lipids still have their original orientation (Figure 1.2). As electric field amplitude increases, the presence of hydrophilic pores becomes

energetically more favorable, which leads to the formation of pores with an average radius corresponding to the minimum of the free-energy curve (Figure 1.3, the upper curve). Further increase of the field amplitude pushes this curve downward, and eventually the energy minimum disappears (Figure 1.3 the lower curve), resulting in a complete breakdown of the membrane, which corresponds to irreversible electroporation.

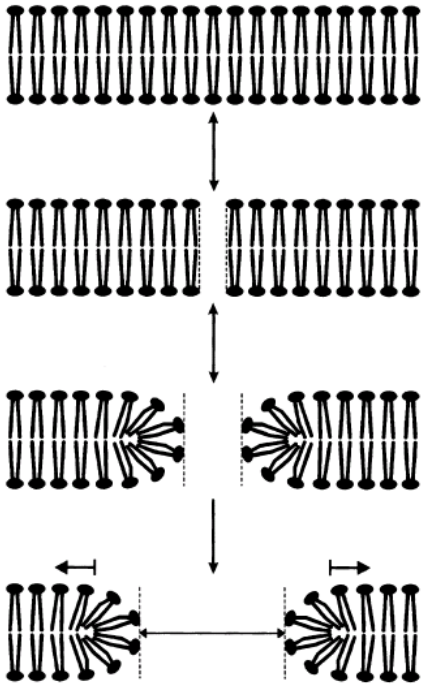

Figure 1.2. Formation of an aqueous pore shown for transmembrane voltage increasing from top to bottom: a non-porated membrane, formation of a hydrophobic pore, transformation into a hydrophilic pore (reversible electroporation), and enlargement beyond the stable size (irreversible electroporation).

(Adapted from reference,[6] with permission from Elsevier.)

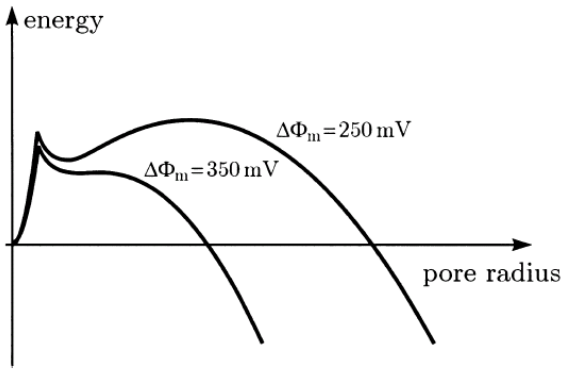

Figure 1.3. A schematic representation of the amount of energy required for formation of an aqueous pore of a given radius for a transmembrane voltage that yields reversible (the upper curve) and irreversible electroporation (lower curve). The sharp local maximum corresponds to the transition from hydrophobic to hydrophilic state.

(Adapted from reference,[6] with permission from Elsevier.)

1.3.1 Pore Creation

A theoretical approach describing the creation of pores induced by electric fields is based on energy considerations.[6, 28, 29] According to the Glaser et al. theory of electroporation, all pores are initially created hydrophobic at a rate determined by their energy[30]

$$E(r) = E_*\left(\frac{r}{r_*}\right)^2 \tag{1.3}$$

where r_* and E_* are the minimum radius and energy barrier for the creation of conducting pores (Figure 1.4). Most of the hydrophobic pores are quickly destroyed by lipid fluctuations, but if hydrophobic pores of radius $r \geq r_*$ are created, they convert spontaneously to long-lived hydrophilic pores. The energy of hydrophilic or conducting pores is given by the following:

$$E(r) = \left(\frac{C}{r}\right)^4 + 2\pi\gamma r - \Gamma\pi r^2 \tag{1.4}$$

Here, C is the steric repulsion coefficient, γ is the pore edge energy, and Γ is membrane surface tension. The first term in Eq. 1.4 represents the steric repulsion between the lipid heads lining the pore and is responsible for the increase in pore energy with shrinking radius.

The pore energy *E(r)* in Figure 1.4 corresponds to the situation when there is no externally applied transmembrane potential. In the presence of a transmembrane potential V_m, the pore energy is denoted by:

$$\varphi(r) = E(r) - \pi a_p V_m^2 r^2 \qquad (1.5)$$

where the term $-\pi a_p V_m^2 r^2$ is the capacitive contribution. The coefficient a_p is a property of the membrane and its aqueous environment.

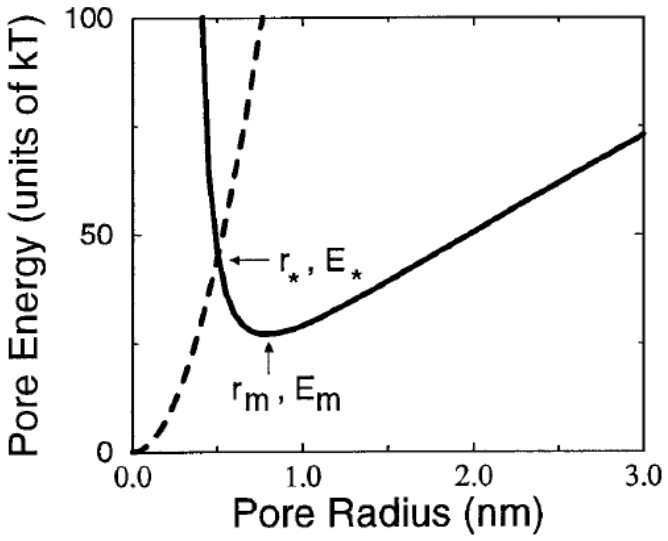

Figure 1.4. The energy of a pore as function of radius at the transmembrane potential V_m = 0 mV. The dashed and solid lines show the energy of hydrophobic and hydrophilic pores, respectively.

(Reprinted from reference,[31] with permission from Elsevier).

1.3.2 Pore Size, Distribution, and Density

A number of models have been described that study the electroporation of a single cell in a uniform electric field. The first model that describes the basic biophysics of electroporation was built by Pastushenko et al. in 1979.[32] This model is based on Smoluchowski equation, a partial differential equation (PDE) that governs the distribution of pores as a function of their radius and time. The Smoluchowsi equation can be described as follows: If *n(r,t)* denotes the distribution function of the pore density, such that the pore density, at a given time *t* and when the number of pores per unit area with radii between *r* and *r+dr*, is *n(r,t)dr*, then *n(r,t)* is governed by the following equation:

$$n_t + D\partial_r\left(-\frac{\varphi}{kT}n - n_r\right) = S(r) \tag{1.6}$$

where *D* is the diffusion constant of pores, φ is the pore energy, *k* is the Boltzmann constant, *T* is the absolute temperature, and *S(r)*is the source term that represents the creation of pores. Subscript *t* denotes differentiation with respect to time, subscript *r* or ∂_r denotes differentiation with respect to pore radius.

Investigating the electroporation process using PDE has several drawbacks. First, this equation requires knowledge of several constants whose values cannot be measured directly. Most of these constants have been estimated by theoretical arguments and are known only in orders of magnitude. Because of these uncertainties in the values of the parameters, the solution to Eq. 1.6 gives only a qualitative picture of the electroporation process.

A model that provides a closer relationship between theory and experiments is developed by DeBruin and Krassowska.[31, 33, 34] In this model, they simplified the Smoluchowski equation

from PDE to an ordinary differential equation (ODE). This ODE describes the dynamics of the pore density by the following equation:

$$\frac{dN}{dt} = \alpha e^{(V_m / V_{ep})^2} \left(1 - \frac{N}{N_{eq}(V_m)} \right) \tag{1.7}$$

where N is the pore density, V_m is the transmembrane potential, V_{ep} is the characteristic voltage of electroporation (0.25 V), and α is the creation rate coefficient. N_{eq} is the equilibrium pore density for a given voltage V_m

$$N_{eq}(V_m) = N_0 e^{q(V_m / V_{ep})^2} \tag{1.8}$$

where N_o is the equilibrium pore density for V_m=0, and $q=(r_m/r_*)^2$, with r_m the mimimum energy radius at V_m=0, and r_* the minimum radius of a hydrophilic pore. This model has been used to determine transmembrane potential, number of pores, and the distribution of pore radii as functions of both time and position on the cell surface. Based upon this model, the pore density of a spherical cell exposed to an external electric field can be high in the order of 10^9 pores/cm^2, of which > 97% are small pores (~1 nm radius). The highest pore density occurs on the depolarized and hyperpolarized poles but the largest pores, which may grow to ~0.5 μm, are on the border of the electroporated regions of the cell.

1.4 ELECTROPORATION PARAMETERS

1.4.1 Pulse Parameters

The pulse parameters and experimental conditions of electroporation should be chosen such that they yield the highest fraction of permeabilized and live cells. Also, in cases of bulk

electroporation, it is necessary that the optimal pulse parameters should be chosen so that a certain quantity of molecular uptake takes place in each cell. For these reasons, the role of pulse parameters and experimental conditions is usually investigated through a combination of tests that estimate the fraction of permeabilized cells, the fraction of cells surviving the treatment, and the average amount of exogenous molecules introduced into the cell.

1.4.1.1 The Role of Field Strength, Pulse Duration, and Number of Pulses

Cell permeabilization occurs on the part of the cell membrane where potential difference has been brought to its critical value. The critical value has been evaluated to be of the order of ~250 mV for most cell types. Permeabilization is therefore controlled by the field strength, and it occurs only when the field intensity E, larger than a critical value, E_p, is applied. The field strength determines the area of the cell surface that is affected.[10, 35] Increase in E results in an increase in the percentage of permeabilized cells; however, this is also accompanied by a decrease in percentage of dead cells. The pulse duration and/ or number of pulses on the other hand control the density of pores in the area where cell permeabilization takes place.[36] Rols and Teissie have shown in Chinese hamster ovary cells that the critical pulse amplitude of electroporation performed in a bulk mode is lowered if the number and/or duration of the pulses is increased.[35] The transmembrane transport of molecules into permeabilized cells depends on the proper choice of the pulsing conditions. Pucihar et al. studied the influence of pulse amplitude and pulse duration on the transport of small molecule such as propidium iodide into Chinese hamster ovary cells.[37] They found that the transport of propidium iodide was faster and larger for higher pulse amplitudes and/ or longer pulse durations. Electrophoresis plays an important role in the transport of macromolecules across the membrane and a sufficiently long pulse duration is crucial for adequate uptake.[38] Zahroff et al. demonstrated in 4T1 murine

mammary carcinoma cell lines that low-voltage and long duration pulses were more effective than high voltage and short duration pulses for macromolecular delivery into permeabilized cells.[39] Typically, pulse durations for the uptake of smaller molecules are in the range of hundreds of microseconds, while for macromolecules, durations from several milliseconds to several tens of milliseconds are usually required.

1.4.1.2 Role of Pulse Shape

The role of pulse shape in efficiency of electroporation has not been studied in great detail because commercially available pulse generators that provide sufficient voltage for electroporation of cells are mostly limited to rectangular and exponentially decaying pulses. Among the studies on the role of pulse shape in electroporation, Tekle et al. found that the efficiency of DNA transfection in vitro was significantly higher with a bipolar 60-kHz square wave of 400 μs duration than with a unipolar wave of the same frequency and duration.[40] Schoenbach et al. have reported on electropermeabilization with ultrashort (60 ns) pulses.[41] In a study comparing unipolar and bipolar rectangular pulses, Kotnik et al. have shown that with bipolar pulses, the critical voltage of electroporation is lowered considerably, while cell viability remains unaffected.[42]

1.4.2 Cell Factors

1.4.2.1 Cell Size and Shape

The effect of cell size on electroporation is evident from the Schwan equation given in Eq. 1.1. The Schwan equation shows that in bulk electroporation where a homogeneous electric field is applied to a spherical cell, the transmembrane potential depends linearly on the cell

size.[43] Therefore, a large cell would have a higher transmembrane potential which leads to an increased cell permeabilization.

Theoretical and experimental results have shown that permeabilization is not only a function of cell size but also of cell shape and orientation.[44-46] For spherical cells in a homogeneous field, the transmembrane potential is defined by the Schwan equation. Non spherical cells can be approximated as prolate or oblate spheroids. The Schwan equation is extended to calculate transmembrane potential for parallel and perpendicularly oriented spheroids, and for arbitrarily oriented spheroids. The generalized Schwan equation can be written as:

$$\Delta\Phi_i = E\sin\alpha\frac{1}{1-L_x}x + E\cos\alpha\frac{1}{L_z}z \tag{1.9}$$

where L_x and L_z are depolarizing factors which depend on the geometrical properties of the spheroid, variables x and z are the coordinates of a point on the surface of the spheroid, E is strength of the applied electric field, and angle α is the angle between the symmetry axis of the spheroid and the external electric field and defines the cell orientation with respect to the electric field. Gimsa and Wachner[46, 47] extended the Schwan equation to present an analytical solution for the transmembrane potential induced by a homogeneous AC field. Their model describes the dependence of transmembrane potential on cell size and shape, field frequency, the membrane capacitance, the conductivities of cytoplasm, membrane and external medium, the angle dependence, and the orientation of the cell with respect to the external field. Valic et al. showed theoretically and experimentally that for elongated cells, the permeabilization was strongly dependent upon electric field intensity and angle of orientation α.[45] Their results showed that for electric field slightly higher than the threshold, only the cells with their longest axis parallel to the electric field were permeabilized. When the electric field was increased, the cells with

longest axis perpendicular to the direction of the field became permeabilized. However, for an electric field higher than 500 V/cm the cells became permeabilized irrespective of their orientation with the respect to the electric field.

1.4.3 Physicochemical Factors

The composition of the electroporation buffer and ambient temperature play an important role in the efficiency of electroporation.

1.4.3.1 Electroporation Buffer

The electroporation buffer plays an important role in controlling the size of the pores.[48] Studies have shown that the uptake (or release) of molecules is dependent upon ionic composition, ionic strength, conductivity, and osmolality of the buffer.[49] However, there is still some debate on this issue. One study reported that the uptake (or release) increased with decreased buffer conductivity,[50] whereas the other reports have shown opposite results.[2, 51] Wang and Griffiths have shown an increase in transformation efficiency (50-fold) in *vibrio parahaemolyticus* strains when the electroporation was performed in Mg^{2+} free buffer.[52] The Mg^{2+} were replaced by sucrose to maintain the stability of the cell membrane. The buffer pH is also important, and the buffer composition and pH should mimic the cytoplasm of the cell. The usual intracellular pH is around 7.2. When applying high voltage with long duration, lower salt compositions are used to avoid excess Joule heating produced by the high voltage.

1.4.3.2 Temperature

Ambient temperature can influence the efficiency of electroporation. Although conflicting data on the temperature dependence in transfection has been reported, several studies have shown increased permeabilization and shortened resealing times at elevated temperatures.[53, 54] At 37 °C, membrane resealing has been shown to take less than 5 min. Rols et al. showed an increased transfection in Chinese hamster ovary cells when they incubated cells at 4 °C before pulsation, and then after pulsation, incubated cells at 37 °C.[55]

1.5 CELL VIABILITY

It is important to preserve cell viability following electroporation. Cell viability is retained in the case of reversible electroporation where the pores reseal with time, however cells die in irreversible electroporation where the pores do not reseal with time. Studies have shown that cell viability depends on electric field parameters such as field strength,[56, 57] pulse duration,[36] number of pulses delivered,[58, 59] and also on the medium of electroporation.[49] One of the most comprehensive studies of understanding the dependence of cell viability on experimental conditions was carried out by Canatella et al.[60] They used flow cytometry to study viability of prostate cancer DU 145 cells for more than 200 different combinations of experimental conditions. Their results showed that viability has a complex dependence on field strength, pulse length, and number of pulses. Gabriel and Teissie evaluated the role of electric field parameters in short-term and long-term death of Chinese hamster ovary cells following electropermeabilization.[56] Short-term cell death was evaluated in the minute range after electropulsation, and the long-term death was evaluated 24 hours after electropulsation. Their

results showed that the cell death (short-term and long-term) was linearly related to the fraction of the membrane area brought to the permeabilized state.

1.6 SINGLE-CELL ELECTROPORATION

1.6.1 Single-Cell Electroporation with Microelectrodes

Lundqvist et al. developed the first single-cell electroporation method by using carbon fiber microelectrodes to produce highly localized fields on single adherent cells in confluent cultures.[61] Two carbon fiber microelectrodes with outer diameter of 5 μm were positioned 2 to 5 μm from the boundaries of the cell at an at an angle of 0–20° and 160–180° with respect to the object plane. A single 1 ms rectangular low-voltage pulse (~2 V) was used to electroporate cells with high spatial resolution, giving a transfection yield and survival rate of 97 %. Furthermore, to characterize single-cell electroporation using microelectrodes, the above technique was combined with patch clamp technology.[62] A patch-clamp pipette was sealed on the cell at a 90° angle with respect to the microelectrodes. The transmembrane current responses were used to determine the critical transmembrane potential.

Despite high resolution and high transfection efficiency achieved with this technique, there are certain disadvantages of the microelectrode method. The voltage drop at the electrode/solution interface due to the electrode reaction and formation of the double layer needs to be taken into account. At long pulse durations and short cell-electrode distances, there is a possibility of cytotoxic products being produced at the electrode. Also, the cell loading agents need to be added to the buffer solution surrounding the cell or delivered specifically to the

targeted area by using a micropipette. To overcome these problems, new methods of single-cell electroporation have been developed.

1.6.2 Single-Cell Electroporation with Micropipettes and Capillaries

Single-cell electroporation with micropipettes and capillaries has certain advantages over the microelectrode system. The electrode reaction takes place far away from the electroporated cell which decreases the toxic product problem. Also, the cell loading agents can be delivered through the capillaries via electroosmotic and electrophoretic flow.

1.6.2.1 Micropipettes

In the micropipette method the electrode close to the cell is a solute-filled micropipette with a metal electrode inside. Another electrode couples with this micropipette electrode to carry current through the target cells. The small tip size of the micropipettes enables the insertion of compounds in selected regions of single cells.

Single-cell electroporation using micropipette technology was first demonstrated by Karlsson et al.[63] They combined electroporation and pressure-driven microinjection method to load biopolymers and colloidal particles into single-cell unilamellar liposomes. Single liposomes were positioned between a ~2 μm tip diameter solute-filled glass micropipet, equipped with a Pt electrode, and a 5 μm-diameter carbon fiber electrode. A transient, 1-10 ms, rectangular waveform dc voltage pulse (10-40 V/cm) was applied between the electrodes, thus focusing the electric field over the liposome. The induced dielectric membrane breakdown facilitated the penetration of micropipet tip into the liposome, thus injecting a small volume of the loading agent. This method was also applied to load single PC12 cells.

Haas et al. used micropipette technology to permeabilize single neurons and glia in the brain of intact *Xenopus* tadpoles and rat hippocampal slices to deliver DNA and other macromolecules.[64] Transfection was performed using a micropipette with a tip diameter of 0.6-1.0 μm. A silver wire (0.25 mm diameter) was placed inside the micropipette. Voltage pulses (10-80 V), with single and multiple pulses of 1-150 ms were delivered between the micropipette electrode and the silver wire ground electrode. Transfection efficiency was tested for a range of stimulation parameters such as amplitude, duration, and shape of pulse. They obtained highest transfection efficiency (30%) with 200 Hz trains of 1 ms square pulses at 50V.

Rae and Levis improved the transfection efficiency of single-cell electroporation with micropipettes by employing patch-clamp technology and more precise positioning of the micropipette and better visualization of the cells.[65] Cultured cell were indented by a micropipet with a pulled tip ~ 0.5 μm which led to an increase in resistance of 25% due to the indention. Rectangular pulses (2-10 V) from 20 μs to 300 ms durations were used. With optimal parameters, transfection efficiency of more than 80% was achieved. Moreover, small tips electroporated only a limited area and so did little cell damage. Rathenberg et al. also achieved high efficiency of 80 % by using two-photon microscopy for real-time visualization at the cellular level by electroporating single cells in neurons using fluorescently labeled oligonucleotides and plasmid DNA.[66] In their setup, micropipettes with a tip diameter of about 1-2 μm and with resistances of 10-20 MΩ were used. The most efficient electroporation pulse parameter was a single train of 200 square pulses with duration of 1 ms and a 4 ms delay with amplitude of 10 V.

1.6.2.2 Electrolyte-filled Capillary (EFC)

The main differences between the EFC and micropipette are that in case of EFC there is no electrode or filament fused into the wall of the capillary. EFCs are typically placed several microns away from the target cells. The main advantage of the capillaries is that the same EFC can be used for electroporation as well as cell analysis. However, some disadvantages of capillaries are that longer pulse durations and higher voltages are required because of the high resistance inside the EFC.

Single-cell electroporation using EFC was first demonstrated by Nolkrantz et al.[67, 68] A typical electroporation setup is shown in Figure 1.6. A 30 cm long capillary (30 µm inner diameter, 375 µm outer diameter tapered to an outer tip diameter of 50 µm) was placed at a ~5 µm distance from the cells. A large-voltage pulse (2-10 kV, duration 5 s) applied across the EFC was used to produce a small electric field outside the terminus of the EFC causing pore formation in cell membranes. The electroporation was used to deliver fluorogenic dyes into single NG108-15 cells and small populations of cells in organotypic hippocampal cultures in vitro and in vivo. The magnitude of the electric field along the axis of symmetry of the EFC lumen extending out into the solution was given by the following equation:

$$E(Z,\Psi) = \frac{\Psi}{L_c}\left[\frac{Z}{\left[1+(Z)^2\right]^{\frac{1}{2}}} - 1\right] \tag{1.10}$$

where Ψ is the applied potential in volts, L_c is the length of the EFC, Z is the dimensionless distance from the tip of the EFC, z/a, where z is distance from the EFC tip and a is the EFC lumen radius.

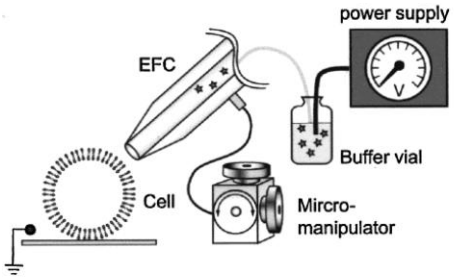

Figure 1.5. Single-cell electroporation using electrolyte-filled capillary.

(Reprinted from reference,[67] with permission from American Chemical Society).

In another set of experiments, Olofsson et al. used larger capillaries (0.4-1.0 mm inner diameter) but lower voltage and shorter duration (gap height 50-100 μm, 200-225 V pulses of 10-25 ms) for a computer-controlled scanning electroporation method.[69] The capillary was scanned over a cell culture to locally deliver both electric field and electroporation agent to the target area without affecting surrounding cells. The instantaneous size of the targeted area was determined by the dimensions of the capillary. Also, they used finite element method simulations to study the spatial distributions of the electric field, concentration of the electroporation agent at the capillary outlet, and fluid dynamics related to the flow of electroporation agent from the capillary.[70] This method was validated for transfection by introduction of a 9-base-pair-long randomized oligonucleotide into PC12, CHO and WSS cells.

1.6.3 Single-Cell Electroporation with Microfabricated Chips

Single-cell electroporation using microchips is growing rapidly as it has many merits: (1) integration with separation and detection and single-cell analysis thereof, (2) small sample amount, (3) high surface/volume ratio that decreases the heat effect, (4) facility to automate

single-cell electroporation with high efficiency and throughput, (5) selectively trap specific target cells. The disadvantages are time-consuming fabrication process and high-cost.

Huang and Rubinsky first developed the microelectroporation chip technology to study and control single-cell electroporation.[71] The chip consists of a three-layer device fabricated using the standard silicon microfabrication technology. The chips were glued together using a high dielectric strength adhesive. A micron-size hole connected the fluid chambers. In a typical experimental setup, cells were introduced into the upper chamber, a negative pressure difference was generated between the bottom and the top chamber to capture individual cell of interest. Once the cell was set in the hole, electric pulse was applied. The individual cells were uploaded with exogenous compounds, and released to be replaced by the next cell. Measurement of current flowing between the electrodes gave information about cell trapping and electroporation status as well as the breakdown voltage. Later they presented a new microchip that uses microfluidic structures that precisely handles cells in a flow through manner, and performs electroporation facilitated gene transfer in each cell consecutively.[72] Membrane impermeable nucleic acid stain YOYO-1 and enhanced green fluorescent protein (EGFP) were loaded into ND-1 cells with a 100% gene transfer rate under controller electroporation. In the experiments performed in flow-through channel micro-electroporation system using conventional DC electrical pulses, it was found that when using large volume of cells, DC pulses caused electrolysis of the solution carrying the cells, thereby resulting in gas bubbles being generated near the electrodes. The gas bubbles migrated towards the micro-channel and causing electrical disconnection in the system. In order to overcome the electrolysis problem, Ziv et al. successfully performed micro-electroporation on mesenchymal stem cells using AC electrical pulses.[73] The effect of AC micro-electroporation on electrolysis was found to be dependent on the AC frequency used.

Khine et al. developed a polydimethylsiloxane (PDMS) microfluidic device to trap individual cells laterally and locally electroporated them in parallel.[74, 75] The advantage of this chip is that it can manipulate an array of cells such that a plurality of cells can be electroporated. Also, it is an easy-to-use chip, which uses low voltages for electroporation (~0.76 V), and has the electrodes placed at a distance from the cell therefore eliminating the potential of adverse products from electrode reactions. Ag/AgCl electrodes and patch clamp amplifier were used to monitor accurate current traces.

Wang and Lu have developed a microfluidic method with high throughput for real-time studies of single-cell electroporation.[76, 77] A continuous DC voltage instead of electrical pulses was applied to produce the electroporation field in the microfluidic channel. The microfluidic channel was geometrically modified in a way that localized high field was created only in the defined section and only this high field section induced electroporation. The exposure time of the cells to this high field was determined by the velocity of the cells and the length of the section. Chinese hamster ovary cells were electroporated reversibly and irreversibly using this technique and the correlation between the swelling rate and cell size for various buffer osmolarities was studied. In a recent study, Wang and Lu used the microfluidics-based electroporation technique to deliver small molecules and genes into Chinese hamster ovary cells.[78]

He et al. developed a new micro pulsed radio-frequency electroporation (μPREP) chip which was fabricated using micro electro-mechanical system (MEMS) technology.[79] A big advantage of this technique is that extensive statistical data can be quickly obtained as large number of cells can be electroporated at different pulse conditions at the same time. They studied the variations of fluorescent intensity and cell viability as functions of the electric pulse amplitude and duration during the electroporation process at the single-cell level. The results of

the parametric study were presented in the “phase diagram”, from which the critical electric field for inducing single-cell electroporation under different conditions could be clearly determined. MEMS-based micro electroporation chip can greatly shorten the experimental time.

1.7 OUTLINE

Single-cell electroporation is not as well developed as bulk electroporation. In single-cell electroporation electric field is focused on one single cell at a time which enables selective permeabilization of the targeted cell without affecting its neighbors. Electroporation of a single cell with a locally applied electric field should not be confused with bulk electroporation of cells cultured on substrates and looked at individually. In the latter case of bulk electroporation, where the cells are exposed to uniform or homogeneous electric fields, the potential drop across the cell membrane is well described by the Schwan equation. According to the Schwan equation, the potential drop across the membrane depends on the magnitude of the homogeneous electric field, the cell size, and the polar angle on the cell surface. In single-cell electroporation on the other hand where a highly focused or an inhomogeneous field is applied to one single cell at a time, there is no model analogous to the Schwan equation, and therefore analytical solutions for calculation of the transmembrane potential for single-cell electroporation experiments are generally not possible. In our lab, we performed single-cell electroporation on fluorescently labeled lung carcinoma A549 cells using electrolyte-filled capillaries. Single, adherent A549 cells were exposed to short electric field pulses (500 V across 15 cm capillary) created at the tip of an electrolyte-filled capillary. We sought to determine experimentally and through numerical

simulations, how experimental and cell parameters influence cell permeabilization and cell viability in single-cell electroporation experiments.

1.8 REFERENCES

(1) Kinosita, K., Jr.; Tsong, T. Y. Voltage-induced pore formation and hemolysis of human erythrocytes. *Biochim et Biophys Acta*. **1977**, *471*, 227-242.

(2) Kinosita, K., Jr.; Tsong, T. Y. Hemolysis of human erythrocytes by a transient electric field. *Proc Natl Acad Sci U S A.* **1977**, *74*, 1923-1927.

(3) Benz, R.; Zimmermann, U. The resealing process of lipid bilayers after reversible electrical breakdown. *Biochim et Biophys Acta*. **1981**, *640*, 169-178.

(4) Neumann, E.; Schaefer-Ridder, M.; Wang, Y.; Hofschneider, P. H. Gene transfer into mouse lyoma cells by electroporation in high electric fields. *EMBO J.* **1982**, *1*, 841-845.

(5) Pliquett, U.; Weaver, J. C. Electroporation of human skin: simultaneous measurement of changes in the transport of two fluorescent molecules and in the passive electrical properties. *Bioelectrochem Bioenerg.* **1996**, *39*, 1-12.

(6) Weaver, J. C.; Chizmadzhev, Y. A. Theory of electroporation: A review. *Bioelectrochem Bioenerg.* **1996**, *41*, 135-160.

(7) Kotnik, T.; Bobanovic, F.; Miklavcic, D. Sensitivity of transmembrane voltage induced by applied electric fields-a theoretical analysis. *Bioelectrochem Bioenerg.* **1997**, *43*, 285-291.

(8) Zimmermann, U.; Riemann, F.; Pilwat, G. Enzyme loading of electrically homogeneous human red blood cell ghosts prepared by dielectric breakdown. *Biochim et Biophys Acta*. **1976**, *436*, 460-474.

(9) Neumann, E. Membrane electroporation and direct gene transfer. *Bioelectrochem Bioenerg.* **1992**, *28*, 247-267.

(10) Escoffre, J.-M.; Portet, T.; Wasungu, L.; Teissie, J.; Dean, D.; Rols, M.-P. What is (Still not) known of the mechanism by which electroporation mediates gene transfer and expression in cells and tissues. *Mol Biotechnol*. **2009**, *41*, 286-295.

(11) Faurie, C.; Golzio, M.; Phez, E.; Teissie, J.; Rols, M. P. Electric field-induced cell membrane permeabilization and gene transfer: Theory and experiments. *Eng Life Sci*. **2005**, *5*, 179-186.

(12) Xie, T. D.; Tsong, T. Y. Study of mechanisms of electric field-induced DNA transfection. II. Transfection by low-amplitude, low-frequency alternating electric fields. *Biophys J*. **1990**, *58*, 897-903.

(13) Xie, T. D.; Sun, L.; Tsong, T. Y. Study of mechanisms of electric field-induced DNA transfection. I. DNA entry by surface binding and diffusion through membrane pores. *Biophys J*. **1990**, *58*, 13-19.

(14) Cemazar, M.; Golzio, M.; Sersa, G.; Hojman, P.; S, K.; Mesojednik, S.; Rols, M.-P.; Teissie, J. Control by pulse parameters of DNA electrotransfer into solid tumors in mice. *Gene Ther*. **2009**, 1-10.

(15) Mir, L. M.; Orlowski, S.; Belehradek, J., Jr. ; Paoletti, C. Electrochemotherapy potentiation of antitumour effect of bleomycin by local electric pulses. *Eur J Cancer (Oxford, England : 1990)*. **1991**, *27*, 68-72.

(16) Miklavcic, D.; Cemazar, M.; Rudolf, Z.; Pucihar, G.; Snoj, M. Electrochemotherapy in treatment of tumours. *EJSO*. **2008**, *34*, 232-240.

(17) Prausnitz, M. R.; Lau, B. S.; Milano, C. D.; Conner, S.; Langer, R.; Weaver, J. C. A quantitative study of electroporation showing a plateau in net molecular transport. *Biophys J*. **1993**, *65*, 414-422.

(18) Prausnitz, M. R.; Bose, V. G.; Langer, R.; Weaver, J. C. Electroporation of mammalian skin: a mechanism to enhance transdermal drug delivery. *Proc Natl Acad Sci U S A.* **1993**, *90*, 10504-10508.

(19) Wong, T. W.; Ko, S. F.; Hui, S. W. Enhancing transdermal drug delivery with electroporation. *Recent Patents on Drug Delivery & Formulation* **2008**, *2*, 51-57.

(20) Bliss, J. G.; Harrison, G. I.; Mourant, J. R.; Powell, K. T.; Weaver, J. C. Electroporation: the population distribution of macromolecular uptake and shape changes in red blood cells following a single 50 ms square wave pulse. *Bioelectrochem Bioenerg.* **1988**, *20*, 57-71.

(21) Teissie, J.; Eynard, N.; Vernhes, M. C.; Benichou, A.; Ganeva, V.; Galutzov, B.; Cabanes, P. A. Recent biotechnological developments of electropulsation. A prospective review. *Bioelectrochemistry (Amsterdam, Netherlands)*. **2002**, *55*, 107-112.

(22) Gehl, J. Electroporation: Theory and methods, perspectives for drug delivery, gene therapy and research. *Acta Physiol Scand.* **2003**, *177*, 437-447.

(23) Olson, K. J.; Ahmadzadeh, H.; Arriaga, E. A. Within the cell: analytical techniques for subcellular analysis. *Anal Bioanal Chem.* **2005**, *382*, 906-917.

(24) Lu, X.; Huang, W.-H.; Wang, Z.-L.; Cheng, J.-K. Recent developments in single-cell analysis. *Anal Chim Acta*. **2004**, *510*, 127-138.

(25) Brady, G. Expression profiling of single mammalian cells - small is beautiful. *Yeast*. **2000**, *17*, 211-217.

(26) Teissie, J.; Golzio, M.; Rols, M. P. Mechanisms of cell membrane electropermeabilization: A minireview of our present (lack of ?) knowledge. *Biochim et Biophys Acta*. **2005**, *1724*, 270-280.

(27) Gross, D.; Loew, L. M.; Webb, W. W. Optical Imaging of cell membrane potential changes induced by applied electric fields. *Biophys J.* **1986**, *50*, 339-348.

(28) Weaver, J. C.; Mintzer, R. A. Decreased bilayer stability due to transmembrane potentials. *Phys Lett. A.* **1981**, *86A*, 57-59.

(29) Sugar, I. P.; Neumann, E. Stochastic model for electric field-induced membrane pores. Electroporation. *Biophys Chem.* **1984**, *19*, 211-225.

(30) Glaser, R. W.; Leikin, S. L.; Chernomordik, L. V.; Pastushenko, V. F.; Sorkiko, A. I. Reversible electrical breakdown of lipid bilayers: formation and evolution of pores. *Biochim et Biophys Acta*. **1998**, *940*, 275-287.

(31) DeBruin, K. A.; Krassowska, W. Modeling electroporation in a single cell. I. Effects of field strength and rest potential. *Biophys J.* **1999**, *77*, 1213-1224.

(32) Pastushenko, V. F.; Chizmadzhev, Y. A.; Arakelyan, V. B. Electric breakdown of bilayer lipid membranes. II. Calculation of the membrane lifetime in the steady-state diffusion approximation. . *Bioelectrochem Bioenerg.* **1979**, *6*, 53-62.

(33) Smith, K. C.; Neu, J. C.; Krassowska, W. Model of creation and evolution of stable electropores for DNA delivery. *Biophys J.* **2004**, *86*, 2813-2826.

(34) Krassowska, W.; Filev, P. D. Modeling electroporation in a single cell. *Biophys J.* **2007**, *92*, 404-417.

(35) Rols, M. P.; Teissie, J. Electropermeabilization of mammalian cells: quantitative analysis of the phenomenon. *Biophys J.* **1990**, *58*, 1089-1098.

(36) Rols, M.-P.; Teissie, J. Electropermeabilization of mammalian cells to macromolecules: control by pulse duration. *Biophys J.* **1998**, *75*, 1415-1423.

(37) Pucihar, G.; Kotnik, T.; Miklavcic, D.; Teissie, J. Kinetics of Transmembrane Transport of Small Molecules into Electropermeabilized Cells. *Biophys J.* **2008**, *95*, 2837-2848.

(38) Wolf, H.; Rols, M. P.; Boldt, E.; Neumann, E.; Teissie, J. Control by pulse parameters of electric fieldmediated gene transfer in mammalian cells. *Biophys J.* **1994**, *66*, 524-531.

(39) Zahroff, D. A.; Henshaw, J. W.; Mossop, B.; Yuan, F. Mechanistic Analysis of Electroporation-Induced Cellular Uptake of Macromolecules. *Exp Biol Med*. **2008**, *233*, 94-105.

(40) Tekle, E.; Astumian, R. D.; Chock , P. B. Electroporation by using bipolar oscillating electric field: An improved method for DNA transfection of NIH 3T3 cells. *Proc Natl Acad Sci U S A.* **1991**, *88*, 4230-4234.

(41) Schoenbach, K. H.; Peterkin, F. E.; Alden, R. W.; Beebe, S. J. The effects of pulsed electric fields on biological cells: experiments and applications. *IEEE Trans Plasma Sci*. **1997**, *25*, 284-292.

(42) Kotnik, T.; Mir, L. M.; Flisar, K.; Puc, M.; Miklavcic, D. Cell membrane electropermeabilization by symmetrical bipolar rectangular pulses. Part I. Increased efficiency of permeabilization. *Bioelectrochemistry (Amsterdam, Netherlands)*. **2001**, *54*, 83-90.

(43) Grosse, C.; Schwan, H. P. Cellular membrane potentials induced by alternating fields. *Biophys J.* **1992**, *63*, 1632-1642.

(44) Kotnik, T.; Miklavcic, D. Analytical description of transmembrane voltage induced by electric fields on spheroidal cells. *Biophys J.* **2000**, *79*, 670-679.

(45) Valic, B.; Golzio, M.; Pavlin, M.; Schatz, A.; Faurie, C.; Gabriel, B.; Teissie, J.; Rols, M.-P.; Miklavcic, D. Effect of electric field induced transmembrane potential on spheroidal cells: theory and experiment. *Eur Biophys J*. **2003**, *32*, 519-528.

(46) Gimsa, J.; Wachner, D. Analytical description of the transmembrane voltage induced on arbitrarily oriented ellipsoidal and cylindrical cells. *Biophys. J.* **2001**, *81*.

(47) Maswiwat, K.; Wachner, D.; Gimsa, J. Effects of cell orientation and electric field frequency on the transmembrane potential induced in ellipsoidal cells *Bioelectrochemistry*. **2008**, *74*, 130-141.

(48) Pucihar, G.; Kotnik, T.; Kanduser, M.; Miklavcic, D. The influence of medium conductivity on electropermeabilization and survival of cells in vitro. *Bioelectrochemistry*. **2001**, *54*, 107-115.

(49) Djuzenova, C. S.; Zimmermann, U.; Frank, H.; Sukhorukov, V. L.; Richter, E.; Fuhr, G. Effect of medium conductivity and composition on the uptake of propidium iodide into electropermeabilized myeloma cells. *Biochim et Biophys Acta*. **1996**, *1284*, 143-152.

(50) Rols, M.-P.; Teissie, J. Ionic-strength modulation of electrically induced permeabilization and associated fusion of mammalian cells. *Eur J Biochem.* **1989**, *179*, 109-115.

(51) Kinosita, K., Jr.; Tsong, T. Y. Formation and resealing of pores of controlled sizes in human erythrocyte membrane. *Nature*. **1977**, *268*, 438-441.

(52) Wang, H.; Griffiths, M. W. Mg2+-free buffer elevates transformation efficiency of Vibrio parahaemolyticus by electroporation. *Lett Appl Microbiol.* **2009**, *48*, 349-354.

(53) Wards, B. J.; Collins, D. M. Electroporation at elevated temperatures substantially improves transformation efficiency of slow-growing mycobacteria. *FEMS Microbiol Lett.* **1996**, *145*, 101-105.

(54) Gallo, S. A. Temperature-dependent electrical and ultrastructural characterizations of porcine skin upon electroporation. . *Biophys J.* **2002**, *82*, 109-119.

(55) Rols, M. P.; Delteil, C.; Serin, G.; Teissie, J. Temperature effects on electrotransfection of mammalian cells. *Nucleic Acids Res.* **1994**, *22*, 540.

(56) Gabriel, B.; Teissie, J. Control by electrical parameters of short- and long-term cell death resulting from electropermeabilization of Chinese hamster ovary cells. *Biochim et Biophys Acta*. **1995**, *1266*, 171-178.

(57) Loste, F.; Eynard, N.; Teissie, J. Direct monitoring of the field strength during electropulsation. *Bioelectrochem Bioenerg.* **1998**, *47*, 119-127.

(58) Pucihar, G.; Mir, L. M.; Miklavcic, D. The effect of pulse repetition frequency on uptake into electropermeabilized cells in vitro with possible applications in electrochemotherapy. *Bioelectrochemistry*. **2002**, *57*, 167-172.

(59) Brown, R. E.; Bartoletti, D. C.; Harrison, G. I.; Gamble, T. R.; Bliss, J. G.; Powell, K. T.; Weaver, J. C. Multiple-pulse electroporation: uptake of a macromolecule by individual cells of Saccharomyces cerevisiae. *Bioelectrochem Bioenerg.* **1992**, *28*, 235-245.

(60) Canatella, P. J.; Karr, J. F.; Petros, J. A.; Prausnitz, M. R. Quantitative study of electroporation-mediated molecular uptake and cell viability. *Biophys J.* **2001**, *80*, 755-764.

(61) Lundqvist, J.; Anders. Sahlin, F.; Aberg, M. A. I.; Stromberg, A.; Eriksson, P. S.; Orwar, O. Altering the biochemical state of individual cultured cells and organelles with ultramicroelectrodes. *Proc Natl Acad Sci U S A.* **1998**, *95*, 10356-10360.

(62) Ryttsen, F.; Farre, C.; Brennan, C.; Weber, S. G.; Nolkrantz, K.; Jardemark, K.; Chiu, D. T.; Orwar, O. Characterization of single-cell electroporation by using patch-clamp and fluorescence microscopy. *Biophys J.* **2000**, *79*, 1993-2001.

(63) Karlsson, M.; Nolkrantz, K.; Davidson, M. J.; Stroemberg, A.; Ryttsen, F.; Kerman, B.; Orwar, O. Electroinjection of colloid particles and biopolymers into single unilamellar liposomes and cells for bioanalytical applications. *Anal Chem.* **2000**, *72*, 5857-5862.

(64) Haas, K.; Sin, W.-C.; Javaherian, A.; Li, Z.; Cline, H. T. Single-cell electroporation for gene transfer in vivo. *Neuron*. **2001**, *29*, 583-591.

(65) Rae, J. L.; Levis, R. A. Single-cell electroporation. *Pfluegers Arch.* **2002**, *443*, 664-670.

(66) Rathenberg, J.; Nevian, T.; Witzemann, V. High-efficiency transfection of individual neurons using modified electrophysiology techniques. *J Neurosci Meth.* **2003**, *126*, 91-98.

(67) Nolkrantz, K.; Farre, C.; Brederlau, A.; Karlsson, R. I. D.; Brennan, C.; Eriksson, P. S.; Weber, S. G.; Sandberg, M.; Orwar, O. Electroporation of single cells and tissues with an electrolyte-filled capillary. *Anal Chem.* **2001**, *73*, 4469-4477.

(68) Nolkrantz, K.; Farre, C.; Hurtig, K. J.; Rylander, P.; Orwar, O. Functional screening of intracellular proteins in single cells and in patterned cell arrays using electroporation. *Anal Chem.* **2002**, *74*, 4300-4305.

(69) Olofsson, J.; Levin, M.; Stromberg, A.; Weber, S. G.; Ryetesen, F.; Orwar, O. Scanning electroporation of selected areas of adherent cell cultures. *Anal Chem.* **2007**, *79*, 4410-4418.

(70) Olofsson, J.; Levin, M.; Stromberg, A.; Weber, S. G.; Ryetesen, F.; Orwar, O. Generation of focused electric field patterns at dielectric surfaces. *Anal Chem.* **2005**, *77*, 4667-4672.

(71) Huang, Y.; Rubinsky, B. Microfabricated electroporation chip for single cell membrane permeabilization. *Sensor Actuat A-Phys.* **2001**, *A89*, 242-249.

(72) Huang, Y.; Rubinsky, B. Flow-through micro-electroporation chip for high efficiency single-cell genetic manipulation. *Sensor Actuat A-Phys.* **2003**, *A104*, 205-212.

(73) Ziv, R.; Steinhardt, Y.; Pelled, G.; Gazit, D.; Rubinsky, B. Micro-electroporation of mesenchymal stem cells with alternating electrical current pulses. *Biomed Microdevices*. **2009**, *11*, 95-101.

(74) Khine, M.; Lau, A.; Ionescu-Zanetti, C.; Seo, J.; Lee, L. P. A single cell electroporation chip. *Lab Chip.* **2005**, *5*, 38-43.

(75) Khine, M.; Ionescu-Zanetti, C.; Blatz, A.; Wang, L.; Lee, L. P. Single-cell electroporation arrays with real-time monitoring and feedback control. *Lab Chip.* **2007**, *7*, 457-462.

(76) Wang, H. Y.; Lu, C. Electroporation of Mammalian Cells in a Microfluidic Channel with Geometric Variation. *Anal Chem.* **2006**, *78*, 5158-5164.

(77) Wang, H. Y.; Lu, C. High-throughput and real-time study of single cell electroporation using microfluidics: effects of medium osmolarity. *Bioelectrochem Bioenerg.* **2006**, *95*, 1116-1125.

(78) Lu, C.; Wang, H.-Y. Microfluidic Electroporation for Delivery of Small Molecules and Genes Into Cells Using a Common DC Power Supply. *Biotechnol Bioeng.* **2008**, *100*, 579-586.

(79) He, H.; Chang, D. C.; Lee, Y.-K. Micro pulsed radio-frequency electroporation chips. *Bioelectrochemistry*. **2006**, *68*, 89-97.

2.0 SIMULTANEOUS MAXIMIZATION OF CELL PERMEABILIZATION AND VIABILITY IN SINGLE-CELL ELECTROPORATION USING AN ELECTROLYTE-FILLED CAPILLARY

This work has been published in *Analytical Chemistry*, **2007**, *79*, 161-167.

2.1 ABSTRACT

A549 cells were briefly exposed to Thioglo -1 which converts thiols to fluorescent adducts. The fluorescent cells were exposed to short (50 - 300 ms) electric field pulses (500 V across a 15 cm capillary) created at the tip of an electrolyte - filled capillary. Fluorescence microscopy revealed varying degrees of cell permeabilization depending on conditions. Longer pulses and shorter cell - capillary tip distance led to a greater decrease in a cell's fluorescence. Live/dead (calcein AM and propidium iodide) testing revealed that a certain fraction of cells died. Longer pulses and shorter cell – capillary tip distances were more deadly. An optimum condition exists at a cell – capillary tip distance of 3.5 μm – 4.5 μm and a pulse duration of 120 ms - 150 ms. At these conditions > 90 % of the cells are permeabilized and 80 – 90% survive.

2.2 INTRODUCTION

Electroporation uses electric field pulses to temporarily permeabilize the cell membrane.[1-3] When the membrane potential reaches a critical value which is around 0.2 - 1.5 V^4 dielectric membrane breakdown occurs resulting in the formation of transient pores.[5-7] Electroporation is most frequently used to introduce charged, polar molecules such as DNA, dyes, drugs or proteins into the interior of the cell. This technique is now used in many fields such as in cellular biology and biotechnology for gene transfer,[8-11] and in medical applications for gene therapy,[12, 13] cancer chemotherapy,[14] and transdermal drug delivery.[15, 16]

Traditionally, electroporation has been done in batch or bulk mode on cells in suspension.[4, 6, 17-22] In the bulk mode, a whole population of cells is subjected to homogeneous fields of a few kilovolts per centimeter which results in permeabilization of numerous cells at the same time. Data collected from such bulk electroporation gives a statistical distribution of cellular states.[23] In other areas of research, single cell analysis is now gaining considerable significance as it allows an understanding of complex cellular heterogeneity within a population of cells. Data collected from single cells generates unique information about cell - to - cell variations and avoids information loss due to averaging across the population of cells.[24-27]

Lundqvist et al. (1998) developed the first single cell electroporation method by using carbon fiber microelectrodes[28] to produce highly localized fields on single adherent cells in confluent cultures. Since then, other single cell electroporation techniques have been developed such as electrolyte-filled capillaries[29] and micropipettes,[30] and microfabricated chip systems.[31-34] These techniques require either an isolation of a cell or a fine focus of the electric field to target a particular cell.[35] A few other high resolution techniques such as optoporation,[36, 37] micro-

electroinjection,[38] and microinjection[39] exist to control and manipulate the biochemical machinery of single cells.

The efficiency of electroporation for a given molecule depends on controlling and optimizing the parameters that lead to cell permeabilization. For example, electric field parameters such as pulse amplitude, pulse duration, number of delivered pulses, and conditions such as temperature, osmotic pressure, and the presence of co-factors such as facilitators of nuclear transfer, edge-actants and cellular characteristics all play a part in electroporation.[40-45] With proper values of electric field parameters, electroporation can be made reversible so that the cells can return to their normal physiological state following permeabilization. However, if these experimental conditions exceed certain values, *e.g.*, amplitude of pulses is too high or pulse duration is too long, cells can be irreversibly electroporated which leads to cell death.[46]

Ultimately, the influence of the electrical parameters is on the transmembrane potential. The transmembrane potential is easily predicted for spherical cells in the homogeneous electric field of bulk electroporation.[4, 47] Electrolyte filled capillaries produce highly focused and inhomogeneous electric fields. The shape of the electric field in solution depends on the geometry. Olofsson et al. has developed a method to create highly focused electric field gradients in the washer-shaped layer of solution existing between the wall of a capillary's butt end and the surface of the cell-containing dish.[48] By using finite element method simulations, they demonstrated that the field and its distribution could be controlled by varying the inner and outer diameters of the capillary, the height between the capillary end and the surface, or the applied current density. For the pulled capillaries used in this work, in which the capillary-substrate distance is greater than the lumen opening, and in which the tip is cone-like, the same sort of distribution does not exist. Rather, the field decays away from the tip with a characteristic

distance related to the diameter of the lumen.[29] In this technique, therefore, the cell – tip distance is a simple way to control the field at the membrane. The electrolyte-filled capillary is fairly resistive, thus the electrical response time is not as short as in bulk electroporation, so another important parameter, pulse length, needs to be longer than is normally used in bulk electroporation. Therefore, the range of useful pulse lengths is somewhat different than the range used in bulk electroporation. For these reasons, we have explored the influence of pulse length and tip – cell distance on electroporation and cell death.

In this study, we developed an assay based on diffusion of fluorescently labeled thiol adducts from preloaded cells through pores induced by transient electric fields. The diffusion of these fluorescently labeled thiol adducts was monitored in real time. In contrast to assays that rely on internalization of dyes, the escape of dyes allows for direct quantification of translocated species by fluorescence microscopy. Direct observation has many advantages, only some of which are realized in this report, namely: observation of mass transport dynamics both inside and outside the cell, immediate feedback to the experimenter on success/failure, it is less demanding than using, e.g., transfection in that there is no need to keep track of where individual cells are on a plate (though assay of live/dead requires this). Furthermore, watching the effect of electroporation in real time does not preclude transfection being done at the same time. Single-cell electroporation was performed using small-sized electrolyte-filled capillaries. Due to the small size of these electrolyte-filled capillaries, high spatial resolution could be achieved with this technique. Furthermore, variability in electroporation led to cell death to some extent in almost all experimental conditions. However, in spite of variability, there are optimal conditions that lead to cell permeabilization and cell survivability.

2.3 EXPERIMENTAL SECTION

Materials. The chemicals used for buffer preparations were all analytical grade and were purchased from Sigma (St. Louis, MO). Thioglo-1 was purchased from Covalent Associates (Woburn, MA). Propidium iodide and calcein AM were purchased from Invitogen/Molecular probes (Eugene, OR). A549 cell lines were obtained from American Type Culture Association (Manassas, VA). Basal medium Eagle (BME), Trypsin-EDTA, fetal bovine serum (FBS), L-glutamine and penicillin were all obtained from Gibco-BRL (Carlsbad, CA). Milli-Q (Millipore Synthesis A 10, Billerica, MA) water was used. Intracellular buffer consisted of NaCl, 5 mM; KCl, 140 mM; $MgCl_2$, 1.5 mM; D-glucose, 10 mM; HEPES, 20 mM; pH adjusted to 7.4.

Cell culture. Basal medium Eagle, supplemented with 10 % fetal bovine serum, and 1 % antibiotic was used to culture human lung cancer A549 cells. Cells were grown in 75 ml cell culture flasks in a CO_2 cell culture incubator (HERA cell incubator, Newtown, CT) at 37° C and 5 % CO_2 to about 80 % confluency. Before the experiments, cells were plated on 35 mm glass bottom cell-culture dishes (MatTek Corporation, Ashland, MA) and were grown for 1-3 days. Experiments were performed on the 2^{nd} and 3^{rd} day following the cell plating.

Cell staining. Prior to the experiments, the cells were stained with the dye Thioglo-1 (2 µM in intracellular buffer) for 30 seconds at room temperature. Thioglo-1 is a cell permeable maleimide-based reagent which gives a highly fluorescent product upon its reaction with active –SH groups in proteins, enzymes, and small peptides.[49, 50] To remove excess uncaptured dye, the cells were washed in intracellular buffer. Cells were bathed in the buffer and mounted on the cell chamber (DH 35i culture dish incubator, Warner Instruments, Holliston, MA) and transferred to the stage of the microscope.

Probe preparation. To perform electroporation experiments, fused-silica capillaries from Polymicro Technology (Phoenix, AZ) were used as a probe. The dimensions of the fused-silica capillary were: outer diameter (o.d.): 367 µm, inner diameter (i.d.): 100 µm. Capillaries were pulled at one end by using a CO_2 laser puller (Sutter Instruments Co. P-2000, Novato, CA). Before pulling the capillaries, 40 cm long capillaries were flushed with filtered Milli-Q water followed by burning of a 2 cm center section of the capillary to remove the protective coating. These capillaries were pulled using a one line program i.e., Heat: 260; Filament: 0; Velocity: 30; Delay: 128; Pull: 0. This one line program created reproducible capillaries with a short pulled tip with an inner diameter of 5 µm. The final length of the capillaries was 15 cm. Before experiments, capillaries were filled with the intracellular buffer.

Electroporation Setup. Single cell electroporation was performed using the electrolyte filled fused-silica capillaries. The experimental setup is depicted in Figure 2.1.

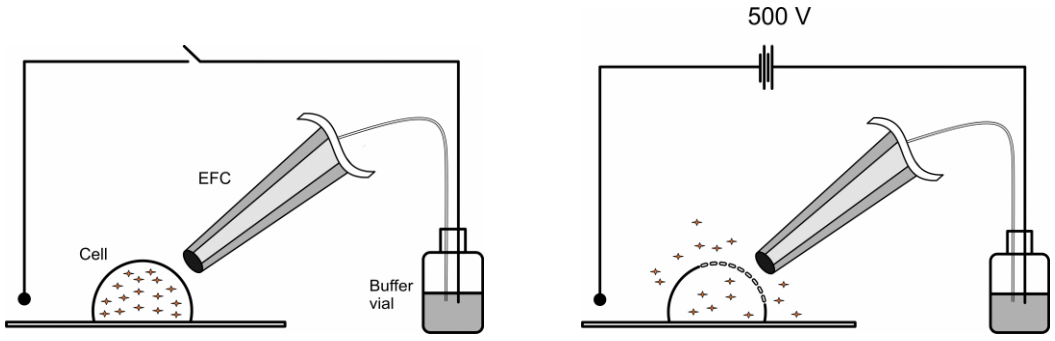

Figure 2.1. Schematic picture of the experimental setup.

A high-graduation micromanipulator (Narishige, NMN-21, Tokyo, Japan) was used to position the capillary close to the cell. The capillary was first positioned at about a 45° angle with respect to the cell dish normal a few micrometers above the surface (h=5 µm) A single fluorescent cell was brought into focus by observing the cells under the microscope. The capillary tip was placed at a desired distance from the cell. The observed distance between the capillary tip and the cell (d_m) was the projection of the capillary image in the horizontal imaging

plane (cell dish surface). These distances (d_m) were 2.0 µm, 3.5 µm, 5.0 µm, 7.0 µm, and 10.0 µm. The actual tip-cell distances are somewhat longer. The other end of the capillary was placed in a vial filled with intracellular buffer. The height of the vial was adjusted to avoid siphoning of the solution. A platinum electrode placed in this vial was connected to the electroporator (ECM 830, BTX Instruments, San Diego, CA) and the electrical circuit was completed with a grounded platinum electrode placed in the cell dish.

Fluorescence Imaging. Cells were observed through a 40X 1.3 NA oil immersion objective using an inverted microscope (Olympus, IX 71, Melville, NY) equipped with an HBO 100-W mercury lamp as the excitation source. For Thioglo-1, an Omega fluorescence cube (especially built, Omega, Brattleboro, VT) was used with filters for excitation at 378 nm and emission at 480 nm. For live/dead imaging, a triple band 'Pinkel' filter set from Semrock (Rochester, NY) was used (exciter 1 387 nm, exciter 2 494 nm; exciter 3 575 nm; dichroic mirror: 394– 414 nm, 484 – 504 nm, 566 – 586 nm, emitter: 457, 530, 628 nm). A CCD camera (Hamamatsu, ORCA-285, Bridgewater, NJ) imaged cells. The image collection frequency was 1 frame/s. Image processing was performed by the image acquisition software Simple PCI (Compix, Inc., Sewickley, PA). All the data were corrected for bleaching by extrapolating the first 25 points (time before pulse was applied) for each cell into a straight line and adding to the data, at each time point, the difference between the baseline of the cell and the extrapolated line.

Electroporation. Cells were exposed to single pulses of 500 V of various pulse durations ranging from 50 ms-300 ms. This will be referred as 'pulsing' of the cells. The pulse shape was monitored by differentially connecting a high voltage differential probe (Tektronix, P-5205, Richardson, TX) and a 2 channel digital oscilloscope (Tektronix, P-3052, Richardson, TX) to the output of the power supply. For all these pulsing conditions the distance between the tip of the

capillary and the cell varied from 2.0 µm-10 µm. The pulse was applied at 25.0 seconds from the start of the acquisition. Diffusive loss of fluorescent thiol adducts from the cell interior was determined quantitatively with Simple PCI software (Compix). The smallest distinguishable intensity change was about 4% of the signal. This was chosen as a threshold value for determination of electroporation success. For a cell to be considered permeabilized it had to loose 4% or more of its fluorescence intensity within 90 s of electroporation.

Cell Viability Assay. Following electroporation experiments, the buffer in the cell dish was replaced by 2 mL of fresh growth medium. The cells were allowed 5-6 hours of recovery in the 37° C incubator with 5% CO_2. Following the recovery period, the growth medium was replaced by 2 µM calcein AM and 2 µM propidium iodide. The cells were incubated for 30 min at 37° C and washed in intracellular buffer. Fluorescence microscopy was used for cell imaging. Cell survival percentage was calculated for each experimental condition based on this live/dead assay. It is important to note that a measurement of cell viability was made on each cell that was electroporated.

2.4 RESULTS

Visualization of electroporation. Table 2.1 summarizes the total number of cells tested in different cell dishes at each condition of pulse duration and cell-capillary tip distance. Figure 2.2A is an overlay of fluorescence and differential interference contrast image. The scale bar shows that the capillary is positioned at a distance d_m=5 µm from the cell. This cell was pulsed for 200 ms. A sequence of fluorescence micrographs obtained before and after the application of the pulse can be seen in Figure 2.2B. The images demonstrate that the cell becomes darker with

time due to the release of fluorescent thiol adducts from the cell interior to the surrounding medium through the nano-scale pores[4] formed upon electroporation. Figure 2.2D illustrates analysis of the change in average fluorescence intensity with time for the region selected inside the cell (Figure 2.2C, region 1). The analysis shows that application of the pulse results in a decrease in fluorescence intensity inside the cell.

Figure 2.2E is a plot of change with time of the average fluorescence intensity for the five regions outside the cell (Figure 2.2C, regions 2 to 6). The plot demonstrates that at the time of application of the pulse, region 2, which is closest to the cell, shows a sharp increase in fluorescence intensity followed by a gradual decrease. Regions 3 to 6 show a delay in the change of the fluorescence intensity, the delay increasing with the distance from the cell. Furthermore, peak of the fluorescence intensity decreases as the distance from the cell increases. These results are consistent with the previous graphs that fluorescent thiol adducts are being released upon permeabilization of the cell membrane and rapidly diffusing away from the cell into the surrounding medium.

Table 2.1. Total number of cells electroporated in each condition of pulse duration and cell-capillary tip distance. [a] *n* refers to the total number of cells electroporated in *m* separate experiments.

	Distance between cell and the capillary tip (μm)				
Pulse Duration (ms)	2.0	3.5	5.0	7.0	10.0
50	n=18 m=3	n=15 m=2	n=15 m=2	n=15 m=3	n=15 m=2
100	n=23 m=3	n=20 m=2	n=36 m=4	n=15 m=2	n=15 m=2
200	n=18 m=2	n=15 m=2	n=20 m=2	n=15 m=2	n=15 m=2
300	n=15 m=2	n=16 m=2	n=22 m=3	n=15 m=2	n=15 m=2

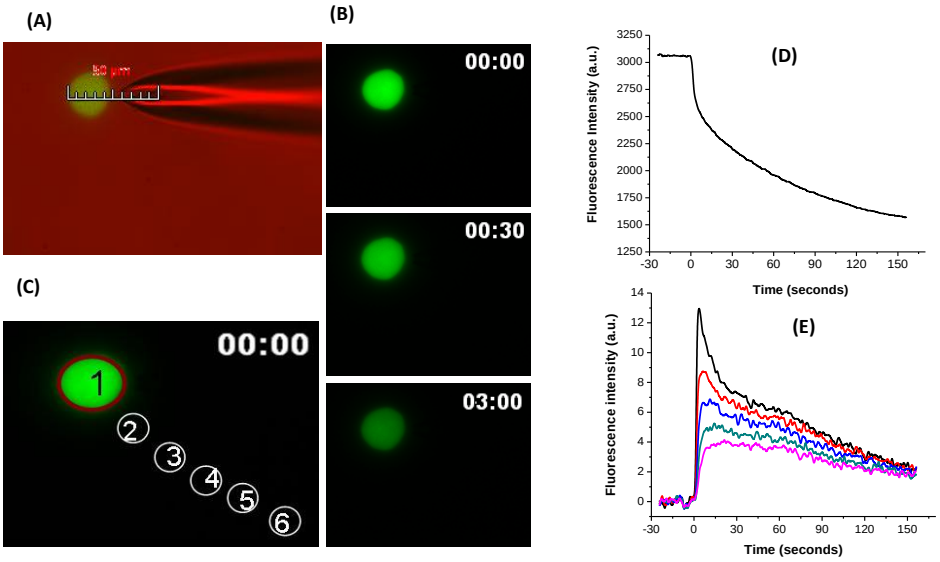

Figure 2.2. Visualization of single cell electroporation. (A) Photomicrograph produced by an overlay of fluorescence and differential interference contrast images. The image shows the placement of the capillary at a distance of *5* µm from the cell. (B) Fluorescence images before pulsation (0 s), and after pulsation (30 s and 3 min from the start of acquisition). (D) Change in average fluorescence intensity for region 1 (C) against time. (E) Change in average fluorescence intensity for regions 2-6 (C) outside the cell against time. All the data were corrected for bleaching.

Spatial resolution. Spatial resolution, or the ability to permeabilize selectively a targeted cell without affecting neighboring cells, can be demonstrated by placing the electrolyte-filled capillary closer to one cell than the others in a group. Figure 2.3A shows two adjacent cells before and after the application of the pulse. In this example, the distance between cells is 10 µm, the probe is 2.0 µm away from cell A (about 24 µm from cell B), and a 200 ms pulse was applied. Upon application of the pulse, Cell A becomes darker as is evidenced by micrographs at 30 s and 2 min. On the other hand, no apparent change in fluorescence intensity other than from photobleaching is seen for cell B. Measurement of average fluorescence intensity presented in Figure 2.3B supports these observations.

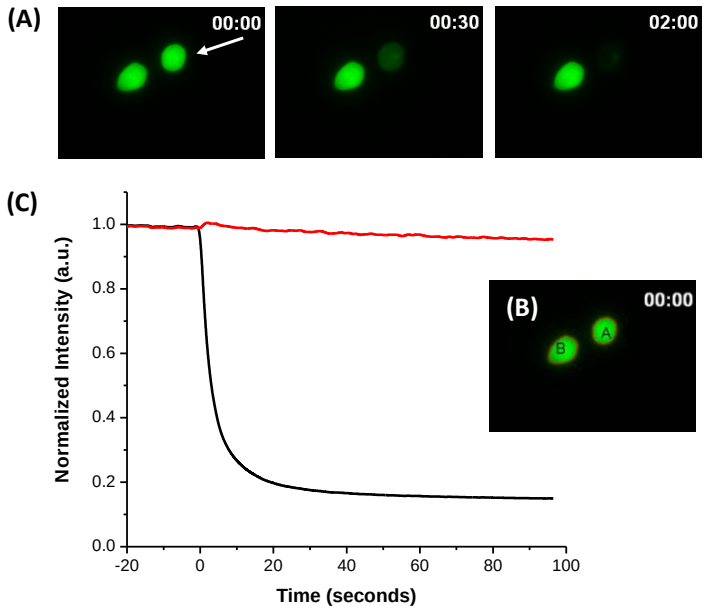

Figure 2.3. High spatial resolution achieved with single cell electroporation. (A) Fluorescence micrograph of 2 fluorescent cells ~ 10 µm from each other. The arrow shows the approximate position of the capillary. The images were taken before pulsation (0 s), and after pulsation (30 s, and 2 min after the start of the acquisition). (C) Normalized average fluorescence intensity for cells A and B (B) against time. All the data were corrected for bleaching.

Cell-capillary tip distance. Experiments were carried out by controlling the distance between the cell and the capillary tip. Figure 2.4A shows change in the average fluorescence intensity with time for all cells pulsed for 200 ms, and cell-capillary tip distance ranging from 2.0 µm to 10 µm. As the cell-to-tip distance increases, the fluorescence decreases to a smaller degree suggesting less permeabilization.

Pulse duration. Electroporation experiments were also conducted for various pulse durations (50 ms to 300 ms). Figure 2.4B shows the change in average fluorescence intensity with time for all cells pulsed for various durations and at a constant cell-capillary tip distance of 3.5 µm. The data show that longer pulse duration results in a larger change in the fluorescence intensity thereby implying greater permeabilization of the cell membrane.

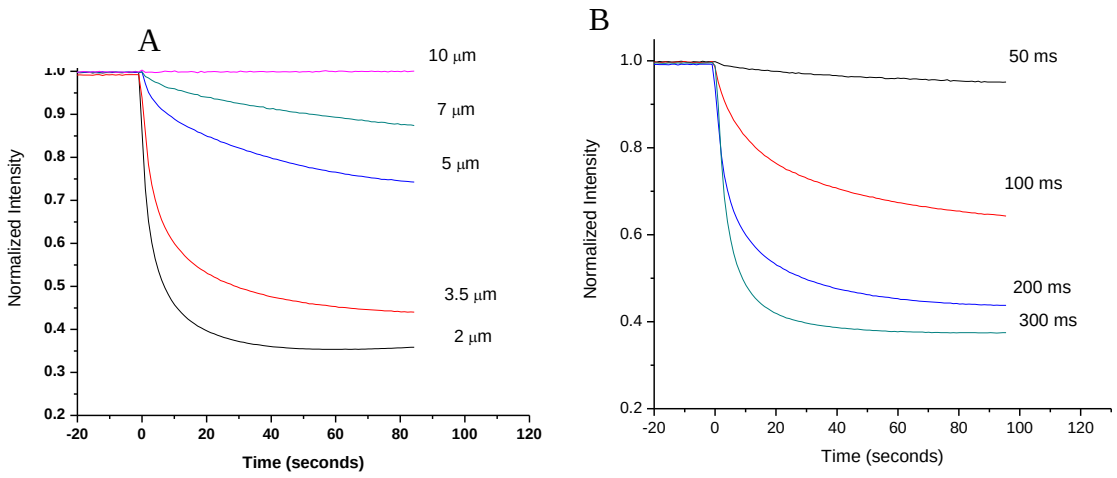

Figure 2.4. Effect of cell-capillary tip distance and pulse duration. (A) Average fluorescence intensity (normalized) vs. time plotted for all cells electroporated with a single pulse of 200 ms and cell-capillary tip distance of 2.0-10.0 μm at 500 V. (B) Average fluorescence intensity (normalized) vs. time plotted for all cell electroporated with a single pulse of varying pulse durations (50 ms to 300 ms), and cell-capillary tip distance of 3.5 μm at 500 V.

Contour Plots. Figure 2.5 is a contour plot of cell survival percentage as a function of pulse duration and cell-capillary tip distance. In this contour plot, lighter shades delineate areas with a larger fraction of live cells whereas darker shades represent a larger fraction of dead cells. Not only is it important to know what fraction of cells survived in these experimental conditions, but also the fraction of cells that were electroporated. A contour plot of the fraction of cells electroporated is superimposed on the contour plot of cell survivability in Figure 2.5. From this figure it can be seen that both the fraction of electroporated cells and the fraction of dead cells increases with a decrease in cell-capillary tip distance and increases with an increase in pulse duration.

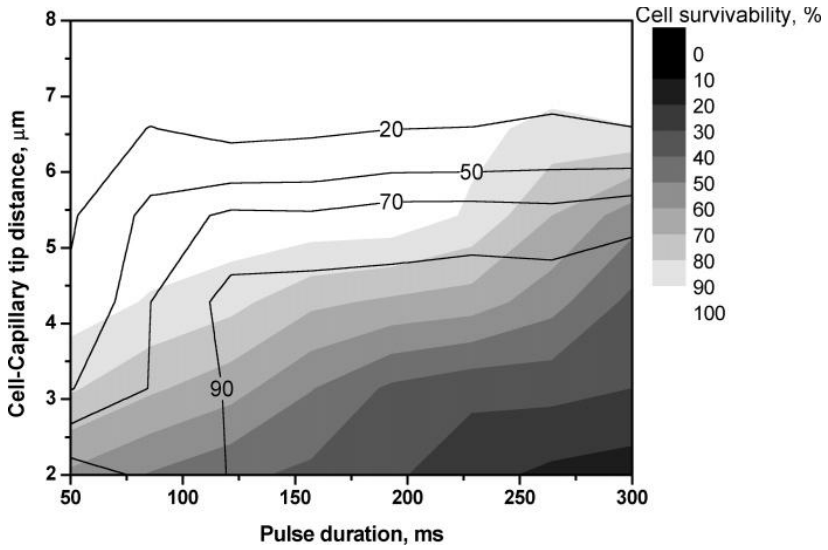

Figure 2.5. Determination of optimal parameters to achieve maximum cell survivability and electroporation. Contour plot of fraction of electroporated cells superimposed on contour plot of cell survivability.

2.5 DISCUSSION

In this work, we varied conditions for single cell electroporation using an electrolyte filled capillary. The diffusion of fluorescent thiol adducts from the cell interior revealed the permeabilization of the membrane by the decrease in fluorescence intensity with time. Permeabilization of the cell membrane is also confirmed by the sharp increase in fluorescence intensity at the time of application of the pulse for the regions outside the cell (Figure 2.2E). Electroporation has been quantified in previous research by studying the uptake and release of molecules and factors that influence this transport in bulk electroporation.[51, 52] Quantitation of ATP by bioluminescence from a cell suspension has also been studied previously.[53] Our results differ from these observations as we monitor directly the real time release of fluorescent thiol adducts from the single cells. In contrast to transfection done via electroporation, which takes

hours to produce proteins by expressing transfected genes,[54] we were able to visualize electroporation within seconds after the application of the pulse.

Electroporation of the cell membrane can be split into two different phases. One is the permeabilization phase that takes place during the pulse and the other is the resealing phase that takes place after the pulse.[4, 43] There are three mechanisms by which molecules can be transported through the pores: electrophoresis, electroosmosis, and diffusion. During the pulse application, the pulse length, amplitude, and molecular properties contribute to the transport rate of molecules. After the end of the pulse application, transport can take place by diffusion and migration until the membrane reseals completely. Migration may occur from the establishment of local diffusion potential gradients within the solution.[55] To minimize diffusion potentials arising from ion concentration gradients, we have used an intracellular buffer. Thus, our results primarily reflect diffusion. During this post-shock period pores are gradually resealing. This process causes the average permeability of the membrane to decrease over time. The characteristic intensity decay curve with time thus is a combination of the diffusion and pore resealing processes. Various models have been developed to quantitatively describe these processes. For example, Puc et al. developed an analytical expression (called a pharmacokinetic model) relating pulse parameters to uptake (or release) of small molecules from a cell. In this model pore resealing is an exponential (first order) process with a rate constant $\alpha = 0.0038\ s^{-1}$.

One of the major advantages of single cell electroporation is that high spatial resolution can be achieved. The resolution can be controlled by controlling the tip diameter of the capillary. Previous studies from Orwar using electrolyte filled capillaries achieved a resolution of > 15 μm.[29] In our experiments capillary tips were typically smaller than 5 μm in diameter and because A 549 cells are on average 20 μm in diameter we easily achieved single cell electroporation. In

fact, a resolution of 10 μm (see Figure 2.3) or better (data not shown) was achieved with this technique.

A number of electric field parameters such as field strength, pulse duration, number of pulses and delay between the pulses can be controlled simultaneously. All these parameters control the extent of electroporation in a certain way. In our experiments, we studied the effect of field strength and pulse duration on electroporation keeping other parameters constant.

Experiments were performed where the electric field was controlled by changing the cell to capillary tip distance. The results in Figure 2.4A show that an increase in the cell-capillary tip distance results in a decrease in the fluorescence intensity indicating less permeabilization of the cell membrane. This suggests that increasing cell-capillary tip distance decreases the field strength experienced by the cell. Previous research has proven that the field strength controls the area of the cell that is electroporated.[53] The higher the field strength applied, the greater the electroporated area of the cell surface. Therefore it can be hypothesized that increasing the cell-capillary tip distance results in decrease of electric field strength which thus results in a smaller area of the cell being permeabilized.

Experiments were also performed where cells were pulsed for various durations keeping other parameters constant. Results, in Figure 2.4B, exhibit that increasing pulse duration results in an increase in the fluorescence intensity change indicating in greater permeabilization. This could be because the pulse duration controls the increase in size of these pores.[41]

As seen in the standard deviation values of fluorescence intensity at 90 seconds in Table 2.2, a large variability exists in cell response at particular conditions. This diverse response in fluorescence intensity and cell viability has been observed before in single cells, both electroporated in a chip,[33] and with an electrolyte-filled capillary.[29] Variability has also been

observed in bulk electroporation. An example of this can be seen in Teissie et al.[46] They showed that there was a significant variability in cell permeation under constant conditions and even larger variability in long term cell survival abilities at the same conditions. For bulk electroporation the variability has been attributed to the cell size distribution around the mean.[43] We assume that this is in part true also for single cell experiments. In bulk electroporation all cells are pulsed simultaneously and therefore experience very similar conditions. In single cell electroporation, the electric field strength variation from experiment to experiment is possible due to cell shape uncertainties (they are rarely perfectly hemispherical) and capillary-to-cell distance measurements. We considered variations of the capillary resistance but variation in the permeabilization level was large even among experiments performed with the same capillary and therefore we ruled out this as significant factor.

Table 2.2. Mean and standard deviation values of fluorescence intensity at 90 seconds from the start of acquisition by pulsing parameters.

	Distance between cell and the capillary tip (μm)									
Pulse Duration (ms)	2.0		3.5		5.0		7.0		10.0	
50	0.55	0.29	0.96	0.06	0.98	0.01	0.99	0.01	1.00	0.00
100	0.68	0.26	0.67	0.24	0.77	0.17	0.99	0.01	1.00	0.00
200	0.35	0.12	0.45	0.22	0.76	0.16	0.99	0.01	1.00	0.00
300	0.34	0.23	0.38	0.27	0.48	0.21	1.00	0.00	1.00	0.00

Even though a large variability exists in the response of individual cells, we were able to find optimum conditions for electroporation and cell viability. The contour plot (Figure 2.5) shows two surfaces. One is the percentage of permeabilized cells, while the other is the percent of cells surviving electroporation. It can be deduced from this plot that at fixed pulse duration, cell survivability increases as the cell-capillary tip distance increases, and at fixed cell-capillary

tip distance cell survivability increases as the pulse duration decreases. The superimposition shows that when the cell-capillary tip distance is between 3.5 µm and 5.0 µm and the pulse duration is between 120 ms to 150 ms, 80 - 90% of cells survive and > 90% of the cells are electroporated. While optimum conditions may differ with different cells, recent work on single-cell electroporation has indicated the similarity of four different sort of cells.[54] We anticipate at least that these optimum conditions are a very good starting point for other cell types. Therefore, even with the variability of single cells, our results provide guidance to experimental conditions to achieve maximum probability of electroporation with minimal probability of cell death.

2.6 REFERENCES

(1) Teissie, J.; Eynard, N.; Gabriel, B.; Rols, M. P. Electropermeabilization of cell membranes. *Adv Drug Deliver Rev.* **1999**, *35*, 3-19.

(2) Phez, E.; Faurie, C.; Golzio, M.; Teissie, J.; Rols, M.-P. New insights in the visualization of membrane permeabilization and DNA/membrane interaction of cells submitted to electric pulses. *Biochim Biophys Acta*. **2005**, *1724*, 248-254.

(3) Teissie, J.; Golzio, M.; Rols, M. P. Mechanisms of cell membrane electropermeabilization: A minireview of our present (lack of ?) knowledge. *Biochim Biophys Acta*. **2005**, *1724*, 270-280.

(4) Weaver, J. C.; Chizmadzhev, Y. A. Theory of electroporation: A review. *Bioelectrochem Bioenerg.* **1996**, *41*, 135-160.

(5) Weaver, J. C.; Vaughan, T. E.; Chizmadzhev, Y. Theory of electrical creation of aqueous pathways across skin transport barriers. *Adv Drug Delivery Rev.* **1999**, *35*, 21-39.

(6) Weaver, J. C. Electroporation of cells and tissues. *IEEE Transactions on Plasma Science*. **2000**, *28*, 24-33.

(7) Tsong, T. Y. Electroporation of cell membranes. *Biophys. J.* **1991**, *60*, 297-306.

(8) Neumann, E.; Schaefer-Ridder, M.; Wang, Y.; Hofschneider, P. H. Gene transfer into mouse lyoma cells by electroporation in high electric fields. *EMBO J.* **1982**, *1*, 841-845.

(9) Neumann, E. Membrane electroporation and direct gene transfer. *Bioelectrochem Bioenerg.* **1992**, *28*, 247-267.

(10) Zimmermann, U.; Riemann, F.; Pilwat, G. Enzyme loading of electrically homogeneous human red blood cell ghosts prepared by dielectric breakdown. *Biochim. Biophys. Acta*. **1976**, *436*, 460-474.

(11) Faurie, C.; Golzio, M.; Phez, E.; Teissie, J.; Rols, M. P. Electric field-induced cell membrane permeabilization and gene transfer: Theory and experiments. *Eng Life Sci.* **2005**, *5*, 179-186.

(12) Xie, T. D.; Tsong, T. Y. Study of mechanisms of electric field-induced DNA transfection. II. Transfection by low-amplitude, low-frequency alternating electric fields. *Biophys J.* **1990**, *58*, 897-903.

(13) Xie, T. D.; Sun, L.; Tsong, T. Y. Study of mechanisms of electric field-induced DNA transfection. I. DNA entry by surface binding and diffusion through membrane pores. *Biophys J.* **1990**, *58*, 13-19.

(14) Mir, L. M.; Orlowski, S.; Belehradek, J., Jr. ; Paoletti, C. Electrochemotherapy potentiation of antitumour effect of bleomycin by local electric pulses. *Eur J Cancer (Oxford, England :1990).* **1991**, *27*, 68-72.

(15) Prausnitz, M. R.; Lau, B. S.; Milano, C. D.; Conner, S.; Langer, R.; Weaver, J. C. A quantitative study of electroporation showing a plateau in net molecular transport. *Biophys J.* **1993**, *65*, 414-422.

(16) Prausnitz, M. R.; Bose, V. G.; Langer, R.; Weaver, J. C. Electroporation of mammalian skin: a mechanism to enhance transdermal drug delivery. *Proc Natl Acad Sci. U. S. A.* **1993**, *90*, 10504-10508.

(17) Bliss, J. G.; Harrison, G. I.; Mourant, J. R.; Powell, K. T.; Weaver, J. C. Electroporation: the population distribution of macromolecular uptake and shape changes in red blood cells following a single 50 ms square wave pulse. *Bioelectrochem Bioenerg.* **1988**, *20*, 57-71.

(18) Golzio, M.; Teissie, J.; Rols, M.-P. Direct visualization at the single-cell level of electrically mediated gene delivery. *Proc Natl Acad Sci. U. S. A.* **2002**, *99*, 1292-1297.

(19) Gabriel, B.; Teissie, J. Time courses of mammalian cell electropermeabilization observed by millisecond imaging of membrane property changes during the pulse. *Biophys J.* **1999**, *76*, 2158-2165.

(20) Hibino, M.; Itoh, H.; Kinosita, K., Jr. Time courses of cell electroporation as revealed by submicrosecond imaging of transmembrane potential. *Biophys. J.* **1993**, *64*, 1789-1800.

(21) Kotnik, T.; Mir, L. M.; Flisar, K.; Puc, M.; Miklavcic, D. Cell membrane electropermeabilization by symmetrical bipolar rectangular pulses. Part I. Increased efficiency of permeabilization. *Bioelectrochemistry (Amsterdam, Netherlands)*. **2001**, *54*, 83-90.

(22) Kotnik, T.; Miklavcic, D.; Mir, L. M. Cell membrane electropermeabilization by symmetrical bipolar rectangular pulses. Part II. Reduced electrolytic contamination. *Bioelectrochemistry (Amsterdam, Netherlands)*. **2001**, *54*, 91-95.

(23) Pliquett, U.; Weaver, J. C. Electroporation of human skin: simultaneous measurement of changes in the transport of two fluorescent molecules and in the passive electrical properties. *Bioelectrochem Bioenerg.* **1996**, *39*, 1-12.

(24) Olson, K. J.; Ahmadzadeh, H.; Arriaga, E. A. Within the cell: analytical techniques for subcellular analysis. *Anal Bioanal Chem.* **2005**, *382*, 906-917.

(25) Lu, X.; Huang, W.-H.; Wang, Z.-L.; Cheng, J.-K. Recent developments in single-cell analysis. *Anal Chim Acta*. **2004**, *510*, 127-138.

(26) Brady, G. Expression profiling of single mammalian cells - small is beautiful. *Yeast*. **2000**, *17*, 211-217.

(27) Anderson, A. B.; Gergen, J.; Arriaga, E. A. Detection of doxorubicin and metabolites in cell extracts and in single cells by capillary electrophoresis with laser-induced fluorescence detection. *J. Chromatogr B.* **2002**, *769*, 97-106.

(28) Lundqvist, J.; Anders. Sahlin, F.; Aberg, M. A. I.; Stromberg, A.; Eriksson, P. S.; Orwar, O. Altering the biochemical state of individual cultured cells and organelles with ultramicroelectrodes. *Proc Natl Acad Sci. U. S. A.* **1998**, *95*, 10356-10360.

(29) Nolkrantz, K.; Farre, C.; Brederlau, A.; Karlsson, R. I. D.; Brennan, C.; Eriksson, P. S.; Weber, S. G.; Sandberg, M.; Orwar, O. Electroporation of single cells and tissues with an electrolyte-filled capillary. *Anal Chem.* **2001**, *73*, 4469-4477.

(30) Ryttsen, F.; Farre, C.; Brennan, C.; Weber, S. G.; Nolkrantz, K.; Jardemark, K.; Chiu, D. T.; Orwar, O. Characterization of single-cell electroporation by using patch-clamp and fluorescence microscopy. *Biophys J.* **2000**, *79*, 1993-2001.

(31) Huang, Y.; Rubinsky, B. Flow-through micro-electroporation chip for high efficiency single-cell genetic manipulation. *Sensor Actuat A-Phys.* **2003**, *A104*, 205-212.

(32) Khine, M.; Lau, A.; Ionescu-Zanetti, C.; Seo, J.; Lee, L. P. A single cell electroporation chip. *Lab Chip.* **2005**, *5*, 38-43.

(33) He, H.; Chang, D. C.; Lee, Y.-K. Micro pulsed radio-frequency electroporation chips. *Bioelectrochemistry*. **2006**, *68*, 89-97.

(34) Huang, Y.; Rubinsky, B. Microfabricated electroporation chip for single cell membrane permeabilization. *Sensor Actuat A-Phys.* **2001**, *A89*, 242-249.

(35) Olofsson, J.; Nolkrantz, K.; Ryttsen, F.; Lambie, B. A.; Weber, S. G.; Orwar, O. Single-cell electroporation. *Curr Opin Biotechnol.* **2003**, *14*, 29-34.

(36) Tao, W.; Wilkinson, J.; Stanbridge, E. J.; Berns, M. W. Direct gene transfer into human cultured cells facilitated by laser micropuncture of the cell membrane. *Proc Natl Acad Sci U S A.* **1987**, *84*, 4180-4184.

(37) Soughayer, J. S.; Krasieva, T. J.; Ramsey., S. C.; Michael., J.; Tromberg, B. J.; Allbritton, N. L. Characterization of Cellular Optoporation with Distance. *Anal Chem.* **2000**, *72*, 1342-1347.

(38) Orwar, O.; Karlsson, M.; Chiu, D.; (Cellectricon AB, Swed.). Application: WO, 2002, pp 30

(39) Capecchi, M. R. High efficiency transformation by direct microinjection of DNA into cultured mammalian cells. *Cell*. **1980**, *22*, 479-488.

(40) Valic, B.; Golzio, M.; Pavlin, M.; Schatz, A.; Faurie, C.; Gabriel, B.; Teissie, J.; Rols, M.-P.; Miklavcic, D. Effect of electric field induced transmembrane potential on spheroidal cells: theory and experiment. *Euro Biophys J.* **2003**, *32*, 519-528.

(41) Rols, M.-P.; Teissie, J. Electropermeabilization of mammalian cells to macromolecules: control by pulse duration. *Biophys J.* **1998**, *75*, 1415-1423.

(42) Loste, F.; Eynard, N.; Teissie, J. Direct monitoring of the field strength during electropulsation. *Bioelectrochem Bioenerg.* **1998**, *47*, 119-127.

(43) Puc, M.; Kotnik, T.; Mir, L. M.; Miklavcic, D. Quantitative model of small molecules uptake after in vitro cell electropermeabilization. *Bioelectrochemistry*. **2003**, *60*, 1-10.

(44) Kotnik, T.; Pucihar, G.; Rebersek, M.; Miklavcic, D.; Mir, L. M. Role of pulse shape in cell membrane electropermeabilization. *Biochim Biophys Acta*. **2003**, *1614*, 193-200.

(45) Valic, B.; Pavlin, M.; Miklavcic, D. The effect of resting transmembrane voltage on cell electropermeabilization: a numerical analysis. *Bioelectrochemistry*. **2004**, *63*, 311-315.

(46) Gabriel, B.; Teissie, J. Control by electrical parameters of short- and long-term cell death resulting from electropermeabilization of Chinese hamster ovary cells. *Biochim Biophys Acta*. **1995**, *1266*, 171-178.

(47) Teissie, J.; Tsong, T. Y. Electric field induced transient pores in phospholipid bilayer vesicles. *Biochemistry*. **1981**, *20*, 1548-1554.

(48) Olofsson, J.; Levin, M.; Stroemberg, A.; Weber, S. G.; Ryttsen, F.; Orwar, O. Generation of Focused Electric Field Patterns at Dielectric Surfaces. *Anal Chem* **2005**, *77*, 4667-4672.

(49) Fabisiak, J. P.; Sedlov, A.; Kagan, V. E. Quantification of Oxidative/Nitrosative Modification of CYS34 in Human Serum Albumin Using a Fluorescence-Based SDS-PAGE Assay. *Antioxid Redox Signal.* **2002**, *4*, 855-865.

(50) Kagan, V. E.; Kuzmenko, A. I.; Tyurina, Y. Y.; Shvedova, A. A.; Matsura, T.; Yalowich, J. C. Pro-oxidant and antioxidant mechanisms of etoposide in HL-60 cells: role of myeloperoxidase. *Cancer Res.* **2001**, *61*, 7777-7784.

(51) Prausnitz, M. R.; Corbett, J. D.; Gimm, J.; Aura Golan, D. E.; Langer, R.; Weaver, J. C. Millisecond measurement of transport during and after an electroporation pulse. *Biophys J.* **1995**, *68*, 1864-1870.

(52) Tekle, E.; Astumian, R. D.; Chock, P. B. Electro-permeabilization of cell membranes: effect of the resting membrane potential. *Biochem Biophys Res Commun.* **1990**, *172*, 282-287.

(53) Rols, M. P.; Teissie, J. Electropermeabilization of mammalian cells: quantitative analysis of the phenomenon. *Biophys J.* **1990**, *58*, 1089-1098.

(54) Rae, J. L.; Levis, R. A. Single-cell electroporation. *Pfluegers Arch.* **2002**, *443*, 664-670.

(55) Newman, J.; Tomas-Alyea, K. E. Electrochemical Systems. 2004, 3rd Edition, pp 149-168

3.0 EFFECT OF CELL SIZE AND SHAPE ON SINGLE-CELL ELECTROPORATION

This work has been published in Analytical Chemistry, **2007**, *79*, 3589-3596. Reproduced with permission from *Analytical Chemistry*.

3.1 ABSTRACT

Single cell electroporation was performed using electrolyte-filled capillaries on fluorescently labeled A549 cells. Cells were exposed to brief pulses (50 – 300 ms) at various cell-capillary tip distances. Cell viability and electroporation success were measured. In order to understand the variability in single cell electroporation, logistic regression was used to determine whether the probabilities of cell survival and electroporation depend on experimental conditions and cell properties. Both experimental conditions and cell properties (size and shape) have a significant effect on the outcome. Finite element simulations were used to compare bulk electroporation to single-cell electroporation in terms of cell size and shape. Cells are more readily permeabilized and are more likely to survive if they are large and hemispherical as opposed to small and ellipsoidal with a high aspect ratio. The dependence of the maximum transmembrane potential across the cell membrane on cell size is much weaker than it is for bulk electroporation. Observed survival probabilities are related to the calculated fraction of the cell's

surface area that is electroporated. Observed success of electroporation is related to the maximum transmembrane potential achieved.

3.2 INTRODUCTION

The cell membrane acts as a barrier to the free diffusion of molecules and ions such as DNA, RNA, proteins, drugs, etc. between the cytoplasm and the external medium. Electroporation[1-5] is a technique that uses electric fields to temporarily permeabilize the cell membrane by inducing a transmembrane potential. When the transmembrane potential reaches a critical value of about 250 mV, transient pores appear in the membrane. During the effective pore open time, impermeable molecules can freely diffuse into the cell interior. It is now routinely used in cell biology and biotechnology for gene transfection,[2, 6-8] and in medical applications for gene therapy[9] and cancer chemotherapy.[10]

A biological cell placed in a uniform electric field results in a local distortion of the field near the cell. As the conductivity of the cell membrane is several orders of magnitude lower than the cytoplasm and the extracellular medium, most of the field is concentrated across the membrane. Analytical solutions exist for the transmembrane potential for spherical cells in a uniform electric field. The most general form of the steady-state transmembrane potential induced on the spherical cells is given by the Schwan equation [11]:

$$\Delta\Phi = \frac{3}{2} Er\cos\theta \tag{3.1}$$

where $\Delta\Phi$ is the induced transmembrane potential, E is the external electric field, r is the radius of the cell, and θ is the polar angle measured from the center of the cell with respect to the

direction of the field. The steady state, to which Eq. 3.1 applies, is reached on the microsecond timescale.[12] Schwan's equation shows that at a given electric field transmembrane potential depends on the cell size. Schwan's equation has now been further extended to calculate the transmembrane potential on prolate and oblate spheroidal cells. Kotnik et al.[13] have proposed an analytical solution of transmembrane potential on spheroidal cells in homogeneous electric fields with the polar radius parallel to the electric field vector. Further, Gimsa et al.[14, 15] have calculated the transmembrane potential on arbitrarily oriented spheroidal cells in an electric field. However, all these calculations apply for a uniform electric field.

Single-cell electroporation has been performed using modified patch clamp techniques,[16] micropipettes,[17] and electrolyte-filled capillary.[18] Unlike bulk electroporation,[3-5, 19] fields produced in single-cell electroporation are highly focused and inhomogeneous. The inhomogeneity is particularly evident when the tip opening diameter is smaller than the cell diameter, and the tip is near the cell. The Schwan equation does not apply if the electric field is inhomogeneous.

The analysis of the cytoplasmic contents of single cells using microfluidics and separations (capillary electrophoresis) is a burgeoning field.[20-29] Typically, the single cells are destroyed in the process of analysis. While we do not realize this goal in the present paper, we do look forward to the analysis of single, adherent (i.e., in a 'natural' state) cells without killing them in the process. Recent reports using nanoelectrodes[30] and chemical permeabilizing agents to introduce enzyme substrates into single cells[31] justify our optimism. Single-cell electroporation has the capability to open a 'window' onto the cell's contents permitting (in principle) analysis of cytoplasmic effluent. However, as an approach to single-cell sampling, it

must be reproducible, and the dependence of the outcome on experimental and cellular parameters must be known.

Thus, we performed single-cell electroporation using an electrolyte-filled capillary at various pulse durations and d_m. From these experiments we determined the electroporation success and cell viability. Logistic regression was carried out on cell viability and electroporation success. From the regression results it was found that both the experimentally controlled parameters and the cell attributes (size and shape) play a significant role in cell permeabilization ($p < 0.05$). Further, finite element method simulations were performed to compare the single-cell electroporation results with bulk electroporation.

3.3 EXPERIMENTAL SECTION

Materials. The chemicals used for buffer preparations were all analytical grade and were purchased from Sigma (St. Louis, MO). Thioglo-1 was purchased from Covalent Associates (Woburn, MA). Propidium iodide and calcein AM were purchased from Invitrogen/Molecular probes (Eugene, OR). A549 cell lines were obtained from American Type Culture Collection (Manassas, VA). Basal medium Eagle (BME), Trypsin-EDTA, fetal bovine serum (FBS), L-glutamine and penicillin were all obtained from Gibco-BRL (Carlsbad, CA). Milli-Q (Millipore Synthesis A 10, Billerica, MA) water was used. Intracellular buffer consisted of NaCl, 5 mM; KCl, 140 mM; $MgCl_2$, 1.5 mM; D-glucose, 10 mM; HEPES, 20 mM; pH adjusted to 7.4.

Cell culture. Human lung cancer A549 cells were cultured in BME supplemented with 10 % fetal bovine serum, 100 U/mL penicillin, and 100 µg/mL streptomycin. Cells were grown as a monolayer in 75-mL cell culture flasks at 37 °C and 95% air/5% CO_2 (HERA cell incubator,

Newtown, CT). Before the experiments, cells were plated on 35-mm, glass-bottom cell culture dishes (MatTek Corp., Ashland, MA) and were grown for up to 3 days. Experiments were performed on the second and third days following the cell plating. Details of single-cell electroporation can be found elsewhere.[32]

Cell staining. The cells were stained with cell-permeable dye Thioglo-1 (2 μM in intracellular buffer) for 30 seconds at room temperature. Thioglo-1 is a maleimide-based reagent that gives a highly fluorescent product upon its reaction with active –SH groups in proteins, enzymes, and small peptides.[33, 34] Cells were washed and bathed in the intracellular buffer and mounted on the cell chamber (DH 35i culture dish incubator, Warner Instruments, Holliston, MA) and transferred to the stage of the microscope.

Probe preparation. To perform electroporation experiments, fused-silica capillaries from Polymicro Technology (Phoenix, AZ) were used as a probe. Capillaries were pulled with a CO_2 laser puller (Sutter Instruments Co. P-2000, Novato, CA) using a one line program, i.e., Heat: 260; Filament: 0; Velocity: 30; Delay: 128; Pull: 0. This one line program created reproducible capillaries with a short pulled tip with an inner diameter of about 5 μm. The final length of the capillaries was 15 cm.

Electroporation Setup. The experimental setup is depicted in Figure 3.1. The 15-cm long pulled capillary with a tip about 5 μm in diameter was positioned using a high-graduation micromanipulator (Narishige, NMN-21, Tokyo, Japan). The observed distance between the capillary tip and the cell (d_m) was the projection of the capillary image in the horizontal imaging plane (cell dish surface). These d_m were 2.0 μm, 3.5 μm, 5.0 μm, 7.0 μm, and 10.0 μm. The other end of the capillary was placed in a vial filled with intracellular buffer. A platinum electrode placed in this vial was connected to the electroporator (ECM 830, BTX Instruments, San Diego,

CA) and the electrical circuit was completed with a grounded platinum electrode placed in the cell dish. For elongated cells the capillary tip was always positioned near the 'long' side of the cell, thus the major axis of the hemispheroidal cell and the symmetry axis of the capillary are perpendicular.

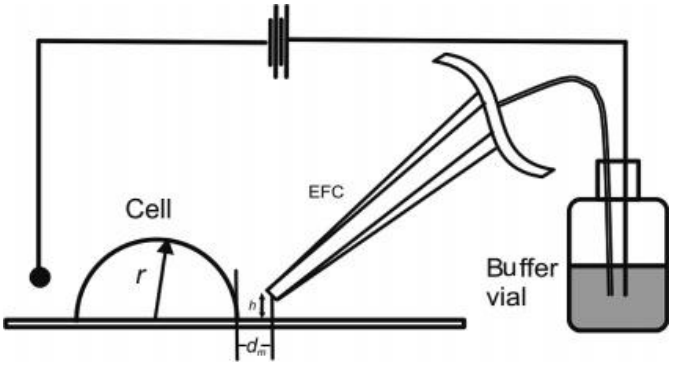

Figure 3.1. Schematic diagram of the experimental setup.

Electroporation. Cells were exposed to single pulses of 500 V with pulse durations ranging from 50 ms-300 ms. This will be referred as 'pulsing' of the cells. For all these pulsing conditions the d_m varied from 2.0 µm-10 µm. The pulse was applied at 25.0 seconds from the start of the acquisition. Diffusive loss of fluorescent thiol adducts from the cell interior was determined quantitatively with Simple PCI software (Compix, Inc., Sewickley, PA). The smallest distinguishable intensity change was about 4% of the signal. This was chosen as a threshold value for determination of electroporation success. For a cell to be considered permeabilized it had to loose 4% or more of its fluorescence intensity within 90 s of electroporation.

Fluorescence Imaging. Cells were observed through a 40X 1.3 NA oil immersion objective using an inverted microscope (Olympus, IX 71, Melville, NY) equipped with an HBO 100-W mercury lamp as the excitation source. For Thioglo-1, an Omega fluorescence cube (specially built, Omega, Brattleboro, VT) was used with filters for excitation at 378 nm and emission at

480 nm. For live/dead imaging, a triple band 'Pinkel' filter set from Semrock (Rochester, NY) was used (exciter 1 387 nm, exciter 2 494 nm; exciter 3 575 nm; dichroic mirror: 394– 414 nm, 484 – 504 nm, 566 – 586 nm, emitter: 457, 530, 628 nm). A CCD camera (Hamamatsu, ORCA-285, Bridgewater, NJ) imaged cells. The image collection frequency was 1 frame/s. Image processing was performed by the image acquisition software Simple PCI (Compix, Inc., Sewickley, PA). All the data were corrected for photobleaching.

Cell Viability Assay. Following electroporation experiments, live/dead analysis was performed on the cells using calcein AM and propidium iodide.[35] Cell survival percentage was calculated for each experimental condition based on this live/dead assay. It is important to note that a measurement of cell viability was made on each cell that was electroporated.

Cell properties. The cell properties were obtained by using the Compix software. A macro file was set to a certain critical value. The cell measurements were then done according to the cell size, cell shape and intensity. The cell size factors used were area, diameter, perimeter, breadth and width. The shape factor used was the aspect ratio (maximum length/maximum breadth). The intensity factors used were grey-level and standard deviation of the grey level. The parameter 'grey-level' is the average of the grey-level intensity of each pixel in the object corresponding to the average fluorescence intensity.

Simulation. The finite element method was used to compute the potential distribution in the experimental system using Comsol 3.2a (Comsol Inc., Burlington, MA). This enables the calculation of a transmembrane potential for cells. The transmembrane potential varies across the cell surface. Electroporation occurs when transmembrane potential is greater than some critical value, TMP_c which is often given as 0.25 V. The area of the cell membrane over which the transmembrane potential is greater than TMP_c is called A^*. The fraction of the hemispherical

cell's area corresponding to A^* will be called F^*. The capillary is positioned 45 degrees with respect to surface normal (Figure 3.1). The center of the tip opening in all calculations is positioned 5 μm above the surface and at the specified distance from the cell. In comparison to prior computational work on electroporation from the top (capillary 90 ^{o}C to the surface) in which cylindrical symmetry could be invoked,[36] a full, three-dimensional simulation was performed. In single-cell electroporation simulations, a realistic model of the capillary tip shape was used. For the simulation geometries, the equation $\nabla(\sigma\nabla V) = 0$ was solved to determine the potential inside and outside the cell, with appropriate boundary conditions. Here V is the potential and σ is the conductivity. A steady state condition was assumed. It is important, especially in 3-D simulations, to avoid simulating unnecessary parts of the experiment. One such part is the potential inside the capillary – it is very reproducible in the cylindrically symmetrical calculations as, e.g., d_m changes. Thus, a boundary condition was specified a mere 2.0 μm up into the capillary lumen from the tip. When that potential (which is independent of radius) is 6.76 V it corresponds to the experimental situation in which we apply 500 V at the distal end of the capillary 15 cm away from the tip. The ground electrode was a 90 degree section of the simulated cylindrical bath (0.5 mm radius, 0.5 mm height) opposite the tip opening. Parameters of the solutions and membrane used in the simulations are in Zudans et al.[36]

3-D simulations were performed for hemispherical cells of three sizes: small, median, and large cell with diameters 19 μm, 25 μm, and 39 μm respectively (corresponding to the 5th, 50th and 95th %ile of our cells). 3-D simulations were also performed for hemispheroidal cells of three sizes: small, median, and large cell with an aspect ratio of 3. The major and minor axes of the spheroidal cells were set so that the projected area was independent of aspect ratio. This allows us to separate the variables of 'size' and 'shape'. The projected area is the apparent area

under the microscope. Simulations were performed for the real conditions where the major axis of the spheroidal cell was perpendicular to the symmetry axis of the capillary. Results of the simulations of the hemispheroidal cells are shown in Figure 3.5.

Statistical analysis. Data from 226 cells from the electroporation experiments were used for statistical analysis. As the outcomes, cell survivability (live/dead) and electroporation success, are binary, logistic regression was used for analysis using the program STATA (Intercooled 9.0). The dependent variables used for logistic regression were the cell properties and the experimental conditions. In the logistic 'model', the effects of the parameters are independent of each other. The cell properties were first transformed in order to get a normal distribution. The logistic regression was run on transformed values of cell properties. These transformed variables were then later untransformed to get the probabilities of cell survivability and electroporation success. The experimental parameters used for logistic regression were pulse duration (50 – 300 ms) and d_m (2-10 μm).

3.4 RESULTS

Logistic Regression. Table 3.1 gives the correlation matrix of the cell properties. It can be seen from the table, and as was expected, that the cell size parameters: area, diameter, perimeter, width are highly correlated. Factor analysis (maximum likelihood estimation with varimax rotation) was performed on all the cell properties to determine the number of factors that explained most of the variance. Also, data were transformed to create near normal distributions for a function of the variables. Three factors explained virtually all of the variance (Table 3.2). Factor loadings greater than or equal to 0.60 are highlighted in the Table. The factors correspond

to ‘size’ (factor 1), ‘shape’ (factor 2), and ‘intensity’ (factor 3). Factor 1 explains 66% of the variance, factor 2 explains 21% of the variance, and factor 3 explains 13% of the variance.

Table 3.1. Correlation matrix of cell properties.

	Area	Diameter	Perimeter	Breadth	Width	Aspect Ratio	Stdev grey-level	Grey-level
Area	1.00							
Diameter	0.99	1.00						
Perimeter	0.92	0.92	1.00					
Breadth	0.68	0.70	0.47	1.00				
Width	0.82	0.81	0.82	0.47	1.00			
Aspect Ratio	0.36	0.36	0.62	-0.02	0.38	1.00		
Stdev grey-level	-0.44	-0.47	-0.37	-0.46	-0.43	-0.07	1.00	
Grey-level	-0.42	-0.42	-0.52	-0.18	-0.45	-0.43	0.47	1.00

Table 3.2. Factor loadings and unique variances. The shaded areas represent absolute values of the factor loading greater than or equal to 0.6.

Variable	Factor 1	Factor 2	Factor 3	Uniqueness
Area	0.97	0.15	-0.14	0.01
Diameter	0.97	0.14	-0.17	0.00
Perimeter	0.84	0.51	-0.13	0.01
Breadth	0.72	-0.34	-0.25	0.30
Width	0.76	0.26	-0.24	0.30
Aspect Ratio	0.25	0.80	-0.04	0.29
Stdev grey-level	-0.38	0.03	0.60	0.51
Grey-level	-0.29	-0.40	0.52	0.50

Ultimately, based on these factor analysis results, the most significant uncorrelated variables were taken. These variables were area, aspect ratio and standard deviation of grey-level. Logistic regression was performed to study the cell survivability and electroporation success based on these cell properties and experimental conditions.

In logistic regression, the following model is used;

$$OR = \frac{P}{1-P} \tag{3.2}$$

$$\mathrm{OR} = \mathrm{e}^{(\mathrm{b}_0 + \mathrm{b}_1\mathrm{x}_1 + \mathrm{b}_2\mathrm{x}_2 + \ldots)} \tag{3.3}$$

where the odds ratio, *OR*, is related to the probability of the event, *P*, as shown in Eq. 3.2. The regression determines the coefficients, b_i, corresponding to independent variables x_i. This sort of regression is applied to problems with a binary outcome (e.g., live/dead, on/off).[37] A linear

regression of "probability" on the variables is not appropriate, as there is nothing inherent in linear regression limiting the outcome to the range of 0 to 1. As Eq. 3.4 shows, the probability is a sigmoidal function of the variables.

$$P = \frac{e^{(b_0 + b_1 x_1 + \ldots)}}{1 + e^{(b_0 + b_1 x_1 + \ldots)}} \tag{3.4}$$

The results from logistic regression analysis on cell survivability are listed in Table 3.3. There are results from two separate regressions. The left three columns correspond to regression on the untransformed, unscaled variables. The right three columns correspond to regression on transformed, scaled variables. Transformation was described above. Scaling is used to yield regression coefficients near unity for convenience. The results indicate that there is a significant ($p < 0.05$) relationship between cell survivability and experimental conditions: pulse duration., d_m, and cell properties: area, and aspect ratio. The standard deviation of the grey-level showed a borderline significance ($p = 0.097$). The results from logistic regression on electroporation success are listed in Table 3.4. The results show that there is significant relationship between electroporation success and experimental conditions: pulse duration, d_m and cell parameter: area. The logistic regression was also carried out to study the effect of cell survivability and electroporation success on the interaction terms between cell properties and experimental conditions. Interaction terms were generated by taking the products of experimental conditions (pulse duration and d_m) and cell properties (area, aspect ratio and standard deviation of grey level). None of the interaction terms showed any effect on cell survivability ($p > 0.05$) and electroporation success ($p > 0.05$).

Table 3.3. Results of logistic regression analysis of cell survivability (Alive) as a function of experimental conditions and cell properties.

Alive	Odds Ratio	p value	Variables (transformed)	Odds Ratio	p value
PulseDuration	0.987	0.000	$\frac{PulseDuration}{50}$	0.50	0.000
Distance	2.27	0.000	Distance	2.30	0.000
Area	1.00	0.036	$\frac{1000}{Area}$	0.41	0.005
Aspect Ratio	0.458	0.030	$\frac{10}{AspectRatio}$	1.37	0.005
Stdev grey-level	$2.79*10^{7}$	0.166	$1000(stdevgreylevel)^{3}$	1.21	0.097

Table 3.4. Results of logistic regression analysis of electroporation success as a function of experimental conditions and cell properties.

Electroporation Success	Odds Ratio	p value	Variables (transformed)	Odds Ratio	p value
PulseDuration	1.01	0.000	$\frac{PulseDuration}{50}$	1.87	0.00
Distance	0.289	0.000	Distance	0.29	0.00
Area	1.00	0.001	$\frac{1000}{Area}$	0.32	0.001

After the logistic regression analysis was carried out, probabilities of cell survivability and electroporation success were computed using Eq. 3.4. The probabilities were computed at the following experimental condition values: pulse duration 50-300 ms and d_m 2-10 μm. For all these experimental conditions, probabilities were computed for three cell sizes: small (5^{th} percentile; diameter: 19 μm), median (50^{th} percentile; diameter: 25 μm), and a large (95^{th} percentile; diameter 39 μm). The aspect ratio for these cell sizes ranged from 1-3. The median value of standard deviation of grey-level was taken. In the 3X3 matrix of contour plots in Figure

3.2, the cell size changes from left to right, and the aspect ratio changes in the vertical direction. In these contour plots, the red grid marks the area where the cell survivability is between 0-50 percent. The black grid marks the area where the electroporation success is between 0-50 percent. The green grid is the good area where there is a greater than 50 percent chance of cell survivability and greater than 50 percent chance of electroporation success. The blue grid which can only be seen in contour plots B, C, F and I, is the area where there is greater than 90 percent chance of both cell survival and electroporation success.

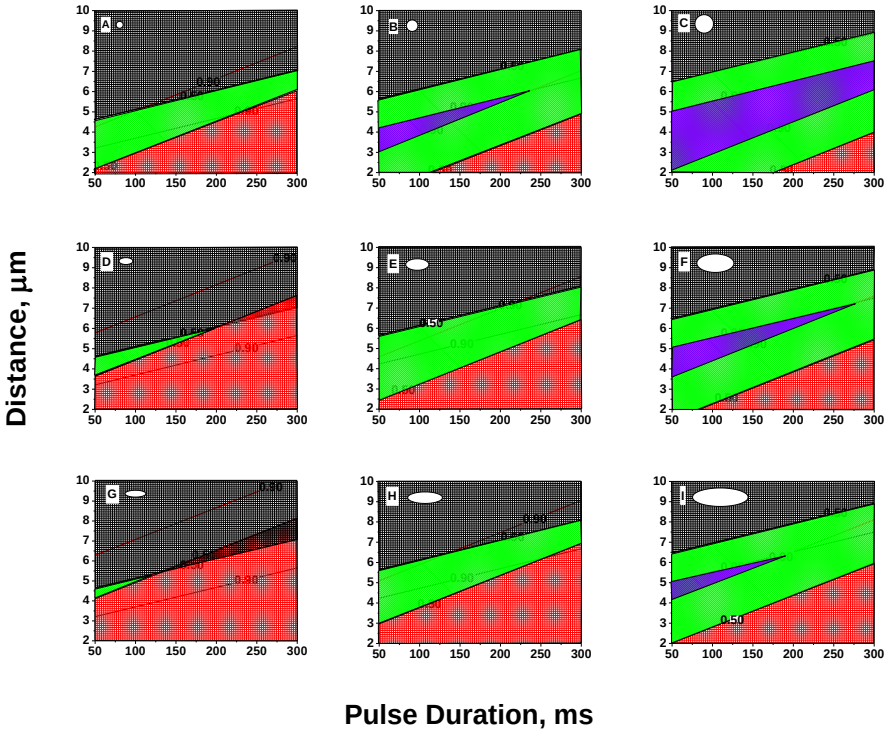

Figure 3.2. Contour plots of probabilities of cell survivability and electroporation success as a function of pulse duration , d_m and cell properties. The cell size changes in the horizontal direction. Aspect ratio changes in the vertical direction. Black grid marks the area of 0-50 % electroporation success. Red grid marks the area of 0-50 % cell survivability. Green grid marks the area of > 50 % electroporation success and > 50% cell survivability. Blue grid marks the area of > 90 % electroporation success and > 90 % cell survivability.

Simulation. Figure 3.3 is a false color image of the transmembrane potential for the three cell sizes.

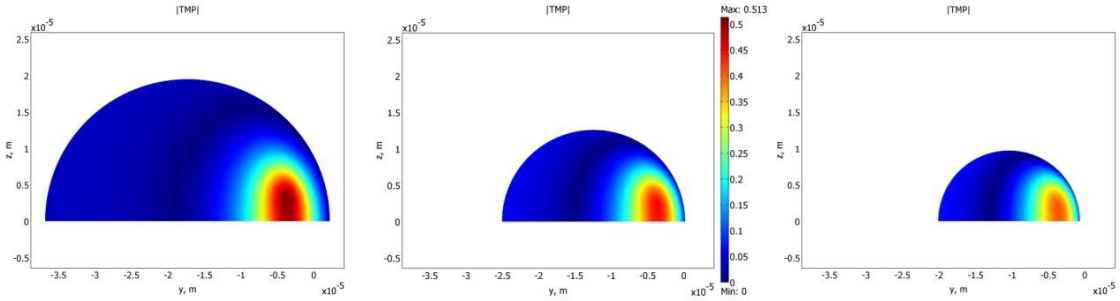

Figure 3.3. Simulated transmembrane potential for three cell sizes (side view): small (5th percentile; diameter: 19 µm), median (50th percentile; diameter: 25 µm), and large (95th percentile; diameter: 39 µm).

Figure 3.4A-C show the maximum transmembrane potential, the area permeabilized (A^*), and the fraction of the cell's surface area permeabilized (F^*) vs. distance.

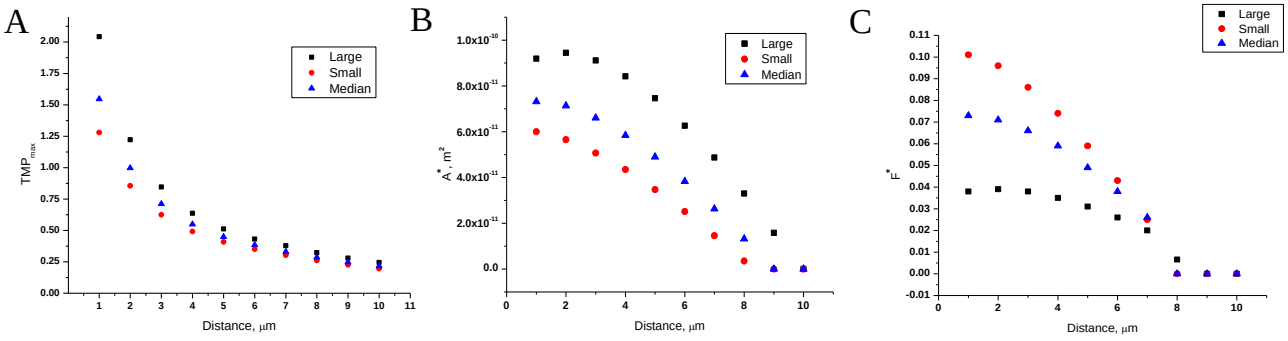

Figure 3.4. (A) TMP_{max} plotted as a function of distance for a large, median, and a small cell.**(B)** Cell area above the TMP_c (A^*) plotted as a function of distance for a large, median, and a small cell. **(C)** Fraction of the cell area above a TMP_c (F^*) plotted as a function of distance for a large, median, and a small cell.

False color, TMP_{max} vs. d_m and F^* vs. distance for cells varying in aspect ratio are qualitatively similar (Figure 3.5A-C).

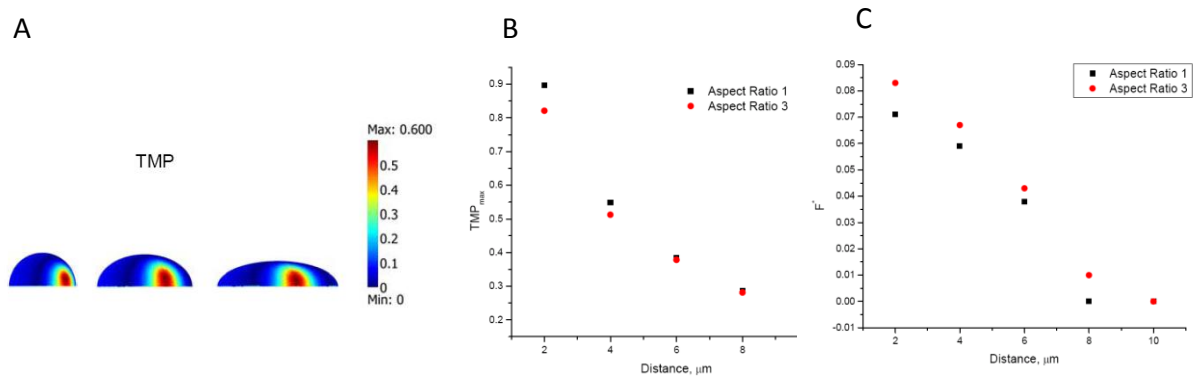

Figure 3.5. (A) Simulated transmembrane potential for three median cells (50th percentile; diameter 25 μm when aspect ratio is 1), with aspect ratio 1, 2, and 3. (B) TMP_{max} as a function of d_m for a median cell (50th percentile; diameter 25 μm when aspect ratio is 1), with aspect ratio 1, 2, and 3 (projected area is constant). (C) F^* as a function of d_m (50th percentile; diameter 25 μm when aspect ratio is 1), with aspect ratio 1, 2, and 3 (projected area is constant).

3.5 DISCUSSION

Variability within a set of experimental conditions is a big issue in bulk and single-cell electroporation. An example of variability in bulk electroporation can be seen in Gabriel and Teissie et al.[38] in which they showed significant variability in cell permeation and cell survivability under constant conditions. Significant variability in electroporation and cell viability under constant conditions is also observed in single-cell electroporation in a chip,[39, 40] and with an electrolyte-filled capillary.[18] In this paper, we have used statistical analysis to understand the variability in single-cell electroporation. We used several cell properties and experimental conditions and studied their effect on cell survivability and electroporation success. The cell properties were area, aspect ratio and standard deviation of the gray level. The experimental variables were pulse duration and d_m. From the results of factor analysis (Table 3.2)

and logistic regression (Tables 3.3 and 3.4), two cell properties were significant ($p < 0.05$); cell size (area) and cell shape (aspect ratio). The intensity factor had borderline significance. More experiments could perhaps resolve whether it is a significant factor or not. Pulse duration and d_m were also highly significant ($p < 0.05$). We have shown in a previous paper[32] that pulse duration and d_m affect cell survivability and electroporation success. Cell survivability decreases, but electroporation success increases as we go from shorter to longer pulses. Upon increasing the d_m, the cell survivability increases, but electroporation success decreases. In this work, our main aim was to understand how the cell properties and experimental conditions influence cell survivability and electroporation success. Analysis was also performed to study the interaction terms between the experimental conditions and the cell properties (for example, regression was run on the product of d_m and cell diameter). The interaction terms did not prove to be significant, thus the prediction of 'success' or 'viability' is not improved by their inclusion.

Figure 3.2 shows how the variables (cell properties and experimental conditions) influence the outcome (cell survivability and electroporation success). It can be seen that the cell properties have a considerable effect on the outcome. The green ('good') area increases from left to right, i.e., as the cell size increases. Furthermore, on moving vertically, the green area increases as the cells become more spherical. From these contour plots we can conclude that a wide range of values of pulse duration and d_m give good results for a large spherical cell (plot C). A small cell with a high aspect ratio (plot G) has the lowest probability of cell survival and electroporation success and there is a narrow range of pulse duration and d_m over which modest success can be expected.

Two cell-based factors are important: size and shape. In bulk electroporation, variability in cell permeabilization has been explained to some extent in terms of cell size. Puc et al.[41] in a

bulk electroporation experiment with 448 cells measured the size distribution of a cell population with flow cytometry. They determined experimentally that cell permeabilization and survival as a function of pulse amplitude can be explained to a large extent by cell size distribution about the mean. In bulk electroporation it is well established from the Schwan equation (Eq. 3.1) that the transmembrane potential for a spherical cell depends linearly on the cell size. A doubling of the cell's diameter leads to a doubling of the transmembrane potential. Higher transmembrane potential is related to greater permeabilization of the cell membrane.

In order to compare our results from single cell experiments with bulk electroporation and their dependence on cell size, we performed 3D simulations on hemispherical cells (Figure 3.3) using the finite element method with diameters corresponding to the 95th, 50th, and 5th percentiles of our cells (39, 25, 19 μm), and for tip-cell distances spanning the critical range (1 – 10 μm). The equation used to calculate the dependence (n) of transmembrane potential on cell radius at various d_m is the slope of a log-log plot:

$$n = \frac{\log(TMP_1 / TMP_2)}{\log(r_1 / r_2)} \tag{3.4}$$

where TMP_1 and TMP_2 are the transmembrane potentials at radii r_1 and r_2 of two different sized cells at a given d_m. The value of n is near 0.3. In bulk electroporation, n = 1. This can be inferred from Eq. 3.1. Thus, in single-cell electroporation the dependence of a cell's response on its size is significantly weaker than for bulk electroporation. The reason for this low dependence on cell size has to do with the relative dimensions of the tip opening diameter and the cell. When the tip opening is smaller than the cell, the field weakens considerably along the 'z' axis (the symmetry axis of the capillary). Thus, the magnitude of the total potential across the cell is dictated primarily by the potential at the cell surface proximal to the tip. A similar analysis comparing

values of A^* in the single-cell experiment to the bulk experiment gives a similar picture. The value of n (Eq. 3.4 with the ratio A^*_1/A^*_2 rather than TMP) is ~ 1 from the single cell simulations, but it is 2 for the bulk experiment.

Although simulation results (Figure 3.3 and Figure 3.4) show that the cell size dependence of transmembrane potential in single-cell electroporation is not very strong, it still helps us in understanding the variability in single-cell electroporation. Figure 3.4 A-C show that the maximum transmembrane potential, A^* and F^* for a small, median and a large cell are different at various cell-capillary tip distances. So, for example, if several cells were electroporated at identical conditions, a large cell would have for example, a smaller F^* than a small cell. This would therefore lead to considerable variability in the results.

Our results from the logistic regression analysis (Table 3.3 and Table 3.4) and the contour plots (Figure 3.2) show that a large, spherical cell has the maximum probability of cell survival and electroporation success. Simulation results (Figure 3.4 A and C) show that a large cell has a larger transmembrane potential but a smaller F^* than a small cell for $d_m < 7$ μm. We infer that the higher transmembrane potential of a large cell is responsible for the higher probability of electroporation success. Furthermore, as large cell has a smaller F^* than a small cell, this could mean that there is a smaller relative efflux of molecules from the cell, hence the probability of its cell survival would be higher. It is also possible that the differing values of transmembrane potential in the three sizes of cells lead to variations in pore size and resealing rates, which leads to differing mass transport rates and viability. However, the effect of transmembrane potential on pore size and kinetics is not very well known and is difficult to determine. It is also clear from the results that smaller cells require more investigation to determine under what conditions the probabilities of success and viability are higher.

The second important factor in our analysis is the shape factor. A recent report on bulk electroporation of cells under a microscope in the presence of a voltage-sensitive dye measured how transmembrane potential varied on irregularly shaped cells.[42] It has also been shown experimentally and numerically that for a spheroidal cell in suspension, the orientation of the cell with respect to a homogeneous field is an important parameter.[43] However, there are no reports that study experimentally the effect of a change in shape of the cell from spherical to spheroidal on cell permeabilization. Gimsa and Wachner[14] have given an analytical solution to calculate transmembrane potential induced by homogeneous fields on arbitrarily oriented cells of ellipsoidal shape. Using this mathematical framework for a homogeneous field, our calculations show that cells with the same projected area, and for the field perpendicular to the major axis, the transmembrane potential decreases as the aspect ratio of the cell increases. Also, our calculations show that at constant aspect ratio, the transmembrane potential increases as the size of the cell increases. In our single-cell electroporation experiments, where we have an inhomogeneous field as opposed to the homogeneous field in bulk electroporation, the change in aspect ratio of the cell shows a slightly different trend. From our 3D simulations (Figure 3.5B), we observed that at a constant projected area, changing the aspect ratio of the cell from 1 to 3 changed TMP_{max} less than 10% at all distances. These simulation results show that in single cell electroporation, transmembrane potential is almost independent of aspect ratio. These simulation results agree well with our logistic regression results (Table 3.4). Logistic regression results (Table 3.4) and also the contour plots (Figure 3.2) show that electroporation success, which is related to transmembrane potential is independent of aspect ratio of the cell as long as the projected area is kept constant. Our simulation results also show that when the aspect ratio of the cell is changed from 1 to 3 (projected area is kept constant), the fraction of cell (F^*) electroporated increases

(Figure 3.5C). This could mean that the cell with a large aspect ratio would have a larger efflux of molecules from the cell, and hence its probability of survival would be lower than a cell with a small aspect ratio. Our results from the contour plots (Figure 3.2) show a similar trend. When the aspect ratio of the cell is increased, but the projected area is kept constant, cell survivability is decreased.

Therefore, cell size and shape are significant parameters in cell permeabilization and inducing variability in electroporation. It is likely that success of electroporation is related to TMP_{max}, and survival is related to the fraction of the surface electroporated.

3.6 REFERENCES

(1) Neumann, E.; Kakorin, S.; Toensing, K. Fundamentals of electroporative delivery of drugs and genes. *Bioelectrochem Bioenerg*. **1999**, *48*, 3-16.

(2) Faurie, C.; Golzio, M.; Phez, E.; Teissie, J.; Rols, M. P. Electric field-induced cell membrane permeabilization and gene transfer: Theory and experiments. *Eng Life Sci.* **2005**, *5*, 179-186.

(3) Bonnafous, P.; Vernhes, M. C.; Teissie, J.; Gabriel, B. The generation of reactive-oxygen species associated with long-lasting pulse-induced electropermeabilization of mammalian cells is based on a non-destructive alteration of the plasma membrane. *Biochim et Biophys Acta, Biomembranes*. **1999**, *1461*, 123-134.

(4) Loste, F.; Eynard, N.; Teissie, J. Direct monitoring of the field strength during electropulsation. *Bioelectrochem Bioenerg*. **1998**, *47*, 119-127.

(5) Gift, E. A.; Weaver, J. C. Simultaneous quantitative determination of electroporative molecular uptake and subsequent cell survival using gel microdrops and flow cytometry. *Cytometry*. **2000**, *39*, 243-249.

(6) Neumann, E. Membrane electroporation and direct gene transfer. *Bioelectrochem Bioenerg*. **1992**, *28*, 247-267.

(7) Neumann, E.; Schaefer-Ridder, M.; Wang, Y.; Hofschneider, P. H. Gene transfer into mouse lyoma cells by electroporation in high electric fields. *EMBO J.* **1982**, *1*, 841-845.

(8) Zimmermann, U.; Riemann, F.; Pilwat, G. Enzyme loading of electrically homogeneous human red blood cell ghosts prepared by dielectric breakdown. *Biochimica et Biophysica Acta, Biomembranes*. **1976**, *436*, 460-474.

(9) Xie, T. D.; Sun, L.; Tsong, T. Y. Study of mechanisms of electric field-induced DNA transfection. I. DNA entry by surface binding and diffusion through membrane pores. *Biophys J.* **1990**, *58*, 13-19.

(10) Mir, L. M.; Orlowski, S.; Belehradek, J., Jr.; Paoletti, C. Electrochemotherapy potentiation of antitumour effect of bleomycin by local electric pulses. *Eur J Cancer (Oxford, England : 1990)*. **1991**, *27*, 68-72.

(11) Grosse, C.; Schwan, H. P. Cellular membrane potentials induced by alternating fields. *Biophys J.* **1992**, *63*, 1632-1642.

(12) Weaver, J. C.; Chizmadzhev, Y. A. Theory of electroporation: A review. *Bioelectrochem Bioenerg*. **1996**, *41*, 135-160.

(13) Kotnik, T.; Miklavcic, D. Analytical description of transmembrane voltage induced by electric fields on spheroidal cells. *Biophys J.* **2000**, *79*, 670-679.

(14) Gimsa, J.; Wachner, D. Analytical description of the transmembrane voltage induced on arbitrarily oriented ellipsoidal and cylindrical cells. *Biophys J.* **2001**, *81*, 1888-1896.

(15) Gimsa, J.; Wachner, D. A polarization model overcoming the geometric restrictions of the laplace solution for spheroidal cells: obtaining new equations for field-induced forces and transmembrane potential. *Biophys J.* **1999**, *77*, 1316-1326.

(16) Rae, J. L.; Levis, R. A. Single-cell electroporation. *Pfluegers Arch.* **2002**, *443*, 664-670.

(17) Haas, K.; Sin, W.-C.; Javaherian, A.; Li, Z.; Cline, H. T. Single-cell electroporation for gene transfer in vivo. *Neuron*. **2001**, *29*, 583-591.

(18) Nolkrantz, K.; Farre, C.; Brederlau, A.; Karlsson, R. I. D.; Brennan, C.; Eriksson, P. S.; Weber, S. G.; Sandberg, M.; Orwar, O. Electroporation of single cells and tissues with an electrolyte-filled capillary. *Anal Chem.* **2001**, *73*, 4469-4477.

(19) Kotnik, T.; Mir, L. M.; Flisar, K.; Puc, M.; Miklavcic, D. Cell membrane electropermeabilization by symmetrical bipolar rectangular pulses. Part I. Increased efficiency of permeabilization. *Bioelectrochemistry (Amsterdam, Netherlands)*. **2001**, *54*, 83-90.

(20) Xia, F.; Jin, W.; Yin, X.; Fang, Z. Single-cell analysis by electrochemical detection with a microfluidic device. *J Chromatogr A.* **2005**, *1063*, 227-233.

(21) Andersson, H.; van den Berg, A. Microtechnologies and nanotechnologies for single-cell analysis. *Curr Opin Biotechnol.* **2003**, *15*, 44-49.

(22) Huang, Y.; Chen, N.; Borninski, J.; Rubinsky, B. A novel microfluidic cell-chip for single cell analysis and manipulation. *Proceedings - IEEE Annual International Conference on Micro Electro Mechanical Systems, 16th, Kyoto, Japan, Jan. 19-23, 2003*. **2003**, 403-406.

(23) Wheeler, A. R.; Throndset, W. R.; Whelan, R. J.; Leach, A. M.; Zare, R. N.; Liao, Y. H.; Farrell, K.; Manger, I. D.; Daridon, A. Microfluidic device for single-cell analysis. *Anal Chem.* **2003**, *75*, 3581-3586.

(24) Stuart, J. N.; Sweedler, J. V. Single-cell analysis by capillary electrophoresis. *Anal Bioanal Chem.* **2003**, *375*, 28-29.

(25) Shaner, L. M.; Brown, P. R. Single cell analysis using capillary electrophoresis. *J Liq Chromatogr.* **2000**, *23*, 975-997.

(26) Krylov, S. N.; Dovichi, N. J. Single-cell analysis using capillary electrophoresis: influence of surface support properties on cell injection into the capillary. *Electrophoresis*. **2000**, *21*, 767-773.

(27) Sims, C. E.; Meredith, G. D.; Krasieva, T. B.; Berns, M. W.; Tromberg, B. J.; Allbritton, N. L. Laser-Micropipet Combination for Single-Cell Analysis. *Anal Chem.* **1998**, *70*, 4570-4577.

(28) Lillard, S. J.; Yeung, E. S. Capillary electrophoresis for the analysis of single cells: laser-induced fluorescence detection. *Handbook of Capillary Electrophoresis (2nd Edition)*. **1997**, 523-544.

(29) Swanek, F. D.; Ferris, S. S.; Ewing, A. G. Capillary electrophoresis for the analysis of single cells: electrochemical, mass spectrometric, and radiochemical detection. *Handbook of Capillary Electrophoresis (2nd Edition)*. **1997**, 495-521.

(30) Fasching, R. J.; Bai, S. J.; Fabian, T.; Prinz, F. B. Nanoscale electrochemical probes for single cell analysis. *Microelectron Eng.* **2006**, *83*, 1638-1641.

(31) Gao, N.; Wang, W.; Zhang, X.; Jin, W.; Yin, X.; Fang, Z. High-Throughput Single-Cell Analysis for Enzyme Activity without Cytolysis. *Anal Chem.* **2006**, *78*, 3213-3220.

(32) Agarwal, A.; Zudans, I.; Orwar, O.; Weber, S. G. Simultaneous maximization of cell permeabilization and viability in single-cell electroporation using an electrolyte-filled capillary. *Anal Chem.* **2007**, *79*, 161-167.

(33) Fabisiak, J. P.; Sedlov, A.; Kagan, V. E. Quantification of Oxidative/Nitrosative Modification of CYS34 in Human Serum Albumin Using a Fluorescence-Based SDS-PAGE Assay. *Antioxid Redox Sign.* **2002**, *4*, 855-865.

(34) Kagan, V. E.; Kuzmenko, A. I.; Tyurina, Y. Y.; Shvedova, A. A.; Matsura, T.; Yalowich, J. C. Pro-oxidant and antioxidant mechanisms of etoposide in HL-60 cells: role of myeloperoxidase. *Cancer Res.* **2001**, *61*, 7777-7784.

(35) Silva, G. A.; Czeisler, C.; Niece, K. L.; Beniash, E.; Harrington, D. A.; Kessler, J. A.; Stupp, S. I. Selective differentiation of neural progenitor cells by high-epitope density nanofibers. *Science*. **2004**, *303*, 1352-1355.

(36) Zudans, I.; Agarwal, A.; Orwar, O.; Weber, S. G. Numerical calculation of single-cell electroporation with an electrolyte-filled capillary. *Biophys J*. **2007**, *92*, 3696-3705.

(37) Weisberg, S. *Applied linear regression*, 2nd ed., 1985.

(38) Gabriel, B.; Teissie, J. Control by electrical parameters of short- and long-term cell death resulting from electropermeabilization of Chinese hamster ovary cells. *Biochim et Biophys Acta, Mol Cell Res*. **1995**, *1266*, 171-178.

(39) Fox, M. B.; Esveld, D. C.; Valero, A.; Luttge, R.; Mastwijk, H. C.; Bartels, P. V.; van den Berg, A.; Boom, R. M. Electroporation of cells in microfluidic devices: a review. *Anal Bioanal Chem*. **2006**, *385*, 474-485.

(40) Khine, M.; Lau, A.; Ionescu-Zanetti, C.; Seo, J.; Lee, L. P. A single cell electroporation chip. *Lab Chip*. **2005**, *5*, 38-43.

(41) Puc, M.; Kotnik, T.; Mir, L. M.; Miklavcic, D. Quantitative model of small molecules uptake after in vitro cell electropermeabilization. *Bioelectrochemistry*. **2003**, *60*, 1-10.

(42) Pucihar, G.; Kotnik, T.; Valic, B.; Miklavcic, D. Numerical determination of transmembrane voltage induced on irregularly shaped cells. *Ann Biomed Eng,*. **2006**, *34*, 642-652.

(43) Valic, B.; Golzio, M.; Pavlin, M.; Schatz, A.; Faurie, C.; Gabriel, B.; Teissie, J.; Rols, M.-P.; Miklavcic, D. Effect of electric field induced transmembrane potential on spheroidal cells: theory and experiment. *Euro Biophys J*. **2003**, *32*, 519-528.

4.0 CONTROL OF THE RELEASE OF FREELY DIFFUSING MOLECULES IN SINGLE-CELL ELECTROPORATION

This work has been submitted to Biophysical Journal

4.1 ABSTRACT

Single-cell electroporation using an electrolyte-filled capillary is an emerging technique for transient pore formation in adherent cells. Because adherent cells do not have a simple and consistent shape, and because the electric field emanating from the tip of the capillary is inhomogeneous, the Schwan equation based on spherical cells in homogeneous electrical fields does not apply. We sought to determine experimental and cell parameters that influence the outcome of a single-cell electroporation experiment. A549 cells were exposed to the thiol-reactive dye Thioglo-1, leading to green fluorescence from intracellular thiol adducts. Electroporation causes a decrease in intracellular fluorescence intensity of Thioglo-1-loaded cells that can be measured as a function of time. The transient curves thus obtained are well-described by a simple model originally developed by Puc *et al.* We find that the steady-state fluorescence following electroporation is related to the capillary tip-to-cell distance and cell size (specifically, $2(A/\pi)^{1/2}$ where A is the area of the cell's image in pixels. This quantity is the diameter if the

image is a circle). In separate experiments, the relationship obtained can be used to control the steady state fluorescence following electroporation by adjusting the tip-to-cell distance based on cell size. The relationship was applied successfully to A549 as well as DU 145, and PC-3 cells. Finally, F-tests show that the variability in the steady state fluorescence (following electroporation) is decreased when the tip-to-cell distance is controlled according to the derived relationship in comparison to experiments in which the tip-cell distance is a constant irrespective of cell size.

4.2 INTRODUCTION

Electroporation [1-9] is a technique that uses electric fields to create transient nanopores in a cell's membrane, dramatically increasing its permeability. This technique has been studied and applied for almost three decades. Over that time, it has been used to transport molecules, chiefly DNA, across cell membranes for a wide range of applications such as gene therapy,[10, 11] molecular biology,[4, 12] and clinical chemotherapy.[13]

There are two types of electroporation, namely bulk electroporation and single-cell electroporation. In bulk electroporation, a batch of cells in suspension is exposed to a macroscopically uniform electric field of a few kilovolts per centimeter resulting in the permeabilization of many cells at the same time.[7, 8, 14-16] Neumann *et al.* in the early 1980s demonstrated gene transfection by bulk electroporation of mammalian cells.[4] Ever since, bulk electroporation has become a standard method for introduction of DNA into cells. However, bulk electroporation results in a distribution of outcomes among the cells in the suspension. It would

be preferable, especially to study the membrane biophysics of cell permeabilization, to electroporate at the single-cell level.

Single-cell electroporation has shown promise, especially for application to natural, adherent cells, but is not as well studied as bulk electroporation. Single-cell electroporation should not be confused with bulk electroporation in which numerous cells are permeabilized, but only individual cells are studied.[17-20] In single-cell electroporation, a localized field is applied to a single adherent cell or a cell in suspension flowing through a microfabricated device, while the neighboring cells are exposed to very low or no field.[21-27] Lundqvist *et al.* first demonstrated single-cell electroporation using carbon-fiber microelectrodes in 1998.[28] Since then, numerous other single-cell electroporation techniques using electrolyte-filled capillaries,[24, 29] micropipettes, [30] microfabricated chips,[31-33] and multi-walled carbon nanotubes[34] have been developed.

In *bulk* electroporation experiments, several workers have determined how to increase transport of DNA, dyes, and drugs across the cell membrane.[35-37] Normally, optimizing conditions for gene transfection in bulk electroporation has been the focus of studies.[4, 38-40] Although transfection is of practical importance, it does not give a direct measure of transport across the membrane because transcription and translation involve many steps in addition to the transport of DNA such as DNA/membrane interaction, the translocation and migration of the plasmid into the cytoplasm, its passage into the nucleus and the activation of expression. Other bulk electroporation studies have measured dye uptake to determine the effect of conditions on the success of electroporation.[36] A few bulk electroporation studies have quantified uptake of small fluorescent molecules using flow cytometry following bulk electroporation.[9, 35] Small molecule uptake in bulk electroporation depends on electroporation parameters such as field strength, pulse length, number of pulses,[41-43] cell size and shape,[18] and other experimental

conditions such as temperature, buffer,[44] *etc*. However, significant variability both in the observed result and in viability under constant conditions is generally observed in bulk electroporation.[43, 45] Prausnitz and Canatella[46] used a statistical approach to predict the uptake of calcein and cell viability following bulk electroporation. Their prediction is based on a nonlinear regression approach to an empirical equation. Based on data for a single cell type, the experimental parameters important to permeabilization and viability were field strength, pulse length, and number of pulses. The empirical expression was useful for sixty different cell types. This rather impressive result solidifies the idea that it is the lipid bilayer's response to an electric field that controls bulk electroporation. We note that the model predicts the average behavior of a large population of cells. It is a telling measure of the inherent variability in the experiment that predictions within a factor of two of the observed result were considered satisfactory. To summarize, there are abundant quantitative studies of the electrical response of a cell in a homogeneous electric field and of the mass transport of molecules into an electroporated cell in bulk electroporation.

There are no experimental reports on a quantitative treatment of single-cell electroporation. An advantage of single-cell electroporation is the ability to relate a result to properties of the cell, not only to experimenter-controlled parameters. However, this dependence is hard to predict because single-cell electroporation lacks the symmetry of bulk electroporation. In the present work, we investigate single cell electroporation quantitatively for the first time. The experimental method is based on first labeling thiols inside the cell with a maleimide-based fluorogenic reagent, Thioglo-1. Loss of fluorescence from diffusion of Thioglo-1 conjugates out of the cell was measured as a function of time. In a first set of experiments, which we will call Set 1, the steady state fluorescence following electroporation was correlated with experimental

variables and parameters of the cell. In a second set of experiments, which we will call Set 2, information from the first set was used to control the steady-state fluorescence following electroporation. We show that a simple model developed for bulk electroporation describing the uptake of small molecules of cells in suspension[45] applies, following suitable modification, to the release of molecules from single, adherent cells. We show that for constant experimental conditions (Set 1), there is considerable variability in the extent of freely diffusing molecule release in single-cell electroporation. Finally, we show that, with statistical significance, we can control the magnitude of molecular flux from single cells, and decrease the variability of the outcome if the size of the individual, adherent cell is taken into account in establishing the electroporation conditions (Set 2).

4.3 EXPERIMENTAL SECTION

Materials. The chemicals used for buffer preparation were all analytical grade and were purchased from Sigma (St. Louis, MO). Thioglo-1 was purchased from Covalent Associates (Woburn, MA). Propidium iodide and calcein AM were purchased from Invitrogen/Molecular Probes (Eugene, OR). The cell lines A549, DU 145, and PC-3 were obtained from ATCC (Manassas, VA). Basal medium Eagle (BME), RPMI-1640, trypsin-EDTA, fetal bovine serum, L-glutamine, penicillin, and streptomycin were all obtained from Gibco-BRL (Carlsbad, CA). Milli-Q (Millipore Synthesis A 10, Billerica, MA) water was used. Extracellular buffer consisted of (mM) NaCl, 140.0; KCl, 5.0; $MgCl_2$, 2.0; $CaCl_2$, 2.0; D-glucose, 10; HEPES, 10.0; pH adjusted to 7.40 with NaOH.

Cell Culture and Staining. Human lung cancer A549 cells were cultured in BME supplemented with 10 % fetal bovine serum, 100 U/mL penicillin, and 100 µg/mL streptomycin. DU 145 and PC-3 cells were grown in RPMI-1640 medium with 0.3 g/L L-glutamine, 10 % fetal bovine serum, 100 U/mL penicillin, and 100 µg/mL streptomycin. Cells were grown as a monolayer in 75-mL cell culture flasks at 37 °C and 95% air/5% CO_2 (HERA cell incubator, Newtown, CT). Before the experiments, cells were plated on 35-mm, glass-bottom cell culture dishes (MatTek Corp., Ashland, MA) and were grown for up to 3 days. Experiments were performed on the second and third days following the cell plating. Before the experiments, the cells were stained with cell-permeable dye Thioglo-1 (2 μM in extracellular buffer) for 30 s at room temperature, then washed with extracellular buffer twice. Thioglo-1 is a maleimide-based reagent that gives a highly fluorescent product upon its reaction with active SH groups.[47, 48] Cell dishes were mounted on the cell chamber (DH 35i culture dish incubator, Warner Instruments, Holliston, MA), and transferred to the stage of the microscope.

Probe Preparation. Fused-silica capillaries from Polymicro Technology (Phoenix, AZ) were used as a probe to perform electroporation experiments. Capillaries were pulled with a CO_2 laser puller (Sutter Instruments Co. P-2000, Novato, CA) to create reproducible capillaries with a short pulled tip having an inner diameter of ~ 5 µm. The final length of the capillaries was 15 cm.

Electroporation setup. To electroporate a cell (Figure 4.1), the pulled tip of the capillary was submerged in the cell dish containing extracellular buffer. The other end of the capillary was placed in a vial filled with extracellular buffer. A platinum electrode placed in this vial was connected to the electroporator (ECM 830, BTX Instruments, San Diego, CA), and the electrical circuit was completed with a grounded platinum electrode placed in the cell dish. The capillary

resistance was measured immediately prior to electroporation. The resistance determining circuit consisted of a synthesized function generator (SRS Model DS 340, Stanford Research Systems, Inc., Sunnyvale, CA) and a lock-in amplifier (SRS Model SR 830 DSP) which has an internal current-to-voltage converter. The function generator applied a continuous 2 V sine wave AC signal at 100 Hz across the aforementioned Pt electrodes with the electrolyte-filled capillary in place. The current resulting from the 2V across the resistance of the capillary was measured by the lock-in amplifier. The resistance informed us about the status of the tip. Tips with an opening of 5 μm that are not clogged have a resistance of about 1.4 x 10^7 Ω. The test circuit is switched off during electroporation.

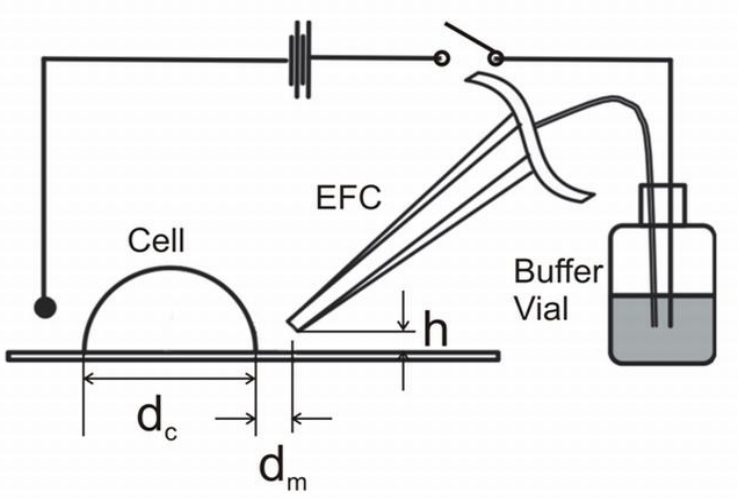

Figure 4.1. Schematic diagram of the experimental setup.

Fluorescence Imaging. Cells were observed through a 40X 1.3 NA oil immersion objective using an inverted microscope (Olympus, IX 71, Melville, NY) equipped with an HBO 100-W mercury lamp as the excitation source. For Thioglo-1, an Omega fluorescence cube (specially built, Omega, Brattleboro, VT) was used with filters for excitation at 378 nm and emission at 480 nm. For live/dead imaging, a triple band 'Pinkel' filter set from Semrock (Rochester, NY) was used (exciter 1 387 nm, exciter 2 494 nm; exciter 3 575 nm; dichroic mirror: 394– 414 nm,

484 – 504 nm, 566 – 586 nm, emitter: 457, 530, 628 nm). A CCD camera (Hamamatsu, ORCA-285, Bridgewater, NJ) imaged cells. The image collection frequency was 1 frame/s. Image processing was performed by the image acquisition software Simple PCI (Compix, Inc., Sewickley, PA).

Electroporation. There were two sets of experiments. In 'Set 1', A549 cells were exposed to single pulses of 500 V. This will be referred as 'pulsing' of the cells. The pulse duration ranged from 300-500 ms, while the tip-cell distance, d_m (see Figure 4.1) was set at 2.0, 3.5 or 5.0 μm. The pulse was applied 25 s from the start of the acquisition of images. Diffusive loss of fluorescent thiol (chiefly reduced glutathione) adducts from the cell was determined quantitatively with Simple PCI software. Further details of single-cell electroporation can be found elsewhere.[29, 49]

In the second set ('Set 2'), A549, PC-3, and DU 145 cells were used. Information from Set 1 experiments was used to determine what value of d_m to use for a given cell, based on its size (the average diameters of the cells were A549: 25 μm, DU 145: 23.5 μm, and PC-3: 23 μm), to achieve a particular steady state fluorescence.

Cell Parameters. Cell parameters representing size, shape, and intensity were obtained by Simple PCI software. The size factors used were area, diameter, perimeter and breadth. The area, A, is the total number of pixels in a cell, the diameter is computed as $2\,(A/\pi)^{1/2}$, the perimeter is the distance traveled around the boundary of the cell, the breadth is the average width of the cell's image. The shape factor is the aspect ratio (maximum length/maximum breadth). Intensity is the average gray level of the pixels in the object.

Measurement of tip-cell distance. A 15-cm-long pulled capillary with a tip of ~ 5 μm in diameter was positioned near a cell using an MP-285 motorized micromanipulator from Sutter

(Novato, CA).The capillary was first positioned at about a 45° angle with respect to the cell dish normal 5 micrometers above the surface (Figure 4.1). The distance between the capillary tip and the cell (d_m) was taken to be from the closest approach of the cell and the projection of the capillary image in the horizontal imaging plane.

Statistical Analysis. Fluorescence decay data from 130 cells comprise the Set 1 data. Stepwise forward and backward linear regression analyses were performed using the program STATA (Intercooled 9.0). The dependent variable was *K*, the ratio of mass transport rate constant to pore resealing rate constant (see below, Eq. 4.2). *K* is also related to the long-time (steady-state or limiting) fluorescence intensity as shown in Eq. 4.1.

$$K = \ln \frac{F^0}{F_{ss}} \tag{4.1}$$

where F^0 is the fluorescence intensity at the time of the application of the pulse and F_{ss} is the steady fluorescence at long times. The independent variables used in the regression were the cell parameters area, diameter, perimeter, breadth, aspect ratio, intensity; and the experimental conditions: d_m and pulse duration. The cell parameters were transformed to get a normal distribution. The transformations are shown in Table 4.1. Regression analysis was based on the transformed variables.

Table 4.1. Cell variables and their transformations

Variable (x)	Transformation
area	$\frac{1}{x}$
diameter	$\frac{1}{x}$
perimeter	$\frac{1}{\sqrt{x}}$
breadth	$\sqrt{x}$
aspect ratio	$\sqrt{x}$
intensity	x^2

Predictive electroporation experiments. In order to validate the regression results, Set 2 electroporation experiments were performed again on the A549 cell line. Further, to validate our results for different cell lines, experiments were performed on two more cell lines: prostate adenocarcinoma cell lines PC-3 and DU 145. For this set of experiments we fixed the percent fluorescence intensity loss 100 (1- F_{ss}/F^0), which we will call ΔF%. For example, in the case of PC-3 cell line, cells were pulsed to achieve a 50% loss. In order to do so, the diameter of the cell to be pulsed was first measured using the Simple PCI software, then according to Eq. 4.4 the d_m at which the cell should be pulsed was determined. Similarly, experiments were performed on A549 cells to obtain ΔF% equal to 20 %, and 40 %, and on cell line DU 145 to obtain ΔF% equal to 40 %.

Cell Viability Assay. Following electroporation experiments, live/dead analysis was performed on the cells. The buffer in the cell dish was replaced by 2 mL of fresh growth medium. The cells were allowed 5-6 h of recovery in the 37 °C incubator with 95% air/5% CO_2, followed by a 30

minute staining with 2 µM (each) calcein AM and propidium iodide. Cell survival percentage was calculated for each experimental condition based on this live/dead assay. It is important to note that a measurement of cell viability was made on each cell that was electroporated.

4.4 RESULTS

In the present work, extracellular buffer (high Na^+) was used to perform the experiments as opposed to intracellular buffer (high K^+) used in our previous work.[29, 49] The range of pulse durations used in the previous experiments performed with intracellular buffer was 50-300 ms at 500 V. The range of pulse durations used in the current work with extracellular buffer was 300-500 ms at 500 V. When using extracellular buffer at pulse durations below 300 ms the electroporation success for A549 cells was very low (< 20 %). Moreover, we found that the survival rate was higher with extracellular buffer as compared to intracellular buffer under the same set of experimental conditions. For example, at pulsing conditions of 300 ms and d_m 2 µm, the survival rate with intracellular buffer was only ~0-5 %, whereas in the case of extracellular buffer, the survival rate was ~ 65 %. At longer distance, e.g. at pulse duration of 300 ms and d_m 5 µm, the survival rate with intracellular buffer was 60 %, whereas in the case of extracellular buffer, it was 95 %. Thus, we have used only extracellular buffer in this work.

In both Set 1 and Set 2 experiments, the function given in Eq. 4.2 was fitted to fluorescence intensity vs. time curves.

$$F = F^0 e^{(-kt)} e^{\left[K\left(e^{-\alpha t}-1\right)\right]} \tag{4.2}$$

Here F is the fluorescence intensity at time t, F^0 is the fluorescence intensity at time zero when the pulse is applied, k is the photobleaching rate constant, $K = \frac{M}{\alpha}$ where M is the first order rate constant for transport of Thioglo-1 labeled molecules out of the cell and α is the first order pore resealing rate constant. This equation results from incorporating a photobleaching term into the equation from Puc *et al.*[45] A program written in Mathcad (Mathsoft, Cambridge, MA) was used to fit decay curves, to estimate the parameters k, K, and α, and provide a goodness of fit R^2. Figure 4.2 gives an example of Eq. 4.2 fitted to a set of data. Here, the circles represent the data from a cell that was pulsed for 300 ms with cell-to-capillary tip distance of 3.5 μm. The solid line is the best fit that was obtained using the Mathcad program. Table 4.2 gives a list of parameter definitions.

Table 4.2. List of parameter definitions.

Parameter	Definition
k	photobleaching rate constant, s^{-1}
K	ratio of mass transport rate constant to pore resealing rate constant, unitless
a	pore resealing rate constant, s^{-1}
d_c	cell diameter, mm
d_m	distance between the capillary tip and the cell, taken from the closest approach of the cell and the projection of the capillary image in the horizontal imaging plane, mm (See Fig. 4.1)

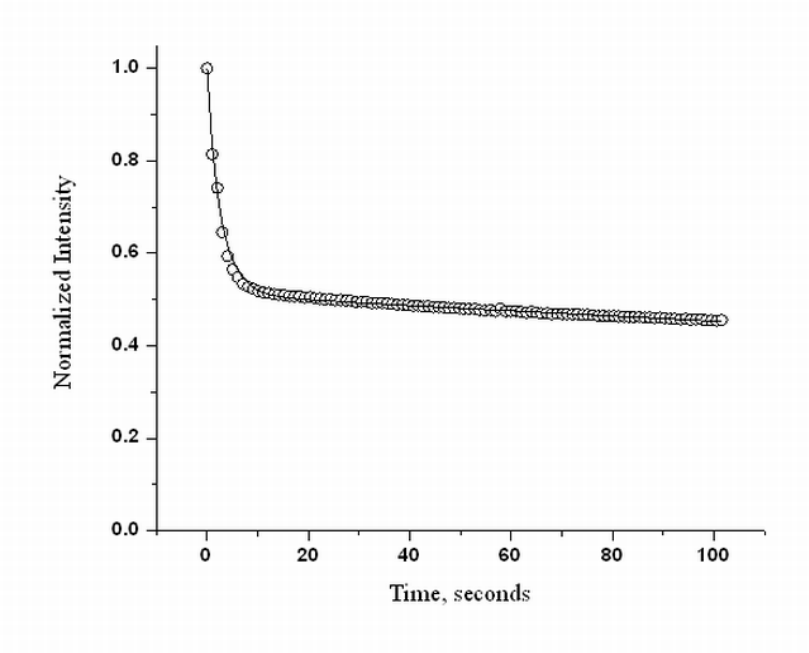

Figure 4.2. A representative curve-fitting of the experimental data (Set 1). Circles represent the experimental data (normalized fluorescence intensity).

In initial explorations of the curve-fitting procedure, we used Eq. 4.3.

$$F = F^0 e^{(-kt)} e^{\left[\frac{M}{\alpha}\left(e^{-\alpha t}-1\right)\right]} \tag{4.3}$$

which, except for the photobleaching term, directly reflects the derivation of Puc *et al.* [45]. It was found that M, and α were somewhat correlated ($\rho_{M\alpha} = 0.48$). When replacing the ratio M/α by the parameter K, we found no correlation between the fit parameters K and α ($\rho_{K\alpha} = -0.06$). By minimizing the correlation between these two fit parameters, the error in the result is also minimized. We should mention that K and α are not 'adjusted' to compensate for photobleaching. Rather, the photobleaching rate constant is one of the parameters determined along with K and α. It turns out that the parameter K is useful in its own right. It is related to the fraction of the cell's fluorescent contents remaining at steady state, as shown above in Eq. 4.1. The value of K is important because it is a time-independent result of electroporation, the

variability of which we seek to control. Our goal is to explain the variability (Set 1 experiments) and then use that understanding to control the result (Set 2 experiments).

Set 1 experiments

Recall that Set 1 experiments represent a survey of ΔF% for a set of cells of various sizes and shapes, and of various tip-cell distances and pulse times. In this set of experiments, the tip-cell distance was set arbitrarily for any given cell. A histogram of ΔF% for all the cells pulsed at 2 μm d_m is shown in Figure 4.3. The average ΔF% for these cells was 53 %, with a standard deviation of percent loss in intensity (ΔF%) of 24 %. The wide distribution ΔF% shows that there is a large variability in the outcome even when the tip-cell distance is constant.

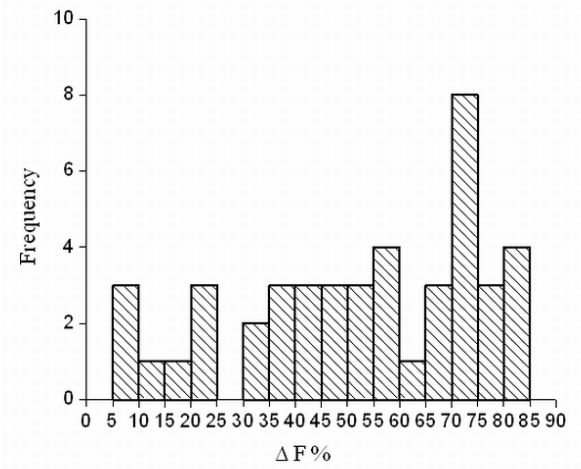

Figure 4.3. Histogram of ΔF% for all the cells electroporated at 2 μm d_m in Set 1 experiments. For the x-axis labeling, the second number which defines the interval is exclusive, whereas the first number is inclusive. e.g., for ΔF of 5-10 %, the interval goes from 5.000 to 9.999.

In order to understand what variables affect *K*, we did multiple linear regression of *K* on the transformed independent variables pulse duration, tip-cell distance d_m, and the cell parameters in Table 4.1. The 'size' (parameters area, diameter, perimeter and breadth) are all highly correlated, but we do not know which is a better predictor (if any) of *K*. Thus, we used stepwise regression. The results from stepwise forward and backward linear regression of *K* on

the transformed variables (Table 4.1) are shown in Table 4.3 and Eq. 4.4. There is significant relationship (r^2 = 0.30, p < 0.001 for the coefficients of d_m and d_c^{-1}, p=0.694 for the constant) between dependent variable K and independent variables d_m and cell diameter d_c (μm).

$$K = -0.175 d_m + \frac{27.8}{d_c} + 0.122 \qquad (4.4)$$

The fact that cell-size parameters other than diameter do not appear in the regression should not be taken to mean that they are not important.

Table 4.3. Results of linear regression analysis of K on experimental conditions and cell parameters. Values of d_m and d_c are in μm.

	Coefficient	Standard Error	p value
d_m *(a)*	-0.18	0.036	< 0.001
$1/d_c$ *(b)*	28	6.8	< 0.001
Constant (c)	0.12	0.31	0.69

The regression results were used to make a contour plot of ΔF% as a function of d_m and d_c (Figure 4.4). The contour plot shows that at a given d_m, a smaller cell has a larger ΔF% than a larger cell. It is instructive to consider the likely spread of values of ΔF% for a fixed d_m given the cell size distribution shown in the Box plot in Figure 4.4. The Box plot in Figure 4.4 represents the distribution of cell sizes in percentiles: 5^{th}, 25^{th}, 50^{th}, 75^{th}, and 95^{th} (12, 19, 22, 27, and 36 μm respectively). It is apparent that the median cell is predicted to lose 50% of its fluorescence at a d_m of about 3.9 μm. The spread of expected values (5 to 95 %ile) of fluorescence loss is fairly

high at any value of d_m. It is clear that fixing the capillary tip-cell distance, d_m, is not sufficient to control tightly the field strength at the cell and thus the outcome of electroporation.

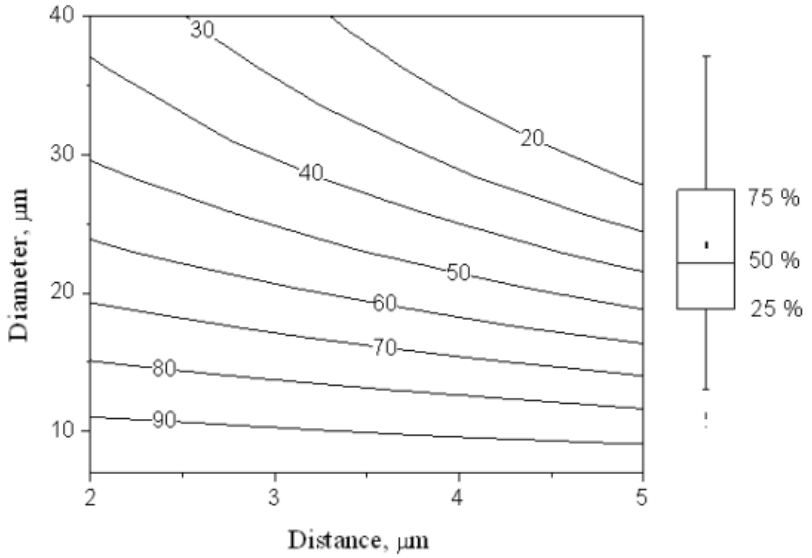

Figure 4.4. Contour plot of ΔF% as a function of cell diameter and cell-capillary tip distance. The box plot gives the 5th, 25th, 50th, 75th, and 95th percentile of cell sizes corresponding to d_c 12, 19, 22, 27, and 36 μm.

Set 2 experiments

Recall that in Set 2, the tip-cell distance was adjusted for each cell to achieve a particular ΔF%. We performed additional electroporation experiments on A549 cells, and also on PC-3, and DU 145 cells. In these experiments, we sought to control ΔF%. Using Eq. 4.1 and Eq. 4.4 we could relate ΔF% to d_m and d_c. A table was created with d_m and d_c that yield a particular ΔF%. The d_m was chosen from this table for each individual cell based on its diameter, d_c. Each cell's transient was recorded, Eq. 4.2 was fit to the data, and a value of ΔF% was obtained. Results are shown in Table 4.4 for three cell types and for several predicted values of ΔF%. For example, the top row shows results from our attempt to obtain a ΔF% of 20 % from A549 cells. The 95 % confidence interval for ΔF% for these cells was [15, 22]. As Table 4.4 shows, the other experiments showed similarly accurate predictions.

Table 4.4. Expected ΔF%, average ΔF% observed, standard error of the mean 95 % confidence interval of the mean, and survival % for cell lines A549, PC-3, and DU 145.

Cell Line (number of cells)	Expected ΔF%	Average ΔF% observed	Standard error of the mean	95 % confidence interval for the mean	Survival %
A549 (15)	20	18	1.9	[15, 22]	100
A549 (21)	40	41	2.4	[36, 45]	95
DU 145 (15)	40	38	2.1	[34, 42]	100
PC-3 (15)	50	52	3.8	[44, 59]	86

Figure 4.5 is a histogram of ΔF% for A549 cells electroporated in Set 1 (d_m = 2 μm) and Set 2 experiments. The large spread in Set 1 experiments shows that there is a large variance in the results (histogram A). Histograms B and C in Figure 4.5 show that we were able to reduce this variance by taking d_c into account (Eq. 4.4) when setting d_m. To further verify this reduction in the variance between Set 1 and Set 2 experiments, an F-test was performed between Set 1 and each of the Set 2 intensity loss observations. The results are shown in Table 4.5. The F-test

results show that the variances in Set 2 experiments were reduced significantly ($p < 0.05$) for all cell types.

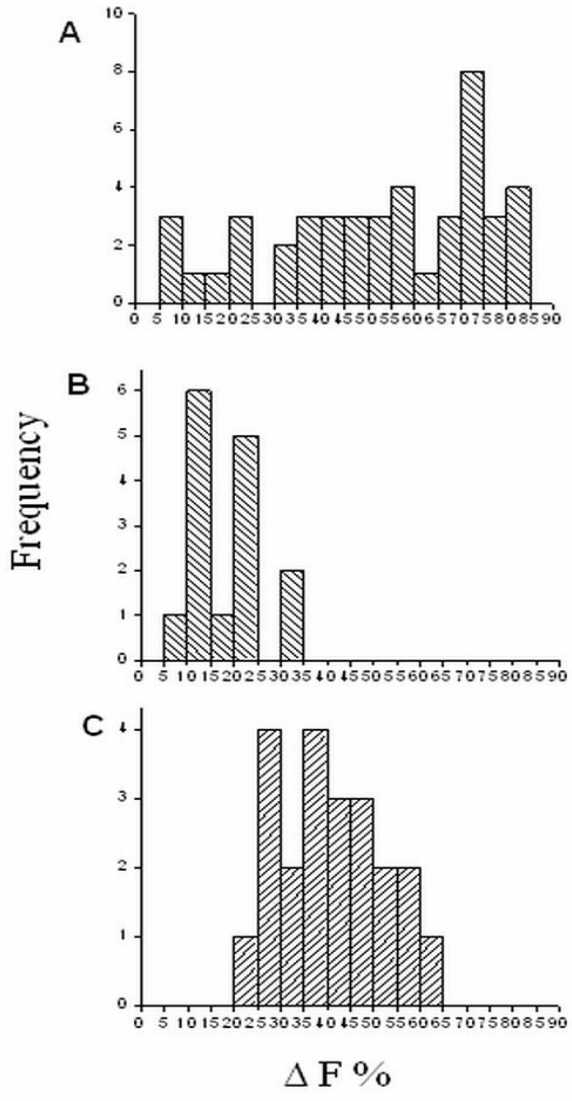

Figure 4.5. Histogram of ΔF% for A549 cells electroporated in set 1 (d_m = 2 μm) (A) and set 2 experiments (B, C) Histogram B represents cells electroporated to achieve ΔF% = 20%, and C represents ΔF% = 40%.

Table 4.5. F-test results on variance in ΔF% between set 1 and set 2 experiments. (*df is degrees of freedom).

Cell Line	Expected ΔF%	df_1*	df_2	F	p value (<)
A549	20	44	14	9.77	0.001
A549	40	44	20	4.22	0.001
DU 145	40	44	14	8.34	0.001
PC-3	50	44	14	2.43	0.05

4.5 DISCUSSION

The issue of variability in electroporation is not new. Large variability in bulk and single-cell electroporation has been observed before.[29, 43] Our aim in the present work is to understand what experimental and cell-based parameters control the release of freely diffusing molecules from single cells following electroporation, and use that understanding to increase predictability and reduce the variability in our experiments. In these experiments, the cells were labeled with a thiol-reactive dye Thioglo-1. As the most abundant thiol in the cell is reduced glutathione, GSH, we can say that the decrease in fluorescence intensity inside the cell following application of the pulse is predominantly due to the efflux of labeled glutathione from the cell. As the GSH-ThioGlo-1 conjugate has a formula weight of 684.7 Da, we view it as an indicator of the flux of freely diffusing molecules.

It is hard to predict membrane permeability upon the exposure to an electric field for adherent cells. For spherical cells exposed to uniform electric fields (bulk electroporation), the potential drop across the membrane is dictated by the Schwan equation.[50] Bulk electroporation of adherent, hemispherical cells would form the same dependence by symmetry as long as the field is parallel to the insulating surface. The potential drop across the membrane depends on the magnitude of the homogeneous electric field, the cell size, and the polar angle on the cell surface. Therefore, part of the variability in bulk electroporation can be attributed to the cell size distribution about the mean.[45] In single-cell experiments, where a highly focused or an inhomogeneous field is applied, there is no simple model analogous to the Schwan equation.[51] Numerical simulations[49] show that the transmembrane potential depends on the tip-cell distance, the polar angle from the long axis of the capillary, and the cell size. The cell-size dependence of the fraction of the cell's surface area that is electroporated is smaller in single-cell electroporation ($\propto d_c^{0.33}$) than in the bulk experiment ($\propto d_c^{1.0}$).[49] In the single-cell experiment, the most critical variable is d_m, as it governs the electric field at the cell for a given applied voltage and capillary length. Thus, it is not surprising to find that both d_c and d_m are significant predictors. Equation 4.4 can be used to estimate the right tip-to-cell distance for a desired concentration decrease (or increase if diffusive flux is inward rather than outward). If, for example, a fluorescence decrease of 50% is desired and the cell diameter is 22 μm, then the equation directs us to use a d_m of 3.9 μm. The prediction of d_m in relation to d_c in controlling release of small molecules is useful also in order to find the right distance for loading cells with small molecules.

The results (Table 4.4) show that for all cell lines (A549, DU 145, and PC-3), the predicted ΔF% lies within the 95 % confidence interval of the observed ΔF%. Further, F-tests

(Table 4.5) show that the variance in Set 2 was significantly reduced compared to Set 1. This is strong evidence that we can control ΔF% by controlling d_m in accordance with Eq. 4.4. To our knowledge, this is the first time that control over small molecule release has been achieved for single-cell electroporation. In our previous research (using high K^+ buffer) we investigated conditions leading to successful electroporation and cell viability. The observations were binary in nature, *i.e.*, either a cell was electroporated or it was not. In those experiments, we observed a large variability (*e.g.*, the average ΔF% for all cells electroporated at 2 μm d_m was 55 % with a standard deviation of 30 %) in success and survivability at a given set of conditions.[29, 49] We found that cell size and shape were significant factors in controlling success and survivability. Thus, at constant experimental conditions, the natural variability of the cells led to variability in the outcome. Nonetheless, we found conditions (experimental and cell parameters) at which we could maximize cell permeabilization and survivability. The present work goes one step beyond that. We have quantified the degree of electroporation. Also, we have not only found one of the factors that induces variability in the experiments, but have also been able to reduce this variability by controlling the d_m according to Eq. 4.4. We note also, see Table 4.4, that the survival rate for the Set 2 experiments is quite acceptable.

The statistical results in Tables 4.4 and 4.5 show two things. Table 4.4 demonstrates that taking into account the cell size in setting the tip-cell distance is critical to achieving a particular ΔF% on average. Table 4.5 demonstrates that taking into account the cell size in setting the tip-cell distance significantly reduces the variability of the outcome of electroporation (in terms of ΔF%). The experimental significance of the reduction in variance is a decrease in the number of experiments required to achieve a particular standard error of the mean given a particular experimental variability. Thus, with statistical rigor, we have demonstrated the advantage of

distance control based on cell size in single-cell electroporation. However, it is also true that the variability is still rather large. At this point, we do not know the cause of the variability, although it is by now well-known that cell-to-cell variability is to be expected in single-cell experiments of any sort. It is very likely that the parameter *K* depends on aspects of cell physiology that we do not now control.

It is interesting to pursue the origin of Eq. 4.4 from a causal rather than an observational (regression) perspective. Transient permeabilization in an electric field results when the transmembrane potential exceeds a critical value. Estimates of the critical value vary, but we have found that the value established by Teissie and Rols[52] of 250 mV is consistent with our observations.[51] We have also previously determined the fraction of a hemispherical cell's exposed area ($\pi d_c^2/2$) that has a transmembrane potential greater than the critical value in single-cell electroporation with an electrolyte-filled capillary.[29] We define f_p as the fraction of the cell's surface area that has a transmembrane potential greater than or equal to the critical value at t=0 (i.e., before the electrical conductance of the membrane increases because of the increased porosity. This permeabilized fraction, f_p is a function of tip-cell distance and of cell diameter.[49] The area of a cell that is permeabilized contributes to the efflux of a chemical species through the membrane.[42] A simple first order rate constant for the loss of material from a cell can be given as

$$M = \frac{A}{V}P \tag{4.5}$$

where *A* is the permeabilized area of the cell, *V* is the cell's volume and *P* is the permeability of the solute through the (porated) membrane. The permeabilized area, *A*, is equal to the product of the cell's surface area, $\pi d_c^2/2$ and the fraction of the area that is permeabilized. The permeabilized area is thus $\frac{\pi}{2} f_p d_c^2$. The cell's volume is $\pi d_c^3/12$.

We can thus write

$$M = \frac{6 f_p P}{d_c} \tag{4.6}$$

This mass transport coefficient is the same as that in Puc *et al.* mentioned above. It is the mass transport coefficient in the presence of the field, assumed constant. Recall from Eq. 4.3 that the time dependent part of the dynamics (pore resealing) is embodied in the time variable – the parameters M, α, and K are time-independent. We also assume here that the mass transport occurs solely by diffusion (e.g., not by electrophoresis) because we do not see experimentally a rapid drop in fluorescence at the time the pulse is applied (called 'g' in Puc *et al.*). The computed values of f_p (called FEA in Figure 6 of Agarwal[49]) fit well to second order polynomials in d_m (See Supplementary Material, Table S4.1). Using these polynomials, we calculated values of the term $6f_p/d_c$. This term is well-described by Eq. 4.7 ($r^2 = 0.87$, p values for coefficients of d_m and d_c^{-1} are <0.0001, for the constant, $p = 0.24$, see Supplementary Material, Table S4.2).

$$\frac{6 f_p}{d_c} = -2.16 \times 10^{-3} d_m + \frac{0.6228}{d_c} - 0.00262 \tag{4.7}$$

This dependence is remarkably similar to the dependence seen for K (Eq. 4.4 and Table 4.3). The magnitudes of the parameters cannot be compared directly for the two equations, however the relative parameter values can be. We note that in both equations the coefficient of d_m is negative, the coefficient of d_c^{-1} is positive and the constant term is statistically indistinguishable from zero (See Supplementary Material, Table S4.2 for regression statistics for Eq. 4.7). Further, the ratios of the coefficients of d_c^{-1} to the coefficients of d_m are similar, on the order of 10^2.

It is possible to make an inference about the electroporation process from this similarity. The functional similarity of Eqs. 4.4 and 4.7 means that the ratio of the two equations is approximately constant (not dependent on the independent variables). Explicit computation of the ratio show that the ratio is approximately constant except for large cells and long distances - cases in which there is little or no fluorescence loss. Algebraically, the ratio of the two quantities

on the left-hand sides of Eqs. 4.4 and 4.7 is equal to P/α. We infer that this ratio is approximately constant.

Krassowska's group has developed a pore formation and closure model based on energies and measured or estimated parameters.[53] In this model, after the electric pulse is removed all pores rapidly shrink to same pore area, *i.e.*, the minimum-energy radius, r_m. Hence, after removal of electric field, cells reseal from the same minimum-energy radius r_m.[53, 54] Thus, the pore resealing rate is considered to be a constant. Indeed, while our measured values vary over a range of values (~0.1 – 1 s^{-1}) values of α were not correlated with any experimental or cell parameter. If the pore resealing rate is approximately constant and the ratio P/α is approximately constant for all cells then we can conclude that, under the conditions of our experiments, the permeability of the cell immediately after the potential is returned to zero (P) is approximately independent of electroporation and cell-based parameters. Further, as we know the ratio P/α, and α, we can estimate P. This is necessarily highly approximate, so only an order of magnitude estimate is justified. We define P as the ratio of diffusion coefficient to membrane thickness, D/l, multiplied by a porosity, ϕ. The porosity ϕ refers to the effective fraction of the electroporated area (itself a fraction of the cell's surface area) through which molecules pass. Using $D \sim 10^{-10}$ m^2s^{-1}, $l \sim 4$ nm, $\alpha \sim 0.1$ s^{-1}, we obtain $\phi \sim 10^{-4}$, a reasonable value.[20, 36]

One important application of our present work of controlled release of small molecules from single cells is in single-cell analysis. The analysis of cytoplasmic contents of single cells using microfluidics and separations has become an important research area.[55-59] This is because highly efficient and sensitive detection of the components in a single cell will explain important physiological processes and therefore improve our understanding of basic cellular processes. Generally, in the process of single-cell analysis, the cell is destroyed. It would be helpful to be

able to sample a cell's cytoplasm over time. Our present work is a major step in this direction as the ability to predict/control small molecular release will provide better handle at reproducibility in single-cell small molecular release experiments.

4.6 REFERENCES

(1) Kinosita, K., Jr.; Tsong, T. Y. Voltage-induced pore formation and hemolysis of human erythrocytes. *Biochim Biophys Acta*. **1977**, *471*, 227-242.

(2) Kinosita, K., Jr.; Tsong, T. Y. Hemolysis of human erythrocytes by a transient electric field. *Proc Natl Acad Sci U S A.* **1977**, *74*, 1923-1927.

(3) Teissie, J.; Tsong, T. Y. Electric field induced transient pores in phospholipid bilayer vesicles. *Biochemistry*. **1981**, *20*, 1548-1554.

(4) Neumann, E.; Schaefer-Ridder, M.; Wang, Y.; Hofschneider, P. H. Gene transfer into mouse lyoma cells by electroporation in high electric fields. *EMBO J.* **1982**, *1*, 841-845.

(5) Sugar, I. P.; Neumann, E. Stochastic model for electric field-induced membrane pores. Electroporation. *Biophys Chem.* **1984**, *19*, 211-225.

(6) Bliss, J. G.; Harrison, G. I.; Mourant, J. R.; Powell, K. T.; Weaver, J. C. Electroporation: the population distribution of macromolecular uptake and shape changes in red blood cells following a single 50 ms square wave pulse. *Bioelectrochem Bioenerg*. **1988**, *20*, 57-71.

(7) Prausnitz, M. R.; Bose, V. G.; Langer, R.; Weaver, J. C. Electroporation of mammalian skin: a mechanism to enhance transdermal drug delivery. *Proc Natl Acad Sci U S A.* **1993**, *90*, 10504-10508.

(8) Pliquett, U.; Weaver, J. C. Electroporation of human skin: simultaneous measurement of changes in the transport of two fluorescent molecules and in the passive electrical properties. *Bioelectrochem Bioenerg*. **1996**, *39*, 1-12.

(9) Gift, E. A.; Weaver, J. C. Simultaneous quantitative determination of electroporative molecular uptake and subsequent cell survival using gel microdrops and flow cytometry. *Cytometry*. **2000**, *39*, 243-249.

(10) Xie, T. D.; Tsong, T. Y. Study of mechanisms of electric field-induced DNA transfection. II. Transfection by low-amplitude, low-frequency alternating electric fields. *Biophys J*. **1990**, *58*, 897-903.

(11) Xie, T. D.; Sun, L.; Tsong, T. Y. Study of mechanisms of electric field-induced DNA transfection. I. DNA entry by surface binding and diffusion through membrane pores. *Biophys J*. **1990**, *58*, 13-19.

(12) Zimmermann, U.; Riemann, F.; Pilwat, G. Enzyme loading of electrically homogeneous human red blood cell ghosts prepared by dielectric breakdown. *Biochim Biophys Acta*. **1976**, *436*, 460-474.

(13) Mir, L. M.; Orlowski, S.; Belehradek, J., Jr. ; Paoletti, C. Electrochemotherapy potentiation of antitumour effect of bleomycin by local electric pulses. *Euro J Cancer (Oxford, England : 1990)*. **1991**, *27*, 68-72.

(14) Teissie, J.; Eynard, N.; Vernhes, M. C.; Benichou, A.; Ganeva, V.; Galutzov, B.; Cabanes, P. A. Recent biotechnological developments of electropulsation. A prospective review. *Bioelectrochemistry (Amsterdam, Netherlands)*. **2002**, *55*, 107-112.

(15) Teissie, J.; Golzio, M.; Rols, M. P. Mechanisms of cell membrane electropermeabilization: A minireview of our present (lack of ?) knowledge. *Biochim Biophys Acta*. **2005**, *1724*, 270-280.

(16) Gehl, J. Electroporation: Theory and methods, perspectives for drug delivery, gene therapy and research. *Acta Physiol Scand.* **2003**, *177*, 437-447.

(17) Sixou, S.; Teissie, J. Exogenous uptake and release of molecules by electroloaded cells: a digitized videomicroscopy study. *Bioelectrochem Bioenerg*. **1993**, *31*, 237-257.

(18) Valic, B.; Golzio, M.; Pavlin, M.; Schatz, A.; Faurie, C.; Gabriel, B.; Teissie, J.; Rols, M.-P.; Miklavcic, D. Effect of electric field induced transmembrane potential on spheroidal cells: theory and experiment. *Euro Biophys J.* **2003**, *32*, 519-528.

(19) Gabriel, B.; Teissie, J. Time courses of mammalian cell electropermeabilization observed by millisecond imaging of membrane property changes during the pulse. *Biophys J*. **1999**, *76*, 2158-2165.

(20) Pucihar, G.; Kotnik, T.; Miklavcic, D.; Teissie, J. Kinetics of Transmembrane Transport of Small Molecules into Electropermeabilized Cells. *Biophys J*. **2008**, *95*, 2837-2848.

(21) Rae, J. L.; Levis, R. A. Single-cell electroporation. *Pfluegers Arch.* **2002**, *443*, 664-670.

(22) Haas, K.; Sin, W.-C.; Javaherian, A.; Li, Z.; Cline, H. T. Single-cell electroporation for gene transfer in vivo. *Neuron*. **2001**, *29*, 583-591.

(23) Olofsson, J.; Nolkrantz, K.; Ryttsen, F.; Lambie, B. A.; Weber, S. G.; Orwar, O. Single-cell electroporation. *Curr Opin Biotechnol.* **2003**, *14*, 29-34.

(24) Nolkrantz, K.; Farre, C.; Brederlau, A.; Karlsson, R. I. D.; Brennan, C.; Eriksson, P. S.; Weber, S. G.; Sandberg, M.; Orwar, O. Electroporation of single cells and tissues with an electrolyte-filled capillary. *Anal Chem.* **2001**, *73*, 4469-4477.

(25) Sims, C. E.; Meredith, G. D.; Krasieva, T. B.; Berns, M. W.; Tromberg, B. J.; Allbritton, N. L. Laser-Micropipet Combination for Single-Cell Analysis. *Anal Chem.* **1998**, *70*, 4570-4577.

(26) Huang, Y.; Sekhon, N. S.; Borninski, J.; Chen, N.; Rubinsky, B. Instantaneous, quantitative single-cell viability assessment by electrical evaluation of cell membrane integrity with microfabricated devices. *Sensor Actuat A-Phys*. **2003**, *A105*, 31-39.

(27) Valero, A.; Post, J. N.; van Nieuwkasteele, J. W.; ter Braak, P. M.; Kruijer, W.; van den Berg, A. Gene transfer and protein dynamics in stem cells using single cell electroporation in a microfluidic device. *Lab Chip*. **2008**, *8*, 62-67.

(28) Lundqvist, J.; Anders. Sahlin, F.; Aberg, M. A. I.; Stromberg, A.; Eriksson, P. S.; Orwar, O. Altering the biochemical state of individual cultured cells and organelles with ultramicroelectrodes. *Proc Natl Acad Sci U S A.* **1998**, *95*, 10356-10360.

(29) Agarwal, A.; Zudans, I.; Orwar, O.; Weber, S. G. Simultaneous maximization of cell permeabilization and viability in single-cell electroporation using an electrolyte-filled capillary. *Anal Chem.* **2007**, *79*, 161-167.

(30) Ryttsen, F.; Farre, C.; Brennan, C.; Weber, S. G.; Nolkrantz, K.; Jardemark, K.; Chiu, D. T.; Orwar, O. Characterization of single-cell electroporation by using patch-clamp and fluorescence microscopy. *Biophys J*. **2000**, *79*, 1993-2001.

(31) Huang, Y.; Rubinsky, B. Microfabricated electroporation chip for single cell membrane permeabilization. *Sensor Actuat A-Phys*. **2001**, *A89*, 242-249.

(32) Khine, M.; Lau, A.; Ionescu-Zanetti, C.; Seo, J.; Lee, L. P. A single cell electroporation chip. *Lab Chip*. **2005**, *5*, 38-43.

(33) He, H.; Chang, D. C.; Lee, Y.-K. Micro pulsed radio-frequency electroporation chips. *Bioelectrochemistry*. **2006**, *68*, 89-97.

(34) Rojas-Chapana, J.; Troszczynska, J.; Firkowska, I.; Morsczeck, C.; Giersig, M. Multi-walled carbon nanotubes for plasmid delivery into *Escherichia coli* cells. *Lab Chip*. **2005**, *5*, 536-539.

(35) Canatella, P. J.; Karr, J. F.; Petros, J. A.; Prausnitz, M. R. Quantitative study of electroporation-mediated molecular uptake and cell viability. *Biophys J*. **2001**, *80*, 755-764.

(36) Neumann, E.; Toensing, K.; Kakorin, S.; Budde, P.; Frey, J. Mechanism of electroporative dye uptake by mouse B cells. *Biophys J*. **1998**, *74*, 98-108.

(37) Rols, M. P.; Teissie, J. Electropermeabilization of mammalian cells: quantitative analysis of the phenomenon. *Biophys J*. **1990**, *58*, 1089-1098.

(38) Faurie, C.; Golzio, M.; Phez, E.; Teissie, J.; Rols, M. P. Electric field-induced cell membrane permeabilization and gene transfer: Theory and experiments. *Eng Life Sci*. **2005**, *5*, 179-186.

(39) Maasho, K.; Marusina, A.; Reynolds, N. M.; Coligan, J. E.; Borrego, F. Efficient gene transfer into the human natural killer cell line, NKL, using the Amaxa nucleofection system. *J Immunol Methods*. **2004**, *284*, 133-140.

(40) Tao, W.; Wilkinson, J.; Stanbridge, E. J.; Berns, M. W. Direct gene transfer into human cultured cells facilitated by laser micropuncture of the cell membrane. *Proc Natl Acad Sci U S A.* **1987**, *84*, 4180-4184.

(41) Loste, F.; Eynard, N.; Teissie, J. Direct monitoring of the field strength during electropulsation. *Bioelectrochem Bioenerg*. **1998**, *47*, 119-127.

(42) Rols, M.-P.; Teissie, J. Electropermeabilization of mammalian cells to macromolecules: control by pulse duration. *Biophys J*. **1998**, *75*, 1415-1423.

(43) Gabriel, B.; Teissie, J. Control by electrical parameters of short- and long-term cell death resulting from electropermeabilization of Chinese hamster ovary cells. *Biochim Biophys Acta*. **1995**, *1266*, 171-178.

(44) Djuzenova, C. S.; Zimmermann, U.; Frank, H.; Sukhorukov, V. L.; Richter, E.; Fuhr, G. Effect of medium conductivity and composition on the uptake of propidium iodide into electropermeabilized myeloma cells. *Biochim Biophys Acta*. **1996**, *1284*, 143-152.

(45) Puc, M.; Kotnik, T.; Mir, L. M.; Miklavcic, D. Quantitative model of small molecules uptake after in vitro cell electropermeabilization. *Bioelectrochemistry*. **2003**, *60*, 1-10.

(46) Canatella, P., J.; Prausnitz, M., R. Prediction and optimization of gene transfection and drug delivery by electroporation. *Gene Ther*. **2001**, *8*, 1464-1469.

(47) Fabisiak, J. P.; Sedlov, A.; Kagan, V. E. Quantification of Oxidative/Nitrosative Modification of CYS34 in Human Serum Albumin Using a Fluorescence-Based SDS-PAGE Assay. *Antioxid Redox Sign*. **2002**, *4*, 855-865.

(48) Kagan, V. E.; Kuzmenko, A. I.; Tyurina, Y. Y.; Shvedova, A. A.; Matsura, T.; Yalowich, J. C. Pro-oxidant and antioxidant mechanisms of etoposide in HL-60 cells: role of myeloperoxidase. *Cancer Res.* **2001**, *61*, 7777-7784.

(49) Agarwal, A.; Zudans, I.; Weber, E., A. ; Olofsson, J.; Orwar, O.; Weber, S. G. Effect of cell size and shape on single-cell electroporation. *Anal Chem.* **2007**, *79*, 3589-3596.

(50) Grosse, C.; Schwan, H. P. Cellular membrane potentials induced by alternating fields. *Biophys J*. **1992**, *63*, 1632-1642.

(51) Zudans, I.; Agarwal, A.; Orwar, O.; Weber, S. G. Numerical calculations of single-cell electroporation with an electrolyte-filled capillary. *Biophys J*. **2007**, *92*, 3696-3705.

(52) Teissie, J.; Rols, M. P. An experimental evaluation of the critical potential difference inducing cell membrane electropermeabilization. *Biophys J*. **1993**, *65*, 409-413.

(53) Smith, K. C.; Neu, J. C.; Krassowska, W. Model of creation and evolution of stable electropores for DNA delivery. *Biophys J*. **2004**, *86*, 2813-2826.

(54) Saulis, G. Pore Disappearance in a Cell after Electroporation: Theoretical Simulation and Comparison with Experiments. *Biophys J*. **1997**, *73*, 1299-1309.

(55) Cannon, D. M., Jr. ; Winograd, N.; Ewing, A. G. Quantitative chemical analysis of single cells. *Ann Rev Bioph Biom*. **2000**, *29*, 239-263, 232 Plates.

(56) Bergquist, J.; Josefsson, E.; Tarkowski, A.; Ekman, R.; Ewing, A. Measurements of catecholamine-mediated apoptosis of immunocompetent cells by capillary electrophoresis. *Electrophoresis*. **1997**, *18*, 1760-1766.

(57) Han, F.; Wang, Y.; Sims, C. E.; Bachman, M.; Chang, R.; Li, G. P.; Allbritton, N. L. Fast Electrical Lysis of Cells for Capillary Electrophoresis. *Anal Chem.* **2003**, *75*, 3688-3696.

(58) Meredith, G. D.; Sims, C. E.; Soughayer, J. S.; Allbritton, N. L. Measurement of kinase activation in single mammalian cells. *Nature Biotech*. **2000**, *18*, 309-312.

(59) Stuart, J. N.; Sweedler, J. V. Single-cell analysis by capillary electrophoresis. *Anal Bioanal Chem*. **2003**, *375*, 28-29.

4.7 SUPPLEMENTARY MATERIAL

Table S4.1.

Fits for f_p vs tip-cell distance over the range 1-7 μm (input data from (49))

Distance/μm	f_p for 39 μm cells
1	0.038
2	0.039
3	0.038
4	0.035
5	0.031
6	0.026
7	0.020

Model: Parabola

Equation: $y = A + Bx + Cx^2$

χ^2/df	r^2
1.7922×10^{-7}	0.99769

Parameter	Value	Error
A	0.03678	0.00066

B	0.00228	0.00038
C	-0.00067	0.00005

Distance/μm	f_p for 19 μm cells
1	0.101
2	0.096
3	0.086
4	0.074
5	0.059
6	0.043
7	0.025

Model: Parabola

Equation: $y = A + Bx + Cx^2$

χ^2/df	r^2
7.7381×10^{-7}	0.99935

Parameter	Value	Error
A	0.10629	0.00137
B	-0.00327	0.00079
C	-0.0012	0.0001

Distance/μm	f_p for 25 μm cells
1	0.073
2	0.071
3	0.066
4	0.059
5	0.049
6	0.038
7	0.026

Model: Parabola

Equation: $y = A + Bx + Cx^2$

χ^2/df	r^2
4.1667×10^{-7}	0.99911

Parameter	Value	Error
A	0.07429	0.00101
B	0.00019	0.00058
C	-0.00102	0.00007

Table S4.2.

Fit for $6f_p/d_c$ vs d_m and d_c^{-1} (Eq. 7)

Param	Value	Error	t-Value	Prob>|t|
Y-Int	-0.00261	0.0031	-0.84	0.41002
d_m	-0.00216	0.00037	-5.86	<0.0001
d_c^{-1}	0.623	0.067	9.32	<0.0001

R-Square(COD)	Adj. R-Square	Root-MSE(SD)
0.	0.85635	0.00338

ANOVA Table:

Item	Degrees of Freedom	Sum of Squares	Mean Square	F Statistic
Model	2	0.00138	0.00069	60.61
Error	18	2.05×10^{-4}	1.1×10^{-5}	
Total	20	0.00159		

Prob>F

<0.0001

5.0 CELL VIABILITY IN SINGLE-CELL ELECTROPORATION

5.1 ABSTRACT

Electroporation is now routinely used in cell and molecular biology and in clinical applications. It is therefore important to preserve cell viability following permeabilization of the cells. Single-cell electroporation using electrolyte-filled capillaries was performed on fluorescently labeled A549 cells. Cells were subjected to brief pulses (300-500 ms) at various cell-capillary tip distances followed by survivability assay on each cell. The loss of fluorescence intensity due to release of Thioglo-1 conjugates from the cell as a result of electroporation was measured as a function of time. A significant relationship exists between cell survival and intensity loss at steady state. It was found that cell survivability could be retained by controlling the magnitude of molecular efflux from single cells. This result was used to control cell survivability of A549, DU 145, and PC-3 cells in a separate set of experiments. It was also found that across the three cell lines, there is a 100 % chance of cell survival by controlling the molecular efflux from single cells at 55 % or less.

5.2 INTRODUCTION

Electroporation is a technique that uses electric fields to induce nanometer-sized pores in the cell membrane thereby allowing impermeable molecules such as DNA, dyes, and drugs to enter a cell.[1-10] Pores are formed in the cell membrane when the transmembrane potential exceeds the dielectric breakdown voltage of the cell membrane (0.2 – 1.0 V).[11, 12] The subsequent growth of the pores is governed by various factors such as pulse duration, number of pulses or the ionic strength of the medium.[13] Depending upon the conditions used for electroporation, the pores can either be transient or short lived in reversible electroporation or long lived in irreversible electroporation. Cell viability is maintained in reversible electroporation as the pores reseal in this case, whereas cell death occurs in irreversible electroporation as the pores do not reseal. The lifetime of the pores in reversible electroporation has been reported to be on the order of seconds to minutes.[14]

One of the important aspects of electroporation is to optimize experimental conditions to achieve reversible electroporation so that the cells can return to their normal physiological state following permeabilization. As electroporation is now routinely being used in cell and molecular biology, and clinical applications such as gene therapy, gene transfection, and drug delivery, there is a need to design protocols such that the cell viability is preserved. Studies have shown that cell viability in both bulk and single-cell electroporation depends on electric field parameters such as field strength,[15-17] pulse duration,[17, 18] number of pulses delivered,[19, 20] cell characteristics such as size and shape,[21-23] medium of electroporation,[24] and temperature. One of the most comprehensive studies of understanding the dependence of cell viability on experimental conditions was carried out by Canatella et al.[25] They used flow cytometry to study viability of prostate cancer DU 145 cells for more than 200 different combinations of experimental conditions. Their results showed

that viability has a complex dependence on field strength, pulse length, and number of pulses. Gabriel and Teissie[15] evaluated the role of electric field parameters in short-term and long-term death of Chinese hamster ovary cells following electropermeabilization. Short-term cell death was evaluated in the minute range after electropulsation, and the long-term death was evaluated 24 hours after electropulsation. Their results showed that the cell death (short-term and long-term) was linearly related to the fraction of the membrane area brought to the permeabilized state. Also, their results showed that high survival rate was obtained with single pulse with high intensity than with repetitive pulses with small intensity.

Although studies have been performed to optimize experimental conditions to achieve reversible electroporation, cell survivability is typically reported as a measure of percentage of cell survival at various conditions of electroporation.[18, 22, 25, 26] The aim of the present work is to determine the relation between molecular efflux from single cells and cell survivability, irrespective of the conditions of electroporation. Such results will be a useful guide in understanding the biochemical processes leading to cell death. In the present work, we studied the diffusion of fluorescently labeled thiol adducts from single cells through pores induced by transient electric fields in real time.[22, 27] In contrast to transfection, which involves a complex multistep DNA transfer into cells, the escape of dyes allows for direct quantification of translocated species by fluorescence microscopy. In the first set of experiments (Set 1), single fluorescent A549 cells were pulsed at various conditions (pulse duration: 300-500 ms, cell-capillary tip distance: 2.0-5.0 μm) followed by cell survivability assay on each cell. The results showed that there is a significant relationship ($p < 0.05$) between cell survivability and intensity loss at steady state. In a separate set of experiments (Set 2), the information from Set 1 experiments was used to successfully control cell viability in A549 and two more cell lines DU

145 and PC-3. Further, combined results from Set 1 and Set 2 experiments showed that cell survivability can be preserved across the three cell lines A549, DU 145, and PC-3 cells by controlling the magnitude of molecular efflux from single cells at 55 % or less.

5.3 EXPERIMENTAL SECTION

Materials. The chemicals used for buffer preparation were all analytical grade and were purchased from Sigma (St. Louis, MO). Thioglo-1 was purchased from Covalent Associates (Woburn, MA). Propidium iodide and calcein AM were purchased from Invitrogen/Molecular Probes (Eugene, OR). The cell lines A549, DU 145, and PC-3 were obtained from ATCC (Manassas, VA). Basal medium Eagle (BME), RPMI-1640, trypsin-EDTA, fetal bovine serum, L-glutamine, penicillin, and streptomycin were all obtained from Gibco-BRL (Carlsbad, CA). Milli-Q (Millipore Synthesis A 10, Billerica, MA) water was used. Extracellular buffer consisted of NaCl, 140.0 mM; KCl, 5.0 mM; $MgCl_2$, 2.0 mM; $CaCl_2$, 2.0 mM; D-glucose, 10 mM; HEPES, 10.0 mM; pH adjusted to 7.40 with NaOH.

Cell Culture and Staining. A549, DU 145, and PC-3 cells were cultured as previously described.[17, 21, 27] Cells were plated on 35-mm, glass-bottom cell culture dishes (MatTek Corp., Ashland, MA) and were grown for 1-3 days. Experiments were performed on the second and third days following the cell plating. The cells were stained with a cell-permeable dye Thioglo-1 (2 μM in extracellular buffer) for 30 s at room temperature. Thioglo-1 is a maleimide-based reagent that gives a highly fluorescent product upon its reaction with active SH groups.[28, 29] Cells were washed and bathed in the extracellular buffer, mounted on the cell chamber (DH 35i culture dish incubator, Warner Instruments, Holliston, MA), and transferred to the stage of the microscope.

Electroporation Setup. Details of single-cell electroporation can be found elsewhere.[17, 21, 27] Briefly, the experimental setup consists of two switchable circuits, the electroporation circuit and the test circuit. The electroporation circuit is depicted in Figure 5.1. A 15-cm-long pulled capillary (prepared in-house)[17] with a tip of ~ 5 μm in diameter was used to perform single-cell electroporation experiments. The capillary was positioned near a single cell at about a 45° angle with respect to the cell dish normal 5 μm above the surface using an MP-285 motorized micromanipulator from Sutter (Novato, CA). The distance between the capillary tip and the cell (d_m) was taken to be from the closest approach of the cell and the projection of the capillary image in the horizontal imaging plane. The other end of the capillary was placed in a vial filled with extracellular buffer. A platinum electrode placed in this vial was connected to the electroporator (ECM 830, BTX Instruments, San Diego, CA), and the electrical circuit was completed with a grounded platinum electrode placed in the cell dish. The test circuit was used to determine the resistance of the capillary prior to electroporation thereby giving information about the status of tip. The test circuit consisted of a synthesized function generator (SRS Model DS 340, Stanford Research Systems, Inc., Sunnyvale, CA) and a lock-in amplifier (SRS Model SR 830 DSP) with an internal current-to-voltage converter. The function generator applied a continuous 2 V sine wave AC signal at 100 Hz across the platinum electrodes with the electrolyte-filled capillary in place. The current resulting from the 2V across the resistance of the capillary was measured by the lock-in amplifier. Tips with an opening of 5 μm that are not clogged have a resistance of about $1.4 \times 10^7\ \Omega$. The test circuit is switched off during electroporation.

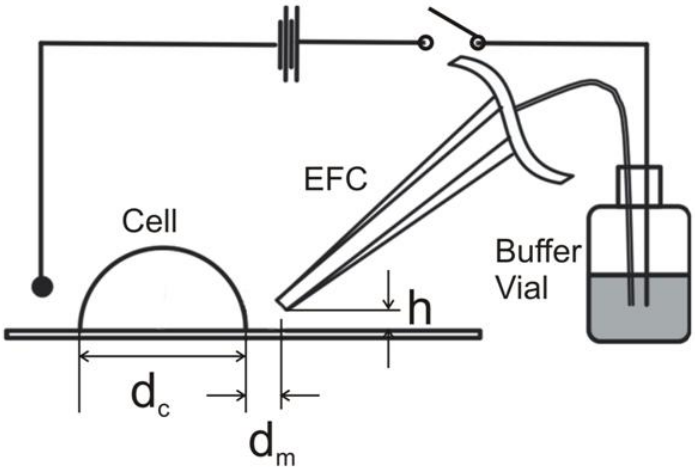

Figure 5.1. Schematic diagram of the experimental setup.

Electroporation. Two sets (Set 1 and Set 2) of electroporation experiments were performed in this study. In Set 1 experiments, fluorescently labeled A549 cells were pulsed at 500V, pulse duration ranging from 300-500 ms, while the tip-cell distance, d_m, was set at 2.0, 3.5 or 5.0 µm. Simple PCI software was used to determine diffusive loss of fluorescent thiol (chiefly reduced glutathione) from the cell.[27]

In the second set (Set 2), electroporation experiments were performed again on A549, and two more cell lines: prostate adenocarcinoma cell line PC-3, and prostate cancer cell line DU 145. In performing Set 2 experiments, the percent fluorescence intensity loss at steady state, which we will call ΔF% was fixed to values at which 100 % cell survival would be expected based upon the information from Set 1 experiments. For example, in the case of PC-3 cell line, cells were pulsed to achieve a 50% loss. In order to do so, the diameter (d_c) of the cell to be pulsed was first measured using the Simple PCI software, then according to the regression equation (Eq. 4 in Agarwal et al.)[27] the d_m at which the cell should be pulsed was determined. Similarly, experiments were performed on A549 cells to obtain ΔF% equal to 20 %, and 40 %, and on cell line DU 145 to obtain ΔF% equal to 40 %.

Imaging. An inverted fluorescent microscope (Olympus, IX 71, Melville, NY) with a 40X 1.3 NA oil immersion objective imaged the cell experiments using a CCD camera (Hamamatsu, ORCA-285, Bridgewater, NJ). The images were collected at a frequency of 1 frame/s. Depending on the fluorescent properties, an appropriate cube was chosen. For Thioglo-1, an Omega fluorescence cube (especially built, Omega, Brattleboro, VT) was used with filters for excitation at 378 nm and emission at 480 nm. For live/dead imaging, a triple band 'Pinkel' filter set from Semrock (Rochester, NY) was used (exciter 1 387 nm, exciter 2 494 nm; exciter 3 575 nm; dichroic mirror: 394– 414 nm, 484 – 504 nm, 566 – 586 nm, emitter: 457, 530, 628 nm). Image acquisition software Simple PCI (Compix, Inc., Sewickley, PA) was used to perform image processing.

Cell Viability Assay. Following electroporation experiments, live/dead analysis was performed on the cells using calcein AM and propidium iodide as described in detail before.[17] Briefly, the buffer in the cell dish was replaced by 2 mL of fresh growth medium. The cells were allowed 5-6 h of recovery in the 37 °C incubator with 95 % air/5% CO_2, followed by a 30 min of 2 μM each of calcein AM and propidium iodide staining. It is important to note that a measurement of the cell viability was made on each cell that was electroporated.

Statistical Analysis. A549 cells electroporated in Set 1 and Set 2 experiments were used for statistical analysis. Logistic regression was performed using the program STATA (Intercooled 9.0) on the outcome cell survivability (live/dead). Logistic regression was done as the outcome cell survivability is binary. The independent variable used was the parameter *K* (described below).

5.4 RESULTS

Figure 5.2 is a contour plot of cell survival percentage of A549 cells in Set 1 electroporation experiments as a function of d_m and pulse duration. In this contour plot, lighter shades represent areas with a larger fraction of live cells, whereas darker shades represent areas with a larger fraction of dead cells. The plot shows that at a given pulse duration, cell survival increases with d_m. As an example, at pulse duration of 400 ms, the cell survivability goes from 75 % at d_m=2.5 µm to 90 % at d_m=4.5 µm. The plot shows that the pulse duration does not have as much of a significant effect on cell survivability as d_m. For example, at d_m=2.25 µm the cell survivability is 70 % for all pulse durations. At d_m=3.5 µm cell survivability is 85 % for pulse durations from 300-430 ms, after which the cell survivability increases to 100 % for 500 ms pulse. Our results (Figure 5.2) also indicate that the cell survival rate with extracellular buffer (high Na^+) is higher than the cell survival rate achieved with intracellular buffer (high K^+).[17] Under similar pulsing conditions (500 V, 300 ms, 2 µm d_m), cell survivability was 65 % with extracellular buffer, whereas it was only 20 % with intracellular buffer. Also pulse duration had a larger influence on cell survivability in intracellular buffer than in extracellular buffer.

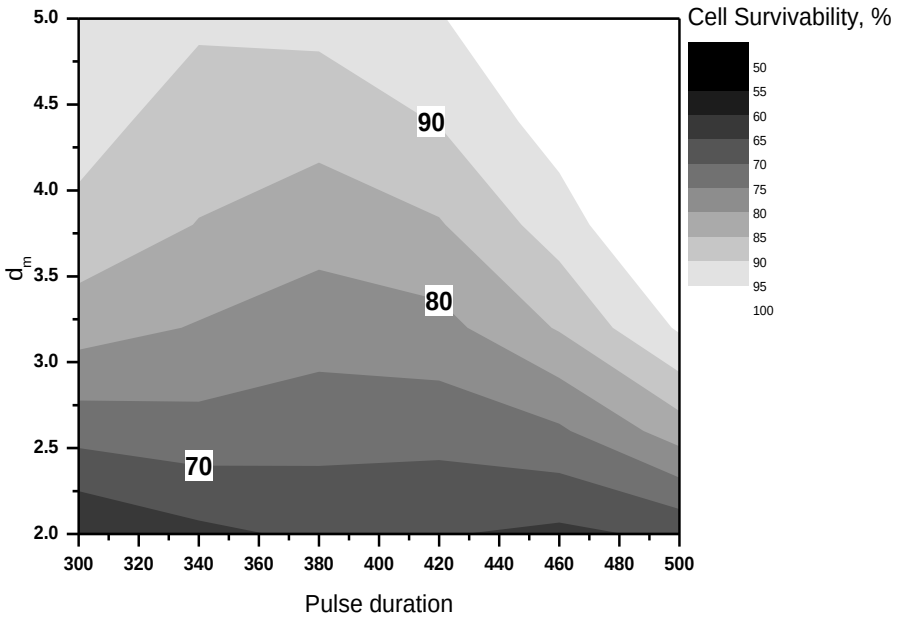

Figure 5.2. Contour plot of percentage of cell survivability of A549 cells electroporated in Set 1 experiments as a function of d_m and pulse duration.

The fluorescence intensity vs. time curves from Set 1 and Set 2 experiments were fitted to a function given in Eq. 5.1.

$$F = F^0 e^{(-kt)} e^{\left[K\left(e^{-\alpha t}-1\right)\right]} \tag{5.1}$$

This equation results from incorporating a photobleaching term into the equation from Puc *et al.*[22] Here F is the fluorescence intensity at time t, F^0 is the fluorescence intensity at time zero when the pulse is applied, k is the photobleaching rate constant, $K = \frac{M}{\alpha}$ where M is the first order rate constant for transport of Thioglo-1 labeled molecules out of the cell, and α is the first order pore resealing rate constant. It should be noted here that the fluorescence intensity versus time data were not corrected for photobleaching. The photobleaching rate constant (k) was one of the parameters determined along with the parameters K and α. A program written in Mathcad (Mathsoft, Cambridge, MA) was used to fit decay curves and to estimate parameters k, K, and α,

and goodness of fit R^2.[27] The parameter K is a useful parameter as it is also related to the fraction of cell's fluorescent contents remaining at steady state as shown in Eq. 5.2.

$$K = \ln \frac{F^0}{F_{ss}} \tag{5.2}$$

Here F^o is the fluorescence intensity at the time of the application of pulse, and F_{ss} is the steady state fluorescence at long times. Our goal in this work is to determine the relationship between K or ΔF % (100 (1- F_{ss}/F^0)) which are the parameters referring to the efflux of freely diffusing molecules from the cells following electroporation and cell survivability.

Figure 5.3 is a plot of computed probabilities of cell survival percentage overlaid over the observed cell survival percentage following electroporation as a function of K for all the A549 cells in Set 1 experiments. The green bars represent live cells, and red bars represent dead cells. Figure 5.3 shows that all the cells subjected to electroporation (500 V, pulse duration: 300-500 ms, and d_m: 2.0-5.0 μm) survived for values of $K \leq 1.0$ (ΔF % = 63 %). The cell survival percentage decreases rapidly at higher values of K. The cell survival decreases from 100 % to 20 % at K values ranging in 1.0-1.4. At higher K values (≥1.4) which corresponds to ΔF % ≥ 75 %, all cells die at the given conditions of electroporation.

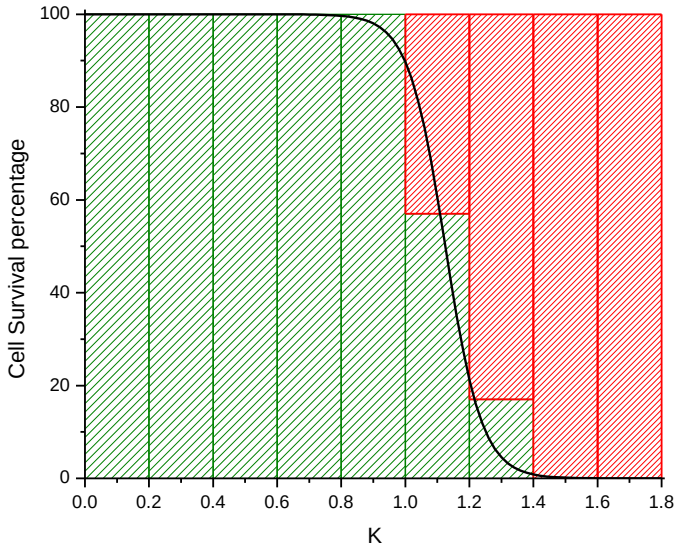

Figure 5.3. Computed probabilities of cell survival (black curve) overlaid over plot of cell survival percentage as a function of *K* for A549 cells electroporated in Set 1 experiments. Green bars represent live cells and red bars represent dead cells.

The black curve in Figure 5.3 shows the computed probabilities of cell survival as a function of *K*. Logistic regression was done to compute the probabilities of cell survival based on *K*. Logistic regression is used when there is a binary outcome (e.g., live/dead). The probability *P* is computed using the following equation:

$$P = \frac{e^{b_0 + b_1 K}}{1 + e^{b_0 + b_1 K}} \tag{5.3}$$

The coefficients in the above model were determined using logistic regression. The estimated values were b_0 = 19.56, and b_1 = -17.39 corresponding to the independent variable *K*. The results indicated a significant relationship ($p < 0.05$) between cell survivability and *K*. The curve shows that at *K* = 1 there is a 90 % chance of cell survival. The curve rapidly decays as a function of *K*. At *K* = 1.1 there is a 50 % chance of cell survival which sharply goes down to 18 % chance of cell survival at *K* = 1.2. The overlay of computed probabilities of cell survival over the observed cell survival shows that the logistic regression model tracks the experimental values closely. For

example, at K = 0.7 probability of cell survival from both the experimental data and model is 1, at K = 1.1 observed probability is 0.61 whereas the model-predicted probability of cell survival is 0.60. Further, at K =1.5 both the model predicted and the observed probabilities of cell survival are 0.

Figure 5.4 is a contour plot of ΔF % and cell survivability as a function of d_m and d_c for all the A549 cells electroporated in Set 1 experiments. The box plot represents the distribution of cell sizes in percentiles: 5^{th}, 25^{th}, 50^{th}, 75^{th}, and 95^{th} corresponding to d_c 12, 19, 22, 27, and 36 μm respectively. It should be mentioned here that a stepwise forward and backward linear regression was done on parameter K and experimental controlled variables d_m and pulse duration and the cell variables. The results from multiple linear regression of K showed a significant relationship (r^2 = 0.30, $p < 0.001$ for the coefficients of d_m and d_c^{-1}) between dependent variable K and independent variables d_m and cell diameter d_c (μm).[27] The regression results (Eq. 4, Agarwal et al.)[27] were used to make the contour plot. The contour lines indicate ΔF %. The plot shows that at a given d_m, a smaller cell has a larger ΔF% than a larger cell. As an example, at d_m = 3.5 μm, a median cell (d_c= 22 μm) loses 54 % fluorescence, whereas a larger cell with a d_c = 27 μm loses 42 % of its fluorescence. The plot is further extended to include cell survivability results from Figure 5.3. The green region represents the area of 100 % cell survivability following electroporation, whereas red region represents the area of 100 % cell death following electroporation. The blue region represents the area where cell survivability decreases rapidly from 100 % to 20 %. The plot shows that at a given d_m, a larger cell has higher chance of cell survival than a smaller cell. For example a median cell (22 μm) pulsed at a d_m = 3.9 μm is predicted to lose 50 % of its fluorescence. As this lies in the green region, the median cell pulsed at 3.9 μm will retain its cell viability. A smaller cell with a d_c = 12 μm pulsed at 3.9 μm would

lose 83 % of its fluorescence. As this lies in the red region, a 12 µm pulsed at 3.9 µm will die. The plot (Figure 5.4) gives a complete guide to predicting the outcome of electroporation as a function of d_m and d_c while preserving cell viability. This is an extension to our previous work where we showed that the ΔF % can be controlled by d_m and d_c. In the present work we show that not just the outcome of electroporation but cell survivability can also be predicted based upon experimenter controlled variable d_m and cell variable d_c.

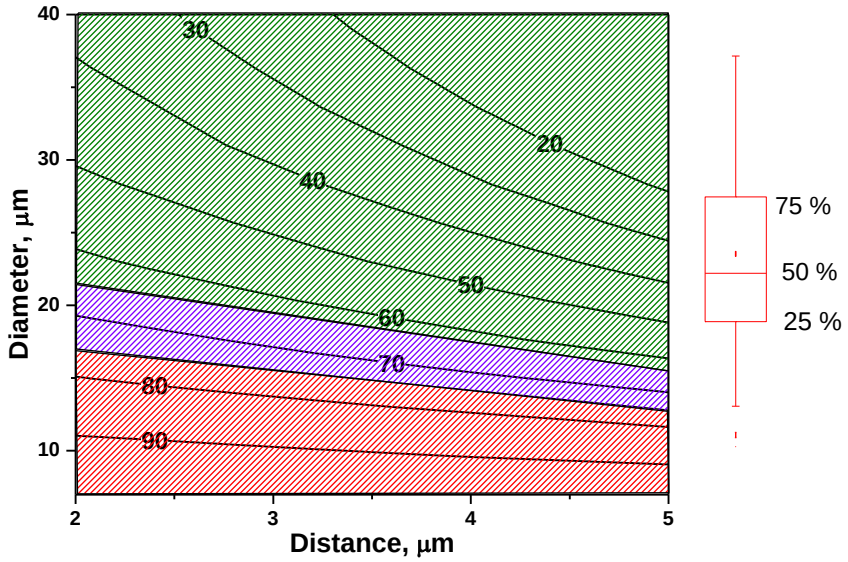

Figure 5.4. Contour plot of percent fluorescence intensity loss and cell survivability as a function of d_m and d_c. Contour lines represent percent fluorescent intensity loss. Green area represents live cells, red area represents dead cells, and blue area represents cell survival between 100 % – 20 %. The box plot gives the 5th, 25th, 50th, 75th, and 95th percentile of cell diameters corresponding to 12, 19, 22, 27, and 36 µm.

In Set 2, we performed additional electroporation experiments on A549 and two more cell lines DU 145 and PC-3. The Set 1 results showed that all the A549 cells pulsed survived at ΔF % ≤ 63 %, therefore in Set 2 experiments, we fixed the ΔF % at < 63 % for all the three cell lines to see if high cell survivability could be achieved. The results (Table 5.1) show the expected, observed (average) and standard error of the mean values for the three cell lines (A549, DU 145, and PC-3) with various values of ΔF %. The survival percentage column shows that high survival

percentage (as high as 100 %) was achieved for all the three cell lines by controlling ΔF %. The results show that cell survivability can be retained for not only A549 cells but also DU 145 and PC-3 cells as long as efflux can be controlled to ≤ 63 %.

Table 5.1. Expected ΔF%, average ΔF% observed, standard error of the mean, and survival % for cell lines A549, PC-3, and DU 145 from Set 2 experiments.

Cell Line (number of cells)	Expected ΔF%	Average ΔF% observed	Standard error of the mean	Survival %
A549 (15)	20	18	1.9	100
A549 (21)	40	41	2.4	95
DU 145 (15)	40	38	2.1	100
PC-3 (15)	50	52	3.8	86

Figure 5.5 is plot of computed probabilities of cell survival percentage overlaid over the observed cell survival percentage following electroporation as a function of *K* for the A549, DU 145, and PC-3 cells electroporated in Set 1 and Set 2 experiments. The green bars represent live cells and the red bars represent dead cells. The combined results from Set 1 and Set 2 data show that all the cells subjected to electroporation remain alive at $K \leq 0.8$ ($\Delta F\ \% \leq 55\%$). The cell

survivability decreases by 10 % at *K* between 0.8-1.0. At higher values of *K*, ranging from 1.0-1.4, cell survivability decreases rapidly from 90% to 20 %. All the cells die at higher values of *K* ($\geq$ 1.4).

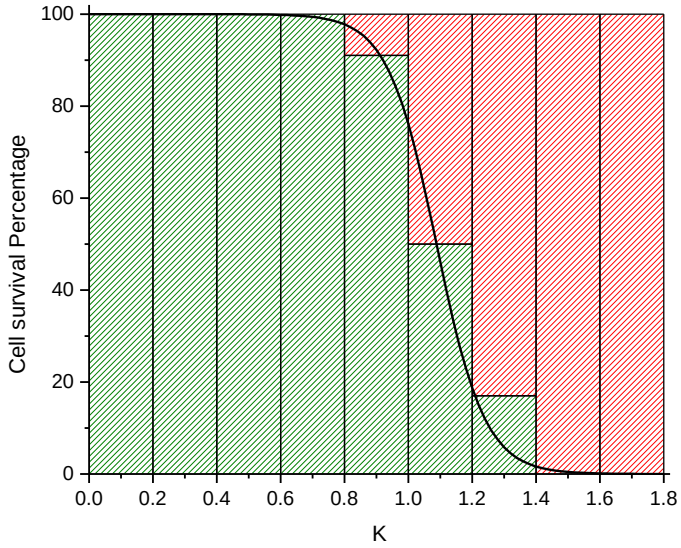

Figure 5.5. Computed probabilities of cell survival (black curve) overlaid over observed cell survival percentage as a function of *K* for A549, DU 145, and PC-3 cells electroporated in Set 1 and Set 2 experiments. Green bars represent live cells and red bars represent dead cells.

The black curve (Figure 5.5) shows the computed probabilities of cell survival (Set 1 and Set 2) based on *K*. Logistic regression was done to compute the probabilities of cell survival based on *K*. The probability *P* was computed using Eq. 5.3. The coefficients of the model were determined using logistic regression. The estimated values were b_0 = 14.31, and b_1 = -13.14 corresponding to the independent variable *K*. The results indicated a significant relationship ($p < 0.05$) between cell survivability and *K*. The curve shows that at *K* = 0.8 there is 98 % chance of cell survival. The curve decreases as a function of *K*. At *K* = 1.1 there is 46 % chance of cell survival which sharply goes down to 18 % at *K* = 1.2. The overlay of computed probabilities of cell survival over the observed cell survival shows that the logistic regression model tracks the experimental values closely as in Fig. 3. For example, at *K* = 0.8 observed cell survival is 1and

model-predicted probability of cell survival is 0.98. At K = 1.1 observed probability is 0.5 whereas the model-predicted probability of cell survival is 0.46. Further, at K =1.5 both the model predicted and the observed probabilities of cell survival are 0.

5.5 DISCUSSION

It is important to preserve cell viability following electroporation. In the present work, our goal is to determine the relation between the release of freely diffusing molecules from single cells following electroporation and cell survivability. Our results from Set 1 (Figure 5.3) experiments show that all the A549 cells remain alive following electroporation till they lose 63 % or less of their intensity. Logistic regression results showed that there is a significant ($p < 0.05$) relationship between cell survivability and the parameter K. We were able to preserve cell viability to a good degree (> 86 %, Table 5.1) for not only A549 but two more cell lines; DU 145 and PC-3, by fixing the percentage release of freely diffusing molecule values at less than 63 %. Further, it was found that across the cell lines (A549, DU 15, and PC-3 from Set 1 and Set 2 experiments, Figure 5.5), all the cells remained alive at a loss of 55 % or less of their intensity. We also showed that the relationship between cell survivability and K can be modeled using logistic regression (Figure 5.3 and Figure 5.5). Our findings indicate that in single cell electroporation, the amount of freely diffusing molecule release can guide us to make estimates of cell survivability (Figure 5.4). One application of our current work is the analysis of the cytoplasmic contents in single living cells.[30-33] Our findings will help design protocols which will allow sampling from single cells by using experimental and cell parameters (d_m and d_c) such that

K is large enough and the cell viability is preserved. In other words *K* will give us information about both the probability of cell survival and the efflux we can expect to get from the cell.

Numerous studies have been performed to determine the fraction of cell survival under various conditions of cell permeabilization. Although this approach helps in developing protocols for optimizing experimental conditions of electroporation, it would be useful to know the fraction of small molecules a cell can release/ uptake before losing its viability. Such results would not only help in gaining better control over electroporation but also help in understanding the biochemical pathways leading to cell death. In this study, the cells were labeled with a cell permeable, thiol-reactive dye Thioglo-1. As reduced glutathione, GSH, is the most abundant thiol in the cells, we can say that the decrease in fluorescence intensity inside the cell following application of the pulse is predominantly due to the efflux of labeled glutathione from the cell. In a cell, glutathione is mainly present in its reduced form, GSH, however under oxidative stress, it is converted into its oxidized form GSSG. The redox status of the GSSG/2GSH couple is an indicator of oxidative stress in the cell and controls various cell processes such as proliferation, differentiation and cell death.[34] The intracellular depletion of GSH ultimately leads to cell death. Gaetjens et al. performed a study on L1210(A) mouse lymphoma cells, in which they depleted the cells of more than 90 % of cellular glutathione content by using the compound L-buthionine-S-R-sulfoximine.[35] Their results showed that cells depleted of glutathione (> 90 %) demonstrated long-term proliferation and no loss in viability. As compared to our results from A549, PC-3, and DU 145 cells that lose cell viability after 60 % efflux, we can say that there are other species the loss of which is more damaging than that of GSH.

Based on the above argument, we can speculate what molecules leak from electropermeabilized cells that lead to cell death. NAD, NADP, and ATP are important

biological molecules that play a major role in mediating cell death. NAD is mostly present in its oxidized form NAD^+. Under physiological conditions, the ratio of cytosolic free NAD^+/NADH is ~ 700 to 1.[34] Alteration of this ratio under oxidative stress or pathological conditions can affect numerous enzymatic activities which may further lead to cell death. . As an example, poly(ADP-ribose) polymerase-1 (PARP-1) is a nuclear enzyme whose excessive activation by DNA damage leads to cell death. Ying et al. have shown that NAD^+ depletion is a key intermediate step in mediating PARP-1 activated cell death.[36] In contrast to NAD^+/NADH, the levels of NADPH are higher than those of $NADP^+$ (~100:1). One of the prominent functions of NADPH is to maintain a pool of reducing equivalents for metabolic systems such that the cells are protected from oxidative stress. Most importantly, NADPH is essential for regeneration of glutathione, thioredoxin, and peroxyredoxins in cells, which are the major oxidative defense systems.[34, 36, 37] Therefore, depletion of NADPH, would lead to oxidative stress in the cells, further leading to cell death. Intracellular ATP levels have been implicated as a determinant of the cell's pathway to die by apoptosis which is a programmed cell death or necrosis which is unnatural death. Eguchi et al. showed that cells treated with a calcium ionophore induced apoptosis under ATP-supplying conditions but necrotic cell death under ATP-depleting conditions, indicating that ATP levels were a determinant of how cell death was manifested.[38]

5.6 REFERENCES

(1) Neumann, E.; Schaefer-Ridder, M.; Wang, Y.; Hofschneider, P. H. Gene transfer into mouse lyoma cells by electroporation in high electric fields. *EMBO J.* **1982**, *1*, 841-845.

(2) Neumann, E. Membrane electroporation and direct gene transfer. *Bioelectrochem Bioenerg*. **1992**, *28*, 247-267.

(3) Neumann, E.; Toensing, K.; Kakorin, S.; Budde, P.; Frey, J. Mechanism of electroporative dye uptake by mouse B cells. *Biophys J.* **1998**, *74*, 98-108.

(4) Neumann, E.; Kakorin, S.; Toensing, K. Fundamentals of electroporative delivery of drugs and genes. *Bioelectrochem Bioenerg*. **1999**, *48*, 3-16.

(5) Prausnitz, M. R.; Bose, V. G.; Langer, R.; Weaver, J. C. Electroporation of mammalian skin: a mechanism to enhance transdermal drug delivery. *Proc Natl Acad Sci U S A.* **1993**, *90*, 10504-10508.

(6) Pliquett, U.; Weaver, J. C. Electroporation of human skin: simultaneous measurement of changes in the transport of two fluorescent molecules and in the passive electrical properties. *Bioelectrochem Bioenerg*. **1996**, *39*, 1-12.

(7) Gift, E. A.; Weaver, J. C. Simultaneous quantitative determination of electroporative molecular uptake and subsequent cell survival using gel microdrops and flow cytometry. *Cytometry*. **2000**, *39*, 243-249.

(8) Xie, T. D.; Tsong, T. Y. Study of mechanisms of electric field-induced DNA transfection. II. Transfection by low-amplitude, low-frequency alternating electric fields. *Biophys J.* **1990**, *58*, 897-903.

(9) Sixou, S.; Teissie, J. Exogenous uptake and release of molecules by electroloaded cells: a digitized videomicroscopy study. *Bioelectrochem Bioenerg*. **1993**, *31*, 237-257.

(10) Faurie, C.; Phez, E.; Golzio, M.; Vossen, C.; Lesbordes, J.-C.; Delteil, C.; Teissie, J.; Rols, M.-P. Effect of electric field vectoriality on electrically mediated gene delivery in mammalian cells. *Biochim et Biophys Acta, Biomembranes*. **2004**, *1665*, 92-100.

(11) Weaver, J. C.; Chizmadzhev, Y. A. Theory of electroporation: A review. *Bioelectrochem Bioenerg*. **1996**, *41*, 135-160.

(12) Tsong, T. Y. Electroporation of cell membranes. *Biophys J.* **1991**, *60*, 297-306.

(13) Kinosita, K., Jr.; Tsong, T. Y. Hemolysis of human erythrocytes by a transient electric field. *Proc Natl Acad Sci U S A.* **1977**, *74*, 1923-1927.

(14) Rols, M. P.; Teissie, J. Electropermeabilization of mammalian cells: quantitative analysis of the phenomenon. *Biophys J.* **1990**, *58*, 1089-1098.

(15) Gabriel, B.; Teissie, J. Control by electrical parameters of short- and long-term cell death resulting from electropermeabilization of Chinese hamster ovary cells. *Biochim et Biophys Acta, Molecular Cell Research*. **1995**, *1266*, 171-178.

(16) Loste, F.; Eynard, N.; Teissie, J. Direct monitoring of the field strength during electropulsation. *Bioelectrochem Bioenerg*. **1998**, *47*, 119-127.

(17) Agarwal, A.; Zudans, I.; Orwar, O.; Weber, S. G. Simultaneous maximization of cell permeabilization and viability in single-cell electroporation using an electrolyte-filled capillary. *Anal Chem.* **2007**, *79*, 161-167.

(18) Rols, M.-P.; Teissie, J. Electropermeabilization of mammalian cells to macromolecules: control by pulse duration. *Biophys J.* **1998**, *75*, 1415-1423.

(19) Pucihar, G.; Mir, L. M.; Miklavcic, D. The effect of pulse repetition frequency on uptake into electropermeabilized cells in vitro with possible applications in electrochemotherapy. *Bioelectrochemistry*. **2002**, *57*, 167-172.

(20) Brown, R. E.; Bartoletti, D. C.; Harrison, G. I.; Gamble, T. R.; Bliss, J. G.; Powell, K. T.; Weaver, J. C. Multiple-pulse electroporation: uptake of a macromolecule by individual cells of *Saccharomyces cerevisiae*. *Bioelectrochem Bioenerg*. **1992**, *28*, 235-245.

(21) Agarwal, A.; Zudans, I.; Weber, E., A; Olofsson, J.; Orwar, O.; Weber, S. G. Effect of cell size and shape on single-cell electroporation. *Anal Chem.* **2007**, *79*, 3589-3596.

(22) Puc, M.; Kotnik, T.; Mir, L. M.; Miklavcic, D. Quantitative model of small molecules uptake after in vitro cell electropermeabilization. *Bioelectrochemistry*. **2003**, *60*, 1-10.

(23) Valic, B.; Golzio, M.; Pavlin, M.; Schatz, A.; Faurie, C.; Gabriel, B.; Teissie, J.; Rols, M.-P.; Miklavcic, D. Effect of electric field induced transmembrane potential on spheroidal cells: theory and experiment. *Euro Biophys J*. **2003**, *32*, 519-528.

(24) Djuzenova, C. S.; Zimmermann, U.; Frank, H.; Sukhorukov, V. L.; Richter, E.; Fuhr, G. Effect of medium conductivity and composition on the uptake of propidium iodide into electropermeabilized myeloma cells. *Biochim Biophys Acta*. **1996**, *1284*, 143-152.

(25) Canatella, P. J.; Karr, J. F.; Petros, J. A.; Prausnitz, M. R. Quantitative study of electroporation-mediated molecular uptake and cell viability. *Biophys J*. **2001**, *80*, 755-764.

(26) Teissie, J.; Eynard, N.; Gabriel, B.; Rols, M. P. Electropermeabilization of cell membranes. *Adv Drug Deliver Rev*. **1999**, *35*, 3-19.

(27) Agarwal, A.; Wang, M.; Olofsson, J.; Orwar, O.; Weber, S. G. Control of small molecule release in single-cell electroporation. *Manuscript submitted*. **2008**.

(28) Fabisiak, J. P.; Sedlov, A.; Kagan, V. E. Quantification of oxidative/nitrosative modification of CYS34 in human serum albumin using a fluorescence-based SDS-PAGE assay. *Antioxid Redox Sign*. **2002**, *4*, 855-865.

(29) Kagan, V. E.; Kuzmenko, A. I.; Tyurina, Y. Y.; Shvedova, A. A.; Matsura, T.; Yalowich, J. C. Pro-oxidant and antioxidant mechanisms of etoposide in HL-60 cells: role of myeloperoxidase. *Cancer Res.* **2001**, *61*, 7777-7784.

(30) Sims, C. E.; Meredith, G. D.; Krasieva, T. B.; Berns, M. W.; Tromberg, B. J.; Allbritton, N. L. Laser-Micropipet Combination for Single-Cell Analysis. *Anal Chem.* **1998**, *70*, 4570-4577.

(31) Han, F.; Wang, Y.; Sims, C. E.; Bachman, M.; Chang, R.; Li, G. P.; Allbritton, N. L. Fast Electrical Lysis of Cells for Capillary Electrophoresis. *Anal Chem.* **2003**, *75*, 3688-3696.

(32) Meredith, G. D.; Sims, C. E.; Soughayer, J. S.; Allbritton, N. L. Measurement of kinase activation in single mammalian cells. *Nat Biotech.* **2000**, *18*, 309-312.

(33) Cannon, D. M., Jr.; Winograd, N.; Ewing, A. G. Quantitative chemical analysis of single cells. *Ann Rev Biophys Biom.* **2000**, *29*, 239-263, 232 Plates.

(34) Schaffer, F. Q.; Buettner, G. R. Redox environment of the cell as viewed through the redox state of the glutathione disulfide/glutathione couple. *Free Rad Biol Med.* **2001**, *30*, 1191-1212.

(35) Gaetjens, E. C.; Chen, P.; Broome, J. D. L1210 (A) mouse lymphoma cells depleted of glutathione with L-buthionine-S-(R)-sulfoximine proliferate in tissue culture. *Biochem. Biophys. Res. Commun.* **1984**, *123*, 626-632.

(36) Ying, W. NAD+/NADH and NADP+/NADPH in cellular functions and cell death: Regulation and biological consequences. *Antioxid Redox Sign.* **2008**, *10*, 179-207.

(37) Pollak, N.; Niere, M.; Zieglar, M. NAD kinase levels control the NADPH concentration in human ells. *J Biol Chem.* **2007**, *282*, 33562-33571.

(38) Eguchi, Y.; Shimizu, S.; Tsujimoto, Y. Intracellular ATP levels determine cell death fate by apoptosis or necrosis. *Cancer Res.* **1997**, *57*, 1835-1840.

APPENDIX A

REGRESSION ANALYSIS

❖ Data Screening

1) Open Intercooled Stata 9.
2) Import data saved in excel format into stata.
   a) *Goto File → Import ASCII data created by a spreadsheet.*
3) Start a log file.
   b) *Goto File → Log → Begin→Save*
4) Screen the data for outliers.
   c) *Goto Graphics → box plot (Univariate outliers)*
   d) *Goto Graphics → Two way graphs → scatterplot (Multivariate outliers)*
      i) The extreme data points detected from box plots and scatterplots can be potential outliers. These data points should be examined for error in data entry, or experimental error.
5) Check the data for normality.
   e) *Command: gladder <variable>*
      ii) Histograms of the variable by transformations with the normal curve superimposed will be created. Select the transformation that is the most normal.

f) *Command: ladder <variable>*

iii) A table of suggested transformations and their chi squared values will be given. Select the transformation with the lowest chi square value.

6) Create a new transformed variable.

g) *Command: newvariable=transformation*(variable)*

iv) Example. variable: diameter, new variable: tdiameter, transformation: log

Command → tdiameter = log(diameter)*

7) Check for Correlation between variables.

h) *Command: scatterplot matrix*

v) If any pair of variables gives high correlation, then to avoid multicollinearity only one of the two variables should be selected.

❖ **Regression Analysis**

1) Logistic Regression.

a) *Command: Logit <dependent variable> <independent variables>*

i) Example: Dependent variable: *success*, Independent variables: *pulse length (plslength), distance, and area*

ii) *Command: Logit success plslength distance area*

iii) Output

Number of Obs[1]	226		
LR $chi^2(3)$[2]	76.26		
Prob > $chi^{2(3)}$	0.00		
Pseudo $R^{2(4)}$	0.39	Log likelihood[5]	-57.6

Success[6]	Coefficient[7]	Standard Error[8]	Z[9]	P>|z|[10]	[95% Conf. Interval][11]	
plslength	0.01	0.00	3.68	0.00	0.01	0.02
distance	-1	0.21	-5.78	0.00	-1	-0.8
area	0.01	0.00	3.27	0.00	0.00	0.01
cons	3	0.96	3.08	0.00	1	5

iv) Interpretation of Results.

(1) Number of observations being analyzed.

(2) Likelihood ratio chi-square with degrees of freedom. One degree of freedom is used for each predictor variable in the logistic regression model.

(3) p-value associated the chi-square. The value of 0.00 indicates that the model as a whole is statistically significant.

(4) Technically, R^2 cannot be computed the same way in logistic regression as it is in OLS regression. The pseudo-R^2, in logistic regression, is defined as $(1 - L_1)/L_0$, where L_0 represents the log likelihood for the "constant-only" model and L_1 is the log likelihood for the full model with constant and predictors.

(5) Values of the log likelihood for the model including the constant and all of the predictors (independent variables) that are computed using the maximum-likelihood logit model.

(6) This column starts with the name of the dependent variable (success) and then lists the names of the predictor variables (pulse duration, distance, area).

(7) The coefficient column gives the values for the logistic regression coefficients. These coefficients indicate the amount of change expected in the log odds when

there is a one unit change in the predictor variable with all of the other variables in the model held constant. A coefficient close to 0 suggests that there is no change due to the predictor variable.

(8) This column contains the standard error for the logistic regression coefficient which is used to compute the z-test for the coefficient.

(9) This column contains the z-statistic testing the logistic coefficient. In the case of the logit command, z = (coef.)/ (Std. Err).

(10) This column contains the two-tail p-value for the z-test.

(11) This column contains the 95% confidence intervals for the logistic regression coefficients. Significant effects are suggested when confidence intervals do not contain 0.

2) Stepwise forward and backward linear regression.

a) *Command: Forward selection: sw, pe(0.05): regress <dependent variable><independent variables>*

b) *Command: backward elimination: sw, pr(0.05): regress <dependent variable> <independent variables>*

i) Example: dependent variable: *K*, Independent variables: *diameter, breadth, width, aspect-ratio, grey-level (grlev), standard deviation grey-level (sdgrlev), pulse length (pldlength), and distance.*

ii) *Command: sw, pe(0.05): regress K diameter breadth width aspect ratio grlev sdgrlev plslength distance*

iii) Output

Source[1]	SS[2]	Df[3]	MS[4]
Model	7.18	2	3.6
Residual	18.3	103	0.18
Total	25.5	105	0.24

Number of Obs[5]	106
F(2, 103)[6]	20.22
Prob > F[6]	0.00
R-squared[7]	0.30
Root MSE[8]	0.42

K[9]	Coefficient[10]	Standard Error[11]	P>|t|[12]	[95% Conf. Interval][13]	
distance	-0.18	0.036	0.00	-0.25	-0.10
diameter	28	6.8	0.00	14	41
cons	0.12	0.31	0.69	-0.49	0.74

iv) Interpretation of the results

(1) Source of variance; Model, Residual, and Total. The Total variance is partitioned into the variance which can be explained by the independent variables (Model) and the variance which is not explained by the independent variables (Residual, sometimes called Error). The Sums of Squares for the Model and Residual add up to the Total Variance.

(2) Sum of Squares associated with the three sources of variance, Total, Model and Residual.

(3) Degrees of freedom associated with the sources of variance. The total variance has N-1 degrees of freedom. The model degrees of freedom correspond to the number of predictors minus 1. The Residual degrees of freedom is the DF total minus the DF model.

(4) Mean Squares, the Sum of Squares divided by their respective DF. These are computed to compute the F ratio (Mean Square Model/Mean Square Residual) to test the significance of the predictors in the model.

(5) Number of observations used in the regression analysis.

(6) The F-value is the Mean Square Model divided by the Mean Square Residual. These values tell us whether the independent variables reliably predict the dependent variable. If $p < 0.05$, then it can be concluded that the independent variables reliably predict the dependent variable. If the $p > 0.05$, then the group of independent variables does not show a statistically significant relationship with the dependent variable, or that the group of independent variables does not reliably predict the dependent variable. This is an overall significance test assessing whether the group of independent variables when used together reliably predict the dependent variable, and does not address the ability of any of the particular independent variables to predict the dependent variable.

(7) R-Squared is the proportion of variance in the dependent variable which can be predicted from the independent variables. This is an overall measure of the strength of association, and does not reflect the extent to which any particular independent variable is associated with the dependent variable.

(8) Root MSE is the standard deviation of the error term, and is the square root of the Mean Square Residual.

(9) This column shows the dependent variable at the top with the independent variables below it.

(10) These are the parameter estimates for the regression equation for predicting the dependent variable from the independent variable.

(11) The standard error is used in t-test for the significance of regression parameter estimates. The standard errors can also be used to form a confidence interval for the parameter, as shown in the last two columns of this table.

(12) *p*-value used in testing the null hypothesis that the parameter is zero. *p*-value is the probability that in the repeated experiments null hypotheses will not be rejected. Hence, a small p-value such as $p < 0.05$ implies that null hypotheses will be rejected 95% of times.

(13) The confidence intervals are related to the p-values such that the coefficient will not be statistically significant if the confidence interval includes 0.

APPENDIX B

MATHCAD PROGRAM

A program was written in Mathcad to get the values of k, K, and alpha.

$$f(X,k,K,\alpha) := \overrightarrow{\left[e^{-k\cdot X}\cdot e^{K\left[e^{-\alpha\cdot(X)}-1\right]}\right]}$$

process (Data) :=

for $i1 \in 0..24$

$ii \leftarrow i1\cdot 2$

$jj \leftarrow ii + 1$

$Y \leftarrow \text{if}\left[\left(\text{Data}^{\langle jj\rangle}\right)_{\text{last}\left(\text{Data}^{\langle jj\rangle}\right)} = 0, \text{submatrix}\left(\text{Data}^{\langle jj\rangle}, 0, \text{submatrix}\left(\text{match}\left(0, \text{Data}^{\langle jj\rangle}\right), 0,0,0,0\right)_0 - 1, 0, 0\right), \text{Data}^{\langle jj\rangle}\right]$

$X \leftarrow \text{if}\left[\left(\text{Data}^{\langle jj\rangle}\right)_{\text{last}\left(\text{Data}^{\langle jj\rangle}\right)} = 0, \text{submatrix}\left(\text{Data}^{\langle ii\rangle}, 0, \text{submatrix}\left(\text{match}\left(0, \text{Data}^{\langle jj\rangle}\right), 0,0,0,0\right)_0 - 1, 0, 0\right), \text{Data}^{\langle ii\rangle}\right]$

$$\text{guess} \leftarrow \begin{pmatrix} 0.001 \\ 0.2 \\ 0.1 \end{pmatrix}$$

$zz \leftarrow \text{genfit}(X, Y, \text{guess}, f)$

$z_{i1,0} \leftarrow zz_0$

$z_{i1,1} \leftarrow zz_1$

$z_{i1,2} \leftarrow zz_2$

$$q \leftarrow \overrightarrow{\left[e^{-z_{i1,0}\cdot X}\cdot e^{z_{i1,1}\left[e^{-z_{i1,2}\cdot(X)}-1\right]}\right]}$$

$rr \leftarrow \text{corr}(q, Y)$

$z_{i1,3} \leftarrow rr$

z

APPENDIX C

C.1 TIPS IN EXPERIMENTAL SECTION

C.1.1 Pulling Capillaries

It is important to maintain reproducibility of the pulled capillaries. There are certain necessary steps and precaution to be taken so that the reproducibility of the capillary can maintained for long periods of time.

A. Sutter P-2000 Puller

1. The retro mirror of the P-2000 Sutter puller should be cleaned with absolute ethanol and lens paper every couple of months.
2. The puller should be kept on a hard flat base in a clean room.
3. Always keep the hood of the puller open when turning the power on.
4. Leave the puller on for 15 minutes before starting to pull the capillaries.

B. Fused-silica capillaries

1. The protective layer of the fused silica capillary where the laser hits should be burned off using an ethanol burner.
2. The capillaries should be flushed with 2-4 ml filtered Mili-Q water before pulling.

C.1.2 Cell Culturing

1) **Clean Room.** Cell culturing should be performed in a clean room.
2) **Incubator.** The incubator where the cells are stored should be cleaned regularly. Especially the water tray should be cleaned regularly and replaced with mili-Q water.
3) **Cross-contamination.** Cross-contamination between cells and tissue cultures should be avoided. As an example, mammalian cells and bacterial cells should not be stored in separate incubators.
4) **Backups.** Cell backups should be prepared in early cell passages e.g. 5-10. Also new batch of cells should be started after ~40 cell passages.